AMERICAN UNIVERSITY OF BEIRUT

Dynamics on the Laplace Surface, Revisited

by

Mohammad Ali Farhat

A thesis
submitted in partial fulfillment of the requirements
for the degree of Master of Science
to the Department of Physics
of the Faculty of Arts and Sciences
at the American University of Beirut

Beirut, Lebanon
June 2019
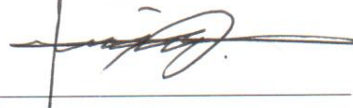
AMERICAN UNIVERSITY OF BEIRUT

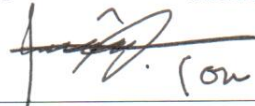## Dynamics on the Laplace Surface, Revisited

by
Mohammad Ali Farhat

Approved by:

Dr. Jihad Touma, Professor and Chair   Advisor

Physics Department

Dr. Scott Tremaine, Richard Black Professor   Member of Committee

Institute for Advanced Study   (on his behalf)
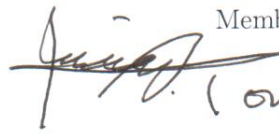
Dr. Leonid Klushin, Professor   Member of Committee

Physics Department   (on his behalf)

Date of thesis defense: June 21, 2019

AMERICAN UNIVERSITY OF BEIRUT

THESIS, DISSERTATION, PROJECT RELEASE FORM

Student Name: __Farhat_____Mohammad_____Ali_____
                             Last   First   Middle

☒ Master's Thesis   ◯ Master's Project   ◯ Doctoral Dissertation

☐   I authorize the American University of Beirut to: (a) reproduce hard or electronic copies of my thesis, dissertation, or project; (b) include such copies in the archives and digital repositories of the University; and (c) make freely available such copies to third parties for research or educational purposes.

☒   I authorize the American University of Beirut, to: (a) reproduce hard or electronic copies of it; (b) include such copies in the archives and digital repositories of the University; and (c) make freely available such copies to third parties for research or educational purposes after: **One** ___ **year from the date of submission of my thesis, dissertation or project.**
           Two X years from the date of submission of my thesis , dissertation or project.
           Three ___ **years from the date of submission of my thesis , dissertation or project.**

_____   28/8/2019
Signature   Date

Dedication

To the martyrs of our land, those who gave their lives so that we can have one. May this work partially cover our negligence and poor efforts in front of your beautiful and altruistic souls.

To Mohammad Jouni (1989-2015)

Acknowledgments

Thoughtful and constructive comments and remarks of Professors Scott Tremaine and Leonid Klushin as thesis committee members are gratefully acknowledged.

I would like to thank fellow friends in the graduate room at our department, especially Rodrique Badr for the continuous help and useful discussions.

I praise God for giving me the chance of apprenticeship for several years as a student of Professor Jihad Touma. He was not only an advisor for this thesis work, but also a life mentor. I thank him for sharing his philosophy of life, the pleasure of exploration, and his skills in our field. I am eternally grateful for his guidance and inspiration.

To my family: Ali, Randa, Hadi, and Nour, nothing would've been done without your continuous support.

To Mariam, thank you for being you.

An Abstract of the Thesis of

Mohammad Ali Farhat   for   Master of Science

Major: Physics

Title: Dynamics on the Laplace Surface, Revisited

We are living through revolutionary times in exo-planetary exploration, both observational and theoretical, with nearly four thousand exo-planetary systems confirmed, and most presenting us with fundamental challenges to cherished theories of planet formation and evolution. Of those, more than a hundred reside in wide binaries, where the stellar binary companion evolves on a fairly eccentric, and possibly inclined orbit. Such a binary companion can strongly perturb both classical processes of planet formation, as well as the resulting planetary system, in the course of its dynamical evolution. Those perturbations can be explored with the help of N-Body simulations, or through semi-analytic, perturbative treatment of the dynamics or both.

In this thesis, we extend the semi-analytic tradition as we study the orbital architecture of systems of self-gravitating particles around a central body (star or planet) which are further affected by a wide, eccentric, hierarchical perturber (stellar binary companion, super-Jupiter, an eccentric debris disk, or a combination of what preceded). To explore equilibrium architecture, we revisit long term dynamical evolution within a classical regime in celestial mechanics, associated with the so-called Laplace Surface. Here equilibrium configurations of a test particle's orbit arise from the combined action of an inner quadrupole (usually from a non-spherical mass distribution associated with an oblate planet, or a planet around the central star), and an outer, inclined perturber, again modelled as a quadrupole. The combined effect allows for equilibrium planes known as the Laplace Planes. Our contribution is in generalizing the classical scenario by allowing for higher order multipoles to account for the breaking of axisymmetry which is introduced by an eccentric perturber. The theory allows for multipoles of arbitrary order and exploits the geometric structure of the dynamics to provide a complete characterization of equilibrium configurations, their stability and bifurcations. We apply the fruits of our theoretical investigations to: i) the familiar setting of a satellite around an oblate planet, with the barycentre following an eccentric orbit ii) the mutual inclination of the Kepler-108 exo-planetary system, and iii) the curiously clustered bunch of trans-Neptunian objects.

Contents

List of Figures

1

Chapter 1

Literature Review

Celestial mechanics after Newton was nothing similar to what it was before him. His work inspired a lot of mathematicians to indulge in the bustle of the field, making it remain at the forefront of mathematical research throughout the eighteenth century. Many people contributed to the development of the subject, and many new mathematical techniques were devised in response to the difficulties that arose. Clairaut, D'Alembert, and Euler were the leaders in the field during the 1740s and 1750s and, when Clairaut died in 1765, the astronomical community could look back on a period of enormous and rapid progress in the theoretical branch of their subject. Some serious problems remained, however. As well as the discrepancies between theory and observation in the case of the secular acceleration of the Moon and the great inequality of Jupiter and Saturn, the most obvious failing was the lack of any general methods that were widely applicable. Over the following 60 years all this changed, primarily due to the efforts of two giants in the history of mathematics, Joseph Louis Lagrange and Pierre-Simon Laplace; the latter, known as the "Newton of France", has been described as possessing a phenomenal natural mathematical faculty superior to that of any of his contemporaries, and is of course, the man who initially inspired the work of this thesis.

Laplace's analytical discussion of the solar system is given in his *Méchanique Céleste* published in five volumes. The first two volumes, published in 1799, contain methods for calculating the motion of the planets, determining their figures, and resolving tidal problems. The third and fourth volumes, published in 1802 and 1805, contain applications of these methods, and several astronomical tables. The fifth volume, published in 1825, is mainly historical, but it gives as appendices the results of Laplace's latest researches.

Difficult to read though Laplace's masterpiece may have been, it was recognized immediately for the outstanding quality of its science. John Playfair referred to it in the Edinburgh Review for January 1808 as 'the highest point to which man

has yet ascended in the scale of intellectual attainment'.

Of the great successes of the book was Laplace's resolution of the cause of the great inequality of Jupiter and Saturn based on perturbation theory. But this also served to highlight the method's intrinsic limitations: The only way to test whether enough terms have been included in the perturbation potential is to compare with observations. His other great success was with the lunar problem: Laplace's final lunar theory, which took into account the secular changes in all elements not only the mean motion, significantly reduced the difference with observation, eventually concluding how the non-spherical shape of the earth is perturbing the moon, which allowed him to predict the oblateness of the earth.

1.1 The Laplace Plane

Of interest to us in Laplace's contribution is his work in Volume 4 of his *Méchanique Céleste* (1); specifically those of Chapter X: On the Excentricities and Inclinations of the Orbits of the Satellites, and Chapter XVII: On The Satellites of Saturn. In these chapters, after determining the oblateness of Jupiter and Saturn, Laplace moves to study the influence of this oblateness on Jupiter's satellites indicating *"the effects of this oblateness on the perijoves of the satellites being very great"*. He also concludes upon his study of inclinations that the great influence of the oblateness of Jupiter gives to each orbit an inclination which is peculiarly adapted to it, and that these satellites move upon planes that pass always between the equator of Jupiter and the orbit of it. The study was clearer with Saturn's satellites because all of them resided constantly in the plane of the ring, except for the outer satellite, which also moves upon a plane passing between Saturn's orbit and equator, through their mutual intersection. This surface known as the *Classical Laplace Surface* has been extensively studied, we discuss some of the literature in what follows.

In 1963, Allan and Cook (2) investigated the long term evolution of an artificial satellite on a circular orbit. Such an object would be perturbed by the oblateness of the Earth and gravitational attractions from the Moon and the Sun. The study is in a region where the the perturbations are of comparable magnitudes, and this covers a wide range of distances. However, the mathematical formalism constrains this range to a few Earth radii: The restriction of the study to circular orbits while neglecting the higher order harmonics in the lunar perturbation sets an upper limit to the radius of the satellite for that assumption to be valid. On the other hand, the period of the tested motion must be appreciably greater than a year for the double averaging in the secular approach to be justifiable, hence this sets a lower limit on the radius.

The motion in such a setting consists of simultaneous precession about the axes: the Earth's axis, the normal of the lunar orbit, and the normal to the ecliptic.

To arrive at a general solution, the authors assume these axes to be fixed and the Moon to be lying in the ecliptic, making the picture analogous to to the motion of the instantaneous axis of rotation of rigid body moving under no forces.

After double averaging the disturbing function and using vector equations of motion, and after imposing the circular condition on the orbit, the authors find three mutually perpendicular directions in which the orbit remains at rest, two of which are stable positions, thus the projection of the normal of the orbit to the unit sphere follows a fixed trajectory around one of the two stable positions. The significance of the Laplace Plane, corresponding to the larger region on the unit sphere, is that the normal of an inclined orbit will regress around the normal of the Laplace plane at a constant rate and inclination.

Neglecting solar perturbations on the satellites, Goldreich in 1965 (3) studied the inclinations of satellites around oblate precessing planets. He shows that if the nodal period of the satellite is short compared to the planet's precession then the satellite will maintain a constant inclination to the planet's equator; a property that proves useful in our discussion below as we will neglect the solar tide causing the planet spin axis to precess as the precession rate of the planetary spin is much smaller than the precession of the solar orbit.

On the other hand, neglecting the oblateness perturbation, and considering only the external perturbation leaves us with a rich history of extensive studies in the so-called Kozai-Lidov regime. In 1961, the secular heirarchical triple systems were addressed by Lidov (4) when he studied the orbital evolution of artificial satellites perturbed by an axisymmetric outer potential. Shortly after that, Kozai (5) studied the effect of Jupiter on inclined asteroids in our solar system. In these cases, we have a Keplerian orbit in the inner binary, perturbed by a far companion on the outer binary. The dynamical behavior of this configuration is a result of the angular momentum exchange between the inner and outer binary. Both Lidov and Kozai found that the inner binary enters a regime of oscillation in both eccentricity and inclination on timescales much larger that the orbital period.

In other words, given the axisymmetric quadrupole approximation of the outer orbit, we have analytical solutions that describe, for an initial mutual inclination between the two binaries between $40°$ and $140°$, large amplitude oscillations between the inner orbit's eccentricity and inclination with respect to the outer orbit. These cycles of oscillation are well bounded by a maximum and a minimum that would limit the motion to a prograde or retrograde regime.

However, it was shown that relaxing the quadrupolar approximation and allowing for higher order terms, mainly the octupole, the eccentricity can reach extremely high values and the system is chaotic in general (6) (7). Moreover, the inclination is no more restricted to oscillate either in a prograde or a retrograde regime, but can flip orientation. This richer and exciting dynamical evolution was one of the factors encouraging us to consider the higher order terms.

4

In 1981, in a further study of the fairly inclined satellite Iapetus, the outermost regular moon of Saturn, Ward attempted to explain why this satellite is off the Laplace Surface (8). Iapetus has an eccentricity of 0.028 and an inclination of 7.5° to the Laplace Surface, and for that to happen something should have pumped its inclination.

Questioning the reason Iapetus maintains this constant inclination to its Laplace plane rather than lying in it, Ward explores the possibility that Iapetus' inclination to the Laplace plane is pumped during the formation process. In fact, upon study of the circumplanetary disk from which the satellites formed, the Laplace plane at the distance of Iapetus would vary during disk dispersal, and a rapid rotation of the plane could generate the specific inclination of Iapetus. Also, out of the possible scenarios for this mechanism, Ward suggests viscous interaction with the solar nebula, as the time scale required for it to accomplish this is comparable to the viscous evolution time-scale of a fully turbulent disk.

Figure 1.1: The orbit of the outermost regular satellite of Saturn. Image created using Celestia software.

The work in this thesis was mainly based on the study of the Laplace plane in 2009 by Tremaine, Touma and Namouni (TTN) (9). This work generalized the study of the Laplace plane, studying its properties, including the stability of it for the full range of obliquities of the planet, and extended the study to eccentric orbits.

TTN studied the classical Laplace plane in the same setting studied by Laplace i.e. an inner quadrupole provided by the planet's oblateness and an outer quadrupole provided by an external perturber, but in the case of the satellite of the Earth. The authors showed that Laplace equilibria exist for both circular and eccentric orbits.

For circular Laplace equilibria, the orbit angular momentum vector has three possible alignments, two of which lie in the principal plane formed by the spin axis of the planet and its orbital angular momentum vector. These two solutions differ by $\pi/2$, and are called the coplanar circular equilibira. One of them is always

Figure 1.2: The warped Classical Laplace Surface structure. This surface combines the local Laplace planes that lie between the planet's equatorial and orbital planes. These planes differ by the planet's obliquity. At the Laplace radius, shown as the thick blue ring, the Laplace plane lies halfway between the planet's equatorial and orbital planes (10).
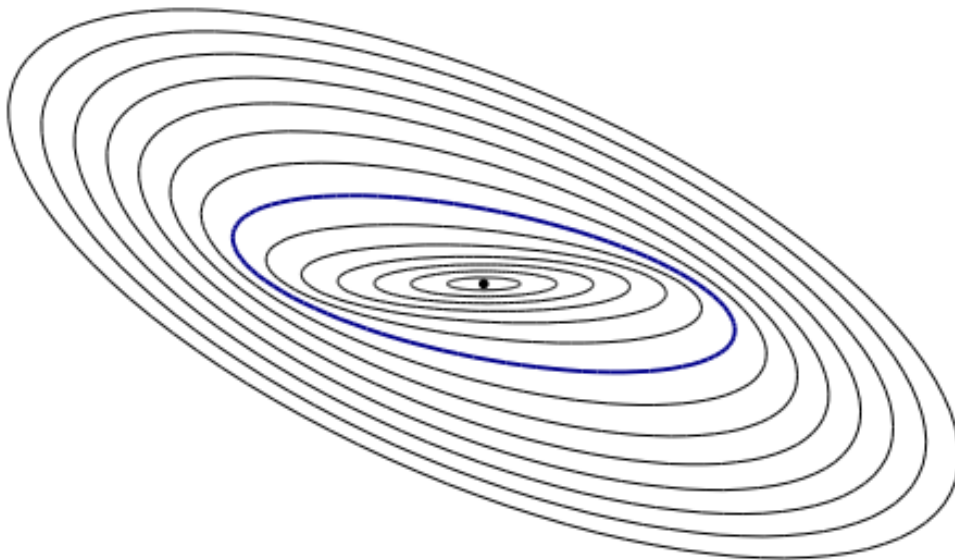
unstable, while the other is stable and described the so-called classical Laplace Surface. This warped surface carries the stable circular equilibria as a function of the semi-major axis. It coincides with the planet's equator at short distances and with its orbital plane at large distances. This warped structure is viewed in figure 1.2. One interesting result that TTN reached was that the stability of the classical Laplace Surface is dependent on the obliquity of the planet. In fact, these circular equilibira are only stable for planetary obliquity of $\phi_\odot < 68.875°$ (or greater than $\pi - 68.875°$) while when it exceeds that, there's a range of distances inside which the rings are rendered unstable.

The third circular Laplace equilbirium is polar, and the set of these orbits is only stable for semi-major axis less that $2^{-1/5}r_L$.

Upon further study, it turned out that in this coplanar-coplanar configuration, when the instability of the circular equilibria kicks in, they bifurcate into eccentric equilibiria. Also stable polar eccentric equilibira bifurcate from circular polar equilibira when they turn unstable at $a = 2^{-1/5}r_L$. The approach for TTN tackling the problem was secular, and a vectorial description of the setting was exploited. The secular description is justified as long as the precession period of the eccentricity and angular momentum vectors of the particle are much larger
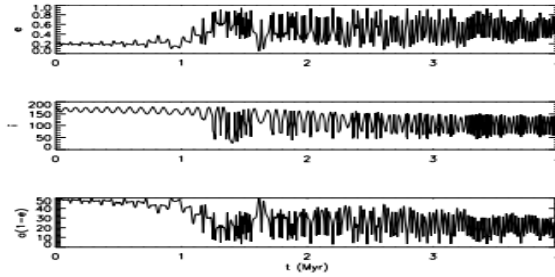
Figure 1.3: Orbital eccentricity (top panel), inclination (middle, in degrees) and pericenter distance (bottom, in planetary radii), plotted vs. time in Myr. The dust particle is slowly evolving inward, but then its dynamics become unstable and the orbital eccentricity and inclination vary chaotically (13).

than its orbital period. This secular approach has some limitations, of which is that it neglects in the regime studied in TTN evection resonance, when the precession rate in the apse due to planetary perturbation equals the mean motion of the planet around the sun. In our study we will use the secular theory bearing in mind these limitations and constraining our selves to ranges in parameter space where this approach is justifiable.

The implications of TTN were various and rich. The Laplace Surface is significant, because it does not only describe satellites around planets, but it also traces the shape of a thin gas of disk or dissipative rings surrounding a planet. The Laplace equilibrium plane provides a qualitative explanation for the overall shape and structure of planetary rings. The study of Laplace planes for planetary rings opens the possibility for warped rings (11).

One interesting application of the results of TTN was an attempt to explain why the regular satellites of Uranus have their hemispherical color asymmetries first detected in 1991 (12). Tamayo et al. in 2011 (13) addressed the following issue: If color assymetries are a result of infalling dust from nearby irregular satellites, why, for example in the Uranian system, the dichotomies in color is among all of the regular satellites, meaning dust has been distributed among all of them and wasn't concentrated on the outermost moon, Oberon, as in the Saturnian case of Iapetus. Based on TTN's results, Uranus' high obliquity (98°), means that it will allow for unstable laplace plane of the particles resulting in chaotic large amplitude variation in the orbit's eccentricity and inclination. This rapid variation in the orbit would allow to access all the regular satellites simultaneously, rather than in sequence. The authors did a numerical analysis for a particle around Uranus depicting the instability shown by TTN for high obliquities; illustration is shown in fig.1.3.

Recently, many studies were done yielding Laplace Planes' modifications. Tamayo et al. (14) generalized the study of TTN to three dimensions i.e. removed the scope of the study from the Laplace plane, and studied orbits inclined to the local Laplace plane. This allowed them to show that orbits with such inclinations are less stable, and the threshold of stability found by TTN is an upper limit because orbits off-Laplace-Plane can go unstable at lower obliquities and over a broader range of semi-major axes.

Other modifications of the Laplace plane were studied when orbits are relaxed from the gravitationally dominated regime and enter a regime of non-gravitational perturbations; radiation pressure for example. This is important in the case of dust grains, as dust grains have an important feature of inward migration by the Poynting-Robertson drag, which provides a natural mechanism for the particle to enter the unstable region. The authors of (14) and (10) found that radiation pressure in such cases can shift the unstable range of semimajor axes; specifically, for prograde(retrograde) orbits it is shifted inwards(outwards).

Of interest to us in this thesis is another attempt on modifying the classical Laplace Surface. We will also be attempting to solve for orbits in the test particle approximation, under perturbation theory. In the studies we've seen, the authors restricted perturbation in the outer tide to an orbit averaged quadrupolar order, where the outer binary's eccentricity, if non-negligible, enters as a parameter without changing the topology of equilibria and their stability. Keeping in mind that outer binaries in many astrophysical settings can be on eccentric orbits, our incentive was to generalize the work of TTN allowing the eccentricity of the outer binary to enter as a variable not only a parameter and alter the classical Laplace equilibria.

Chapter 2

Theoretical Background

2.1 The Hamiltonian Formalism

In all of our studied cases, we have test particles on *Keplerian* obits that are subject to two or more perturbations. So the Hamiltonian of our particle will be a sum of the Keplerian term with whatever perturbations we have. In this section, we start by defining these perturbations and modeling them mathematically.

2.1.1 The Non-Sphericity in the Inner Mass Distribution

As our studies are in the context of Laplace Surface variations, we will always have an inner perturbation that results from the non spherical mass distribution in the inner binary. This non-sphericity appears in two settings: the equatorial bulge contribution of an oblate planet (as in the Moon orbiting the Earth); or the added contribution of planets or satellites orbiting the inner object (as in the effect of the nearly coplanar giant planets orbiting the sun).

In general, the gravitational potential of a continuous body is (15):

$$\Phi(\mathbf{x}) = -G \int \frac{dm'}{\|\mathbf{x} - \mathbf{x}'\|} \tag{2.1}$$

where $dm' = dm(\mathbf{x}', t)$ is an infinitesimal mass element at point $\mathbf{x}'$, and G is the gravitational constant. For spherically symmetric bodies, this integral is easy to evaluate: We choose the origin at the body's center of mass and indicate this by writing $\mathbf{r}$ and $\mathbf{r}'$ instead of $\mathbf{x}$ and $\mathbf{x}'$. And here symmetry implies that mass density is only of radial dependence. Thus, $dm' = \rho(\mathbf{r}')\mathbf{r}'^2 dr' d\Omega$ where $d\Omega$ is the element of solid angle, Thus,

$$\Phi(\mathbf{r}) = -G \int \frac{dm'}{\|\mathbf{r} - \mathbf{r}'\|} = -G \int_0^R \rho' \mathbf{r}'^2 dr' \oint \frac{d\Omega}{\|\mathbf{r} - \mathbf{r}'\|} \tag{2.2}$$

For $r = \|\mathbf{r}\| > r' = \|\mathbf{r}'\|$

$$\oint \frac{d\Omega}{\|\mathbf{r} - \mathbf{r}'\|} = 2\pi \int_0^\pi \frac{\sin\theta d\theta}{[r^2 + r'^2 - 2rr'\cos\theta]^{\frac{1}{2}}} = \frac{4\pi}{r} \qquad (2.3)$$

and the remaining of the integral gives the total mass of the body M. Therefore, the external gravitational potential of a spherically symmetric body is given by:

$$\Phi(\mathbf{r}) = -G \int \frac{dm'}{\|\mathbf{r} - \mathbf{r}'\|} = -\frac{GM}{r} \qquad (2.4)$$

For deviations from spherical symmetry, we expand the potential of a given body in a Taylor series about the center of mass:

$$\frac{1}{\|\mathbf{r} - \mathbf{r}'\|} = \frac{1}{r}[1 + \frac{P_1(\mathbf{rr}')}{r^2} + \frac{P_2(\mathbf{rr}')}{r^4} + ...] \qquad (2.5)$$

$$= \frac{1}{r}[1 + \sum_{n=1}^\infty (\frac{r'}{r})^n P_n(\mathbf{rr}')] \qquad (2.6)$$

where P_n are the Legendre Polynomials, and the expansion of the potential becomes

$$\Phi(\mathbf{r}) = \frac{-G}{r}[M + \frac{1}{r^2}\int P_1(\mathbf{rr}')dm' + \frac{1}{r^4}\int P_2(\mathbf{rr}')dm' + ...] \qquad (2.7)$$

now since the center of the mass is at the origin, P_1 term cancels. We define the inertia tensor ϱ of the body as

$$\varrho_{\mathbf{r}} = \int dm'\mathbf{r}'\mathbf{r}' \wedge \mathbf{r} = \int dm'(r'^2\mathbf{r} - \mathbf{r}'\mathbf{r}' \cdot \mathbf{r}) \qquad (2.8)$$

and the trace of the inertia tensor is the sum of the principal moments of inertia I_1 I_2 I_3, Therefore,

$$\int dm' P_2(\mathbf{rr}') = \int dm'\frac{1}{2}[3(\mathbf{r} \cdot \mathbf{r}')^2 - r^2\mathbf{r}'^2] \qquad (2.9)$$

$$= \frac{1}{2}[r^2 Tr(\varrho) - 3\mathbf{r} \cdot \varrho] \qquad (2.10)$$

$$= \frac{1}{2}\mathbf{r} \cdot \mathbf{Q_r} \qquad (2.11)$$

where we have defined the symmetric tensor $\mathbf{Q_r}$ as

$$\mathbf{Q_r} = \mathbf{r}Tr(\varrho) - 3\varrho \qquad (2.12)$$

In analogy to the electromagnetic terminology, we may refer to $\mathbf{Q_r}$ as the gravitational quadrupole tensor.

The expanded potential can now be written as a *harmonic (multipole) expansion*:

$$\Phi(\mathbf{r}) = \frac{-G}{r}[M + \frac{1}{2}\frac{\mathbf{r} \cdot \mathbf{Q_r}}{r^4} + ...] \tag{2.13}$$

Knowing the inertia tensor of an axisymmetric body with symmetry axis unit vetor $\hat{\boldsymbol{n}}_{\boldsymbol{p}}$ as

$$\varrho_{\mathbf{r}} = I_1\mathbf{r} + (I_3 - I_1)\mathbf{r} \cdot \hat{\boldsymbol{n}}_{\boldsymbol{p}}\hat{\boldsymbol{n}}_{\boldsymbol{p}} \tag{2.14}$$

we can get our symmetric tensor as:

$$\mathbf{Q_r} = (I_3 - I_1)(\mathbf{r} - 3\mathbf{r} \cdot \hat{\boldsymbol{u}}\hat{\boldsymbol{n}}_{\boldsymbol{p}}) \tag{2.15}$$

If we define a dimensionless measure of the oblateness of the body as

$$J_2 = \frac{I_3 - I_1}{MR^2} \tag{2.16}$$

R being the radius of the planet, then the series (6) integrates to a harmonic expansion for the potential with the form:

$$\Phi(\mathbf{r}) = \frac{-GM}{r}\left[1 - \sum_{n=2}^{\infty} J_n \left(\frac{R}{r}\right)^n P_n(\hat{\boldsymbol{r}}\hat{\boldsymbol{n}}_{\boldsymbol{p}})\right] \tag{2.17}$$

Thus the quadrupole term arising from oblateness is:

$$\Phi_p(\mathbf{r}) = \frac{GM}{r^3}R^2 J_2 P_2(\hat{\boldsymbol{r}}\hat{\boldsymbol{n}}_{\boldsymbol{p}}) \tag{2.18}$$

$$= \frac{GMR^2 J_2}{2r^5}\left[3(\mathbf{r} \cdot \hat{\boldsymbol{n}}_{\boldsymbol{p}})^2 - r^2\right] \tag{2.19}$$

This correction to the gravitational potential will be used to account for the oblateness of earth. However, it can be analogously used to account for the contribution of the nearly-coplanar giant planets around the sun by defining:

$$J_2'R^2 = J_2R^2 + \frac{1}{2}\sum_{i=1}^{n}\frac{a_i^2 m_i}{M} \tag{2.20}$$

where the contribution of the oblateness of the sun (16) is negligible compared to the contribution of the giant planets.

2.1.2 External Gravitational Perturbation

Now we move to account for the contribution of an outer perturber on our particle's orbit. This external perturber is identified as the sun in the (Moon-Earth-Sun) system, and as the suggested Planet IX in the study of eTNOs. In general, for $\mathbf{r}, \mathbf{r}'$ being the radii of the inner and outer binaries respectively, the potential of the coupling interaction between the binaries is:

$$\Phi_{ep}(\mathbf{r}, \mathbf{r}') = \frac{-GM_{ep}}{\|\mathbf{r} - \mathbf{r}\|} \tag{2.21}$$

It is proved advantageous to expand the inverse of the separation in terms of r/r' by means of the generating function of the Legendre polynomials:

$$\frac{1}{\|\mathbf{r} - \mathbf{r}'\|} = \frac{1}{r'} \sum_{k=0}^{\infty} \left(\frac{r}{r'}\right)^k P_k(\cos \gamma) \tag{2.22}$$

$$= \frac{1}{r'} \left[1 + \frac{r}{r'} \cos \gamma + \left(\frac{r}{r'}\right)^2 \frac{1}{2} \left(3\cos^2 \gamma - 1\right) + \left(\frac{r}{r'}\right)^3 \frac{1}{2} \left(5\cos^3 \gamma - 3\cos \gamma\right) + \ldots \right] \tag{2.23}$$

Where P_k is the kth Legendre polynomial, and γ is the angle between r and r' such that:

$$\cos \gamma = \frac{\mathbf{r} \cdot \mathbf{r}'}{rr'} \tag{2.24}$$

This allows us to write:

$$\Phi_{ep}(\mathbf{r}, \mathbf{r}') = \frac{-GM_{ep}}{r'} \left[1 + \frac{\mathbf{r} \cdot \mathbf{r}'}{r'^2} - \frac{r^2}{2r'^2} + \frac{3(\mathbf{r} \cdot \mathbf{r}')^2}{2r'^4} + \frac{5}{2} \frac{(\mathbf{r} \cdot \mathbf{r}')^3}{r'^6} - \frac{3}{2} \frac{\mathbf{r} \cdot \mathbf{r}'}{r'^4} r^2 + \ldots \right] \tag{2.25}$$

The first term term is independent of the dynamical variable of the particle $\mathbf{r}$. The second term will cancel out upon averaging in the secular approach next. So the first contributing terms will be the quadrupole (second order in r), and the octupole (third order in r).

2.2 Geometry of Keplerian Orbits

For a test particle in a Keplerian orbit around a spherically symmetric object, energy E and angular momentum $\mathbf{L}$ are conserved and are given by(17):

$$E = -\frac{GM}{2a} \tag{2.26}$$

$$\|\mathbf{L}\| = \left[GMa(1 - e^2)\right]^{\frac{1}{2}} \tag{2.27}$$

M being the mass of the orbited object, a the semi-major axis of the orbit, e the eccentricity. However, for an oblate spheroid, total $\mathbf{L}$ is not conserved, but rather its z-component L_z:

$$L_z = \left[GMa(1 - e^2)^{\frac{1}{2}} cos(i)\right] \tag{2.28}$$

i being the inclination of the orbit.

Using a vecotrial formulation, we define a coordinate system whose equatorial plane lies in the orbital plane of the test particle. Define (9):

$\hat{\boldsymbol{n}}$ as the direction of the particle's angular momentum vector

$\hat{\boldsymbol{u}}$ as the direction towards the pericenter

$\hat{\boldsymbol{v}}$ as the direction of $\hat{\boldsymbol{n}} \times \hat{\boldsymbol{u}}$.

Introducing polar coordinates (r, ϕ) in the orbital plane, r being the radius, and ϕ the *true anomaly*, then the orbital equation is given by (17):

$$r = \frac{a(1 - e^2)}{1 + e \cos\phi} \tag{2.29}$$

$$\mathbf{r} = r\cos\phi\hat{\boldsymbol{u}} + r\sin\phi\hat{\boldsymbol{v}} \tag{2.30}$$

or in terms of the *eccentric anomaly E*:

$$r = a(1 - e\cos E) \tag{2.31}$$

with

$$\cos\phi = \frac{\cos E - e}{1 - e\cos E} \tag{2.32}$$

Keplerian Elements

We know that the trajectories in the bounded two-body problem are ellipses, and by *Kepler's* equation, we can obtain the position of the considered body along its ellipse as a function of time i.e. in cartesian coordinates: $(r(\phi)\cos\phi, r(\phi)\sin\phi, 0)$. However, it's more useful in practice to describe it in an arbitrarily oriented reference frame, and the passage from the two coordinate systems having the same origin would be through rotation, decomposed into three elementary rotations.

Several combinations of rotations are used in celestial mechanics, the most common corresponds to the 3-1-3 combination. In the arbitrarily oriented reference frame, the position of the body is given by:

$$\mathbf{r} = R_3(\Omega)R_1(i)R_3(\omega) \begin{pmatrix} r(\phi)\cos\phi \\ r(\phi)\cos\phi \\ 0 \end{pmatrix} \tag{2.33}$$

where Ω, ω, and i correspond the longitude of the ascending node, the argument of the pericenter, and the inclination of the orbit. By computing explicitly the products of the three rotation matrices, we obtain:

$$\mathbf{r} = r(\phi) \begin{pmatrix} \cos(\omega+\phi)\cos\Omega - \sin(\omega+\phi)\sin\Omega\cos i \\ \cos(\omega+\phi)\sin\Omega + \sin(\omega+\phi)\cos\Omega\cos i \\ \sin(\omega+\phi)\sin i \end{pmatrix} \tag{2.34}$$

Hence we can describe the orbit of the particle by these traditional orbital elements in the barycentric reference frame in which the orbited object lies on one of the focii of the ellipse. Two parameters describe the shape of the ellipse: the semi-major axis (a), and the eccentricity (e). One element gives the position of the particle on the ellipse: the true anomaly (ϕ); while three angles represent the position of the ellipse in a three-dimensional reference frame centred on O (the inclination i, the longitude of ascending node Ω and the argument of pericenter ω).

2.3 Secular Theory

In many problems in celestial mechanics, the variation of orbital elements is slow compared to the orbital period, and because we're neglecting spin-orbit and orbit-orbit resonances, we seek the non-resonant long term evolution of the orbit by neglecting dynamics that happen on shorter timescales. This can be done by averaging our dynamical quantities over the orbital period of the particle. The purpose of this time smoothing procedure is to get rid of the oscillations of the fast varying angle, which is the angle representing the position of the particle in the ellipse. By doing so, we have turned our particle into a ring of mass element proportional to the time spent by the particle in it. In other words, the goal of secular theory is not to describe the motion of the particle on its orbit, but to describe the deformation and the rotation of the orbit itself. Naturally, that kind of description is only possible if the particle follows indeed a slowly deforming Keplerian orbit, that is without catastrophic close encounters or other chaotic phenomena.

The averaging over short times scales as we said is based on eliminating the angles describing the the position of the particle in the ellipse. This can be done via a canonical transformation known as the Von Zeipel transformation (18). In this canonical transformation, a time independent generating function is defined to be periodic in the mean anomalies, allowing the elimination of the short-period terms in the Hamiltonian. Thus we produce a Hamiltonian that is cyclic in these angles, rendering their conjugate momenta conserved, and their conjugate momenta are functions of the semi-major axis, hence in secular description, we are conserving the semi-major axis of the orbit. This would be analogous to averaging whatever quantities we need over orbital periods by saying:

$$\big\langle \Phi(\mathbf{r}) \big\rangle = \frac{1}{P} \int_0^P dt \Phi\big(\mathbf{r}(t)\big) \tag{2.35}$$

where P is the orbital period defined by

$$P = 2\pi \frac{a^{\frac{3}{2}}}{\sqrt{GM}} \tag{2.36}$$

Using the angular momentum definition, and differentiating Kepler's equation, we can get the following differential relations:

$$\frac{dt}{P} = \frac{r dE}{2\pi a} = \frac{r^2 d\phi}{2\pi a b} = \frac{dM}{2\pi} \tag{2.37}$$

where b is the pericenter distance, E is the eccentric anomaly, and M is the mean anomaly. We proceed now to construct out secular Hamiltonian by averaging the perturbations we discussed earlier.

15

The Inner Quadrupole

The inner quadrupole presented in 2.18 can now be averaged:

$$\langle \Phi_p(\mathbf{r}, \phi) \rangle = \frac{GMJ_2R^2}{2}\left[3(\hat{\boldsymbol{u}} \cdot \hat{\boldsymbol{n}}_{\boldsymbol{p}})^2 \langle \frac{\cos^2 \phi}{r^3} \rangle + 3(\hat{\boldsymbol{v}} \cdot \hat{\boldsymbol{n}}_{\boldsymbol{p}})^2 \langle \frac{\sin^2 \phi}{r^3} \rangle \right.$$

$$\left. + 6(\hat{\boldsymbol{u}} \cdot \hat{\boldsymbol{n}}_{\boldsymbol{p}})(\hat{\boldsymbol{v}} \cdot \hat{\boldsymbol{n}}_{\boldsymbol{p}}) \langle \frac{\cos\phi \sin\phi}{r^3} \rangle - \langle \frac{1}{r^3} \rangle \right] \qquad (2.38)$$

and we find:

$$\langle \frac{\cos^2 \phi}{r^3} \rangle = \langle \frac{\sin^2 \phi}{r^3} \rangle = \frac{1}{2a^3(1-e^2)^{\frac{3}{2}}} \qquad (2.39)$$

$$\langle \frac{1}{r^3} \rangle = \frac{1}{a^3(1-e^2)^{\frac{3}{2}}} \qquad (2.40)$$

$$(2.41)$$

Hence we get

$$\langle \Phi_p \rangle = \frac{GMJ_2'R^2}{4a^3(1-e^2)^{\frac{5}{2}}}\left[1 - e^2 - 3(\mathbf{j} \cdot \hat{\boldsymbol{n}}_{\boldsymbol{p}})^2 \right] \qquad (2.42)$$

This shall be used to describe the perturbation of the oblateness of the earth, where $\hat{\boldsymbol{n}}_{\boldsymbol{p}}$ is the spin axis of the Earth, and analogously, the perturbation due to the massive planets, where $\hat{\boldsymbol{n}}_{\boldsymbol{p}}$ in that case would represent the direction of the total angular momentum of the solar system.

The Outer Quadrupole

The gravitational perturbation, arising from the external perturber of mass M_{ep}, presented in 2.25 can be truncated at the order convenient for the analysis. We start by the quadrupolar order given by:

$$\Phi_{quad}(\mathbf{r}, \mathbf{r}') = \frac{-GM_{ep}}{r'}\left[1 + \frac{\mathbf{r} \cdot \mathbf{r}'}{r'^2} - \frac{r^2}{2r'^2} + \frac{3(\mathbf{r} \cdot \mathbf{r}')^2}{2r'^4} \right] \qquad (2.43)$$

Th first term is dropped because is does not depend on our variable, while we drop the second because it averages to zero.

$$\Phi_{quad}(\mathbf{r}, \mathbf{r}') = \frac{-GM_{ep}}{r'}\left[-\frac{r^2}{2r'^2} + 3\left(r^2 \frac{(\cos\phi\hat{\boldsymbol{u}} + \sin\phi\hat{\boldsymbol{v}}) \cdot \mathbf{r}')^2}{2r'^4} \right] \qquad (2.44)$$

hence the averaged potential would be

$$\left\langle \Phi_{quad}(\mathbf{r}, \mathbf{r}') \right\rangle = \frac{GM_{ep}}{2r'^3}\left[\langle r^2 \rangle - \frac{3}{r'^2}\langle r^2 \cos^2\phi \rangle (\hat{\boldsymbol{u}} \cdot \mathbf{r}')^2 - \frac{3}{r'^2}\langle r^2 \sin^2\phi \rangle (\hat{\boldsymbol{v}} \cdot \mathbf{r}')^2 \right.$$

$$\left. - \frac{6}{2r'^4}\langle r^2 \sin\phi \cos\phi \rangle (\hat{\boldsymbol{v}} \cdot \mathbf{r}')(\hat{\boldsymbol{u}} \cdot \mathbf{r}') \right] \qquad (2.45)$$

16

Choosing to average these quantities over the orbit using either the eccentric or the true anomlay, with the appropriate differential defined in 2.37 and using the appropriate orbital equation, we find the follwoing:

$$\langle r^2 \rangle = \frac{a^2}{2}(2 + 3e^2) \qquad\qquad \langle r^2 \cos^2 \phi \rangle = \frac{a^2}{2}(1 + 4e^2) \tag{2.46}$$

$$\langle r^2 \sin^2 \phi \rangle = \frac{a^2}{2}(1 - e^2) \qquad\qquad \langle r^2 \sin\phi \cos\phi \rangle = 0 \tag{2.47}$$

Now set the angular momentum and eccentricity vectors (9):

$$\mathbf{j} = \sqrt{(1 - e^2)}\mathbf{n} \tag{2.48}$$

$$\mathbf{e} = e\hat{\boldsymbol{u}} \tag{2.49}$$

and eliminate the $(\hat{\boldsymbol{v}} \cdot \mathbf{r}')$ terms using

$$r'^2 = (\hat{\boldsymbol{v}} \cdot \mathbf{r}')^2 + (\hat{\boldsymbol{u}} \cdot \mathbf{r}')^2 + (\hat{\boldsymbol{n}} \cdot \mathbf{r}')^2 \tag{2.50}$$

to get

$$\left\langle \Phi_{quad}(\mathbf{r}, \mathbf{r}') \right\rangle = \frac{GM_{ep}a^2}{4r'^3}\left[-1 + 6e^2 - 15\frac{(\mathbf{e} \cdot \mathbf{r}')^2}{r'^2} + 3\frac{(\mathbf{j} \cdot \mathbf{r}')^2}{r'^2} \right] \tag{2.51}$$

Now to average over the outer orbit, assuming the inner quantities are fixed, introduce the outer semi-major axis, eccentricity, and reference triad: $a_\odot$, $e_\odot$, $\hat{\boldsymbol{n}}_\odot$, $\hat{\boldsymbol{u}}_\odot$, $\hat{\boldsymbol{v}}_\odot$, thus:

$$\left\langle\left\langle \Phi_{quad}(\mathbf{r}') \right\rangle\right\rangle = \frac{GM_{ep}a^2}{4}\left[\left\langle \frac{-1}{r'^3} \right\rangle + \left\langle \frac{6e^2}{r'^3} \right\rangle - 15\left\langle \frac{(\mathbf{e} \cdot \mathbf{r}')^2}{r'^5} \right\rangle + 3\left\langle \frac{(\mathbf{j} \cdot \mathbf{r}')^2}{r'^5} \right\rangle \right] \tag{2.52}$$

and we find:

$$\left\langle \frac{1}{r'^3} \right\rangle = \frac{1}{a_\odot^3(1 - e_\odot^2)^{\frac{3}{2}}} \tag{2.53}$$

$$\left\langle \frac{(\mathbf{k} \cdot \mathbf{r}')^2}{r'^5} \right\rangle = \frac{1}{2a_\odot^3(1 - e_\odot^2)^{\frac{3}{2}}}(k^2 - (\mathbf{k} \cdot \hat{\boldsymbol{n}}_\odot)^2) \tag{2.54}$$

Thus we get

$$\left\langle\left\langle \Phi_{quad} \right\rangle\right\rangle = \frac{3GM_{ep}a^2}{4a_\odot^3(1 - e_\odot^2)^{\frac{3}{2}}}\left[\frac{1}{3} - 2e^2 + 5(\mathbf{e} \cdot \hat{\boldsymbol{n}}_\odot)^2 - (\mathbf{j} \cdot \hat{\boldsymbol{n}}_\odot)^2 \right] \tag{2.55}$$

Obviously this quadrupole is a symmetric modelling of the interaction potential. It is invariant under apse orientation variation in the outer orbit if the orbit itself is non-symmetric i.e. eccentric.

Introducing the Outer Octupole

Back to equation 2.25, we now choose to handle the order cubic in the inner radius, thus we trancate the following, resembling the octupolar order:

$$\frac{-GM_{ep}}{r'}\frac{1}{2}\left(5\frac{(\mathbf{r}\cdot\mathbf{r}')^3}{r'^6}-3\frac{(\mathbf{r}\cdot\mathbf{r}')}{r'^4}r^2\right) \tag{2.56}$$

hence if averaged becomes:

$$\left\langle\Phi_{oct}(\mathbf{r},\phi)\right\rangle = \frac{-GM_{ep}}{2r'}\left[\frac{5}{r'^6}\left(\langle r^3\cos^3\phi\rangle(\hat{\boldsymbol{u}}\cdot\mathbf{r}')^3+3\langle r^3\cos^2\phi\sin\phi\rangle(\hat{\boldsymbol{u}}\cdot\mathbf{r}')^2(\hat{\boldsymbol{v}}\cdot\mathbf{r}')\right.\right.$$

$$\left.+\langle r^3\sin^3\phi\rangle(\hat{\boldsymbol{v}}\cdot\mathbf{r}')^3+3\langle r^3\sin^2\phi\cos\phi\rangle(\hat{\boldsymbol{u}}\cdot\mathbf{r}')(\hat{\boldsymbol{v}}\cdot\mathbf{r}')^2\right)$$

$$\left.-\frac{3}{r'}\left(\langle r^3\cos\phi\rangle(\hat{\boldsymbol{u}}\cdot\mathbf{r}')+\langle r^3\sin\phi\rangle(\hat{\boldsymbol{v}}\cdot\mathbf{r}')\right)\right] \tag{2.57}$$

Thus we get the following:

$$\langle r^3\cos^3\phi\rangle = \frac{a^3}{2}(-5e^3-\frac{15}{4}e) \tag{2.58}$$

$$\langle r^3\sin^3\phi\rangle = 0 \tag{2.59}$$

$$\langle r^3\cos\phi\rangle = \frac{5a^3}{2}[-3\frac{e^3}{4}-e] \tag{2.60}$$

$$\langle r^3\sin\phi\rangle = 0 \tag{2.61}$$

$$\langle r^3\sin^2\phi\cos\phi\rangle = \frac{-5a^3}{8}e(1-e^2) \tag{2.62}$$

$$\langle r^3\cos^2\phi\sin\phi\rangle = 0 \tag{2.63}$$

plugging these quantities in we get:

$$\left\langle\Phi_{oct}(\mathbf{r}')\right\rangle = \frac{-5GM_{ep}a^3}{16r'^5}\left[-35\frac{(\mathbf{e}\cdot\mathbf{r}')^3}{r'^2}+3(8e^2-1)(\mathbf{e}\cdot\mathbf{r}')+15\frac{(\mathbf{e}\cdot\mathbf{r}')(\mathbf{j}\cdot\mathbf{r}')^2}{r'^2}\right] \tag{2.64}$$

Now double averaging over the outer orbit:

$$\left\langle\left\langle\Phi_{oct}(\mathbf{r}')\right\rangle\right\rangle = \frac{-5GM_{ep}a^3}{16}\left[-35\left\langle\frac{(\mathbf{e}\cdot\mathbf{r}')^3}{r'^7}\right\rangle+3(8e^2-1)\left\langle\frac{(\mathbf{e}\cdot\mathbf{r}')}{r'^5}\right\rangle+15\left\langle\frac{(\mathbf{e}\cdot\mathbf{r}')(\mathbf{j}\cdot\mathbf{r}')^2}{r'^7}\right\rangle\right] \tag{2.65}$$

Computing these we get:

$$\left\langle\frac{(\mathbf{e}\cdot\mathbf{r}')^3}{r'^7}\right\rangle = \frac{3e_\odot}{4a_\odot^4(1-e_\odot)^{\frac{5}{2}}}\left[e^2(\mathbf{e}\cdot\hat{\boldsymbol{u}}_\odot)-(\mathbf{e}\cdot\hat{\boldsymbol{u}}_\odot)(\mathbf{e}\cdot\hat{\boldsymbol{n}}_\odot)^2\right] \tag{2.66}$$

$$\left\langle \frac{(\mathbf{e} \cdot \mathbf{r'})(\mathbf{j} \cdot \mathbf{r'})^2}{r'^7} \right\rangle = \frac{e_\odot}{4a_\odot^4(1 - e_\odot)^{\frac{5}{2}}} \Big[3(\mathbf{e} \cdot \hat{\boldsymbol{u}}_\odot)(\mathbf{j} \cdot \hat{\boldsymbol{u}}_\odot)^2 + 3(\mathbf{e} \cdot \hat{\boldsymbol{u}}_\odot)(\mathbf{e} \cdot \hat{\boldsymbol{v}}_\odot)^2$$

$$+ 2(\mathbf{e} \cdot \hat{\boldsymbol{v}}_\odot)(\mathbf{j} \cdot \hat{\boldsymbol{v}}_\odot)(\mathbf{j} \cdot \hat{\boldsymbol{u}}_\odot) \Big] \quad (2.67)$$

$$\left\langle \frac{(\mathbf{e} \cdot \mathbf{r'})}{r'^5} \right\rangle = \frac{e_\odot}{4a_\odot^4(1 - e_\odot)^{\frac{5}{2}}}(\mathbf{e} \cdot \hat{\boldsymbol{u}}_\odot) \quad (2.68)$$

Plugging these in we get:

$$\langle\langle \Phi_{oct} \rangle\rangle = \frac{15 G M_{ep} a^3 e_\odot}{64 a_\odot^4 (1 - e_\odot)^{\frac{3}{2}} (1 - e_\odot^2)} \Big[(\mathbf{e} \cdot \hat{\boldsymbol{u}}_\odot)\Big(8e^2 - 1 - 35(\mathbf{e} \cdot \hat{\boldsymbol{n}}_\odot)^2 + 5(\mathbf{j} \cdot \hat{\boldsymbol{n}}_\odot)^2 \Big)$$

$$+ 10(\mathbf{j} \cdot \hat{\boldsymbol{u}}_\odot)(\mathbf{j} \cdot \hat{\boldsymbol{n}}_\odot)(\mathbf{e} \cdot \hat{\boldsymbol{n}}_\odot) \Big] \quad (2.69)$$

Now define (9):

$$\varepsilon_\odot = \frac{M_{ep} a^3}{M a_\odot^3 (1 - e_\odot^2)^{\frac{3}{2}}} \quad (2.70)$$

$$\varepsilon_p = \frac{J_2' R^2}{a^2} \quad (2.71)$$

and we add here:

$$\varepsilon_\otimes = \frac{e_\odot}{1 - e_\odot^2} \frac{a}{a_\odot} \quad (2.72)$$

We can non-dimensionalize our potentials multiplying each by a factor of $\frac{a}{GM}$ to get:

$$\Psi_p = \frac{\varepsilon_p}{4(1 - e^2)^{\frac{5}{2}}} \Big[1 - e^2 - 3(\hat{\boldsymbol{n}}_p \cdot \mathbf{j})^2 \Big] \quad (2.73)$$

$$\Psi_{quad} = \frac{3\varepsilon_\odot}{8} \Big[\frac{1}{3} - 2e^2 + 5(\mathbf{e} \cdot \hat{\boldsymbol{n}}_\odot)^2 - (\mathbf{j} \cdot \hat{\boldsymbol{n}}_\odot)^2 \Big] \quad (2.74)$$

$$\Psi_{oct} = \frac{15}{64} \varepsilon_\odot \varepsilon_\otimes \Big[(\mathbf{e} \cdot \hat{\boldsymbol{u}}_\odot)\big(8e^2 - 1 - 35(\mathbf{e} \cdot \hat{\boldsymbol{n}}_\odot)^2 + 5(\mathbf{j} \cdot \hat{\boldsymbol{n}}_\odot)^2 \big)$$

$$+ 10(\mathbf{j} \cdot \hat{\boldsymbol{u}}_\odot)(\mathbf{j} \cdot \hat{\boldsymbol{n}}_\odot)(\mathbf{e} \cdot \hat{\boldsymbol{n}}_\odot) \Big] \quad (2.75)$$

The breaking of symmetry by the octupole is obvious. Now the Hamiltonian and consequently the dynamical equations of motion will attribute dependence on the orientation of the outer orbit given that it's axisymmetric. The added $(\mathbf{e} \cdot \hat{\boldsymbol{u}}_\odot)$ and $(\mathbf{j} \cdot \hat{\boldsymbol{u}}_\odot)$ components are dependent on the orientation of the pericenter of the outer orbit. That's some added complexity, but it is necessary to fully describe the problem. By this we can write the total Hamiltonian as the sum of the Keplerian part and the added perturbations, namely:

$$H = -\frac{GM}{2a} + \frac{GM}{a}(\Psi_p + \Psi_{quad} + \Psi_{oct}) \quad (2.76)$$

19

2.4 Dynamical Analysis

2.4.1 Equations of Motion

For a set of canonical variables (q,p) the total time derivative of some functions of the canonical variables and time $f_i(q, p, t)$ is (19):

$$\frac{df_i}{dt} = [u, H] + \frac{\partial f_i}{\partial t} \tag{2.77}$$

where $[u, H]$ is the usual poisson bracket. If H is expressed as a $H = H(f_i(q, p, t))$ then:

$$\frac{\partial H}{\partial q} = \frac{\partial H}{\partial f_i} \frac{\partial f_i}{\partial q} \tag{2.78}$$

$$\frac{\partial H}{\partial p} = \frac{\partial H}{\partial f_i} \frac{\partial f_i}{\partial p} \tag{2.79}$$

Hence we can get the equations for the variations of f_i in the form(20):

$$\dot{f} = [f, f_i] \frac{\partial H}{\partial f_i} + \frac{\partial f_i}{\partial t} \tag{2.80}$$

Thus in our system, we have for $f_i = \mathbf{e}, \mathbf{j}$:

$$\frac{d\mathbf{j}}{dt} = [\mathbf{j}, \mathbf{j}] \nabla_{\mathbf{j}} H + [\mathbf{j}, \mathbf{e}] \nabla_{\mathbf{e}} H \tag{2.81}$$

$$\frac{d\mathbf{e}}{dt} = [\mathbf{e}, \mathbf{j}] \nabla_{\mathbf{j}} H + [\mathbf{e}, \mathbf{e}] \nabla_{\mathbf{e}} H \tag{2.82}$$

so after finding the poisson brackets to be:

$$[\mathbf{j}, \mathbf{j}] = -\frac{1}{\sqrt{GMa}} \mathbf{j} \tag{2.83}$$

$$[\mathbf{j}, \mathbf{e}] = -\frac{1}{\sqrt{GMa}} \mathbf{e} \tag{2.84}$$

$$[\mathbf{e}, \mathbf{e}] = -\frac{1}{\sqrt{GMa}} \mathbf{j} \tag{2.85}$$

we find the equations of motion to be:

$$\frac{d\mathbf{j}}{dt} = -\frac{1}{\sqrt{GMa}} (\mathbf{j} \times \nabla_{\mathbf{j}} H + \mathbf{e} \times \nabla_{\mathbf{e}} H) \tag{2.86}$$

$$\frac{d\mathbf{e}}{dt} = -\frac{1}{\sqrt{GMa}} (\mathbf{e} \times \nabla_{\mathbf{j}} H + \mathbf{j} \times \nabla_{\mathbf{e}} H) \tag{2.87}$$

We defined the Hamiltonian of our system earlier as the sum of the Keplerian term with the inner quadrupole and the outer potential, namely:

$$H = H_k + \langle\langle \Phi_p \rangle\rangle + \langle\langle \Phi_{quad} \rangle\rangle + \langle\langle \Phi_{oct} \rangle\rangle \tag{2.88}$$

where the Keplerian contribution vanishes because $\mathbf{e}$ and $\mathbf{j}$ are constants in it, and with τ defined as:

$$\tau = \sqrt{\frac{GM}{a^3}} t; \tag{2.89}$$

So for $H = \Psi = \Psi_p + \Psi_{quad} + \Psi_{oct}$

$$\frac{d\mathbf{j}}{d\tau} = -\mathbf{j} \times \nabla_{\mathbf{j}}\Psi - \mathbf{e} \times \nabla_{\mathbf{e}}\Psi \tag{2.90}$$

$$\frac{d\mathbf{e}}{d\tau} = -\mathbf{e} \times \nabla_{\mathbf{j}}\Psi - \mathbf{j} \times \nabla_{\mathbf{e}}\Psi \tag{2.91}$$

and we compute the gradients:

$$\nabla_{\mathbf{j}}\Psi = -\frac{3}{2}\frac{\varepsilon_p}{(1-e^2)^{\frac{5}{2}}}(\mathbf{j} \cdot \hat{\boldsymbol{n}}_{\boldsymbol{p}})\hat{\boldsymbol{n}}_{\boldsymbol{p}} - \frac{3}{4}\varepsilon_{\odot}(\mathbf{j} \cdot \hat{\boldsymbol{n}}_{\odot})\hat{\boldsymbol{n}}_{\odot} + \frac{75}{32}\varepsilon_{\odot}\varepsilon_{\otimes}(\mathbf{e} \cdot \hat{\boldsymbol{u}}_{\odot})(\mathbf{j} \cdot \hat{\boldsymbol{n}}_{\odot})\hat{\boldsymbol{n}}_{\odot}$$

$$+ \frac{75}{32}\varepsilon_{\odot}\varepsilon_{\otimes}(\mathbf{e} \cdot \hat{\boldsymbol{n}}_{\odot})(\mathbf{j} \cdot \hat{\boldsymbol{u}}_{\odot})\hat{\boldsymbol{n}}_{\odot} + \frac{75}{32}\varepsilon_{\odot}\varepsilon_{\otimes}(\mathbf{e} \cdot \hat{\boldsymbol{n}}_{\odot})(\mathbf{j} \cdot \hat{\boldsymbol{n}}_{\odot})\hat{\boldsymbol{u}}_{\odot} \tag{2.92}$$

$$\nabla_{\mathbf{e}}\Psi = \frac{3}{2}\varepsilon_p \frac{\mathbf{e}}{(1-e^2)^{\frac{5}{2}}} - \frac{15}{4}\varepsilon_p \frac{(\mathbf{j} \cdot \hat{\boldsymbol{n}}_{\boldsymbol{p}})^2}{(1-e^2)^{\frac{7}{2}}}\mathbf{e} + \frac{15}{4}\varepsilon_{\odot}(\mathbf{e} \cdot \hat{\boldsymbol{n}}_{\odot})\hat{\boldsymbol{n}}_{\odot} - \frac{3}{2}\varepsilon_{\odot}\mathbf{e}$$

$$+ \frac{15}{8}\varepsilon_{\odot}\varepsilon_{\otimes}e^2\hat{\boldsymbol{u}}_{\odot} + \frac{15}{4}(\mathbf{e} \cdot \hat{\boldsymbol{u}}_{\odot})\mathbf{e} - \frac{15}{64}\varepsilon_{\odot}\varepsilon_{\otimes}\hat{\boldsymbol{u}}_{\odot}$$

$$- \frac{35 \cdot 15}{64}\varepsilon_{\odot}\varepsilon_{\otimes}(\mathbf{e} \cdot \hat{\boldsymbol{n}}_{\odot})^2\hat{\boldsymbol{u}}_{\odot} - \frac{35 \cdot 15}{64}\varepsilon_{\odot}\varepsilon_{\otimes}(\mathbf{e} \cdot \hat{\boldsymbol{u}}_{\odot})2(\mathbf{e} \cdot \hat{\boldsymbol{n}}_{\odot})\hat{\boldsymbol{n}}_{\odot}$$

$$+ \frac{75}{64}\varepsilon_{\odot}\varepsilon_{\otimes}(\mathbf{j} \cdot \hat{\boldsymbol{n}}_{\odot})^2\hat{\boldsymbol{u}}_{\odot} + \frac{75}{32}\varepsilon_{\odot}\varepsilon_{\otimes}(\mathbf{j} \cdot \hat{\boldsymbol{u}}_{\odot})(\mathbf{j} \cdot \hat{\boldsymbol{n}}_{\odot})\hat{\boldsymbol{n}}_{\odot} \tag{2.93}$$

With that, we can finally present the dynamical equations of motion of a test particle on a Keplerian orbit that is perturbed by an external massive body and by a non-spherical mass distribution inside of it. The following equations of motion are for our dynamical variables: the non-dimensional angular momentum vector $\mathbf{j}$, and the Laplace-Runge-Lenz vector $\mathbf{e}$.

$$\frac{d\mathbf{j}}{d\tau} = \frac{3}{4}\varepsilon_\odot(\mathbf{j}\cdot\hat{\boldsymbol{n}}_\odot)\mathbf{j}\times\hat{\boldsymbol{n}}_\odot - \frac{15}{4}\varepsilon_\odot(\mathbf{e}\cdot\hat{\boldsymbol{n}}_\odot)\mathbf{e}\times\hat{\boldsymbol{n}}_\odot + \frac{3}{2}\varepsilon_p\frac{(\mathbf{j}\cdot\hat{\boldsymbol{n}}_{\boldsymbol{p}})}{(1-e^2)^{\frac{5}{2}}}\mathbf{j}\times\hat{\boldsymbol{n}}_{\boldsymbol{p}}$$

$$-\frac{75}{64}\varepsilon_\odot\varepsilon_\otimes\Bigg[\Big[2\big((\mathbf{e}\cdot\hat{\boldsymbol{u}}_\odot)(\mathbf{j}\cdot\hat{\boldsymbol{n}}_\odot)+(\mathbf{e}\cdot\hat{\boldsymbol{n}}_\odot)(\mathbf{j}\cdot\hat{\boldsymbol{u}}_\odot)\big)\mathbf{j}+2\big(-7(\mathbf{e}\cdot\hat{\boldsymbol{n}}_\odot)(\mathbf{e}\cdot\hat{\boldsymbol{u}}_\odot)+(\mathbf{j}\cdot\hat{\boldsymbol{u}}_\odot)(\mathbf{j}\cdot\hat{\boldsymbol{n}}_\odot)\big)\mathbf{e}\Big]\times\hat{\boldsymbol{n}}_\odot$$

$$+\Big[2(\mathbf{e}\cdot\hat{\boldsymbol{n}}_\odot)(\mathbf{j}\cdot\hat{\boldsymbol{n}}_\odot)\mathbf{j}+\big(-7(\mathbf{e}\cdot\hat{\boldsymbol{n}}_\odot)^2+(\mathbf{j}\cdot\hat{\boldsymbol{n}}_\odot)^2+\frac{8}{5}e^2-\frac{1}{5}\big)\mathbf{e}\Big]\times\hat{\boldsymbol{u}}_\odot\Bigg]\quad(2.94)$$

$$\frac{d\mathbf{e}}{d\tau} = \frac{3}{4}\varepsilon_\odot(\mathbf{j}\cdot\hat{\boldsymbol{n}}_\odot)\mathbf{e}\times\hat{\boldsymbol{n}}_\odot - \frac{15}{4}\varepsilon_\odot(\mathbf{e}\cdot\hat{\boldsymbol{n}}_\odot)\mathbf{j}\times\hat{\boldsymbol{n}}_\odot + \frac{3}{2}\varepsilon_p\frac{(\mathbf{j}\cdot\hat{\boldsymbol{n}}_{\boldsymbol{p}})}{(1-e^2)^{\frac{5}{2}}}\mathbf{e}\times\hat{\boldsymbol{n}}_{\boldsymbol{p}}$$

$$+\Big[\frac{3}{2}\varepsilon_\odot-\frac{3}{4}\varepsilon_p\frac{1-e^2-5(\mathbf{j}\cdot\hat{\boldsymbol{n}}_{\boldsymbol{p}})^2}{(1-e^2)^{\frac{7}{2}}}\Big]\mathbf{j}\times\mathbf{e}$$

$$-\frac{75}{64}\varepsilon_\odot\varepsilon_\otimes\Bigg[\Big[2\big((\mathbf{e}\cdot\hat{\boldsymbol{u}}_\odot)(\mathbf{j}\cdot\hat{\boldsymbol{n}}_\odot)+(\mathbf{e}\cdot\hat{\boldsymbol{n}}_\odot)(\mathbf{j}\cdot\hat{\boldsymbol{u}}_\odot)\big)\mathbf{e}+2\big(-7(\mathbf{e}\cdot\hat{\boldsymbol{u}}_\odot)(\mathbf{e}\cdot\hat{\boldsymbol{n}}_\odot)+(\mathbf{j}\cdot\hat{\boldsymbol{u}}_\odot)(\mathbf{j}\cdot\hat{\boldsymbol{n}}_\odot)\big)\mathbf{j}\Big]\times\hat{\boldsymbol{n}}_\odot$$

$$+\Big[2(\mathbf{e}\cdot\hat{\boldsymbol{n}}_\odot)(\mathbf{j}\cdot\hat{\boldsymbol{n}}_\odot)\mathbf{e}+\big(-7(\mathbf{e}\cdot\hat{\boldsymbol{n}}_\odot)^2+(\mathbf{j}\cdot\hat{\boldsymbol{n}}_\odot)^2+\frac{8}{5}e^2-\frac{1}{5}\big)\mathbf{j}\Big]\times\hat{\boldsymbol{u}}_\odot$$

$$+\frac{16}{5}(\mathbf{e}\cdot\hat{\boldsymbol{u}}_\odot)\mathbf{j}\times\mathbf{e}\Bigg]\quad(2.95)$$

These equations are obviously coupled in the dynamical vectors. Reflection of the inner binary $\mathbf{j}\rightarrow-\mathbf{j}$ takes the equations from $\frac{d\mathbf{j}}{d\tau}\rightarrow-\frac{d\mathbf{j}}{d\tau}$, $\frac{d\mathbf{e}}{d\tau}\rightarrow-\frac{d\mathbf{e}}{d\tau}$, which can be interpreted as reversing the direction of time. Thus $\tau\rightarrow-\tau$ keeps the equations invariant. This is also equivalent in orbital elements to saying $i\rightarrow\pi-i, \omega\rightarrow\pi-\omega, \Omega\rightarrow\Omega+\pi$. Note also that the equations truncated at the quadrupolar level are invariant under the following extra transformations:

$$\mathbf{e}\rightarrow-\mathbf{e}\qquad\text{or}\qquad\hat{\boldsymbol{n}}_\odot\rightarrow-\hat{\boldsymbol{n}}_\odot\qquad\text{or}\qquad\hat{\boldsymbol{n}}_{\boldsymbol{p}}\rightarrow-\hat{\boldsymbol{n}}_{\boldsymbol{p}}$$

However, once we allow for the octupole to enter the game, not all of this symmetry is conserved, and we need to account for multiple configurations. Specifically, symmetry under flipping of the eccentricity vector is no longer maintained. These configurations for a coplanar-coplanar setting, in which all the vectors lie in the same plane, are represented in figure(2.1)
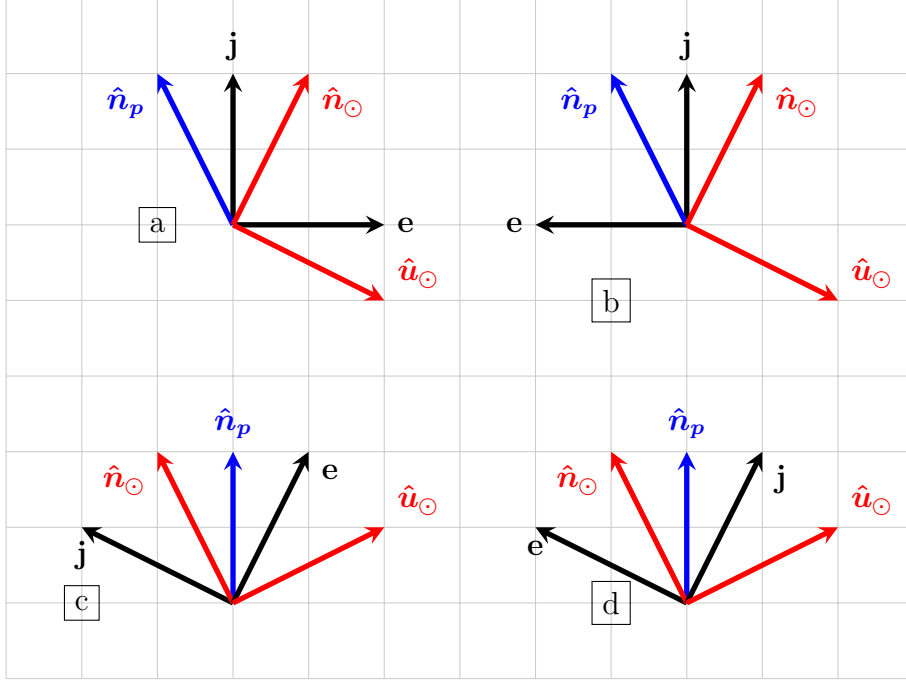
Figure 2.1: Different configurations to consider in the coplanar-coplanar setting.

2.4.2 Linear Stability Analysis

We will proceed further to solve our equations of motion presented earlier, but in order to study the stability of the solutions we will produce, we perform a linear stability analysis. For the vector $\mathbf{x}$ containing our vectorial elements $\mathbf{j}, \mathbf{e}$, a point $\mathbf{x}_0$ is an equilibrium if $\nabla H(\mathbf{x}_0) = 0$. Our study of equilibria stability would be by linearizing the equations of motion assuming $\mathbf{x}_1 = \mathbf{x} - \mathbf{x}_0$ obtaining

$$\dot{\mathbf{x}}_1 = L\mathbf{x}_1 \tag{2.96}$$

Hence we first look for the linearization matrix L by writing $\mathbf{j} = \mathbf{j}_0 + \mathbf{j}_1$ and $\mathbf{e} = \mathbf{e}_0 + \mathbf{e}_1$ then linearizing the equations of motion for arbitrary equilibria $\mathbf{j}_0$ and $\mathbf{e}_0$ up to first order in $\mathbf{j}_1$ and $\mathbf{e}_1$. After linearizing the equations we resolve them into their components considering the outer binary triad as our basis. We obtain the linearization matrix containing vectors: $\mathbf{j}_0, \mathbf{j}_1, \mathbf{e}_0, \mathbf{e}_1, \hat{\boldsymbol{n}}_\odot, \hat{\boldsymbol{n}}_{\boldsymbol{p}}$.
Having found the linearization matrix L, the solution of equation 2.96, for distinct eigenvalues λ_i, is of the form:

$$\mathbf{x}_1(t) = \sum_{i=1}^{i=2n} c_i \mathbf{v}_i \exp(\lambda_i t) \tag{2.97}$$

where $\mathbf{v}_i$ are the eigenvectors of L. The solution has exponentially growing terms unless all eigenvalues lie on the imaginary axis. Thus our stability analysis reduces to finding eigenvalues of L (21). The full stability analysis equations can be found in Appendix A.

2.4.3 The Coplanar-Coplanar Equilibrium Condition

In this setting, vectors $\mathbf{j}, \mathbf{e}, \hat{\boldsymbol{u}}_\odot$ lie in the principal plane of $\hat{\boldsymbol{n}}_\odot, \hat{\boldsymbol{n}}_{\boldsymbol{p}}$. We define ϕ as the angle between $\mathbf{j}$ and $\hat{\boldsymbol{n}}_{\boldsymbol{p}}$, and $\phi_\odot$ as the angle between $\hat{\boldsymbol{n}}_{\boldsymbol{p}}$ and $\hat{\boldsymbol{n}}_\odot$. Then it is trivial to transform our set of equations of motion in 3D into two one-dimensional equations as the cross products of all vectors involved is always in the same direction, namely the direction $\hat{\boldsymbol{v}}_\odot$. Doing that, we would be solving for (e, ϕ) by the following conditions:

$$
\begin{aligned}
0 = &-\frac{3}{4}\varepsilon_\odot(1-e^2)\cos(\phi_\odot-\phi)\sin(\phi_\odot-\phi) - \frac{15}{4}\varepsilon_\odot e^2\sin(\phi_\odot-\phi)\cos(\phi_\odot-\phi) \\
&+\frac{3}{2}\varepsilon_p\frac{\cos\phi\sin\phi}{(1-e^2)^{\frac{3}{2}}} - \frac{75}{64}\varepsilon_\odot\varepsilon_\otimes\Bigg[-2e(1-e^2)\cos^2(\phi_\odot-\phi)\sin(\phi_\odot-\phi) \\
&+2e(1-e^2)\sin^3(\phi_\odot-\phi) - 14e^3\cos^2(\phi_\odot-\phi)\sin(\phi_\odot-\phi) + 7e^3\sin^3(\phi_\odot-\phi) \\
&-2e(1-e^2)\cos^2(\phi_\odot-\phi)\sin(\phi_\odot-\phi) - 2e(1-e^2)\cos^2(\phi_\odot-\phi)\sin(\phi_\odot-\phi) \\
&-\frac{8}{5}e^3\sin(\phi_\odot-\phi) - e(1-e^2)\cos^2(\phi_\odot-\phi)\sin(\phi_\odot-\phi) + \frac{1}{5}e\sin(\phi_\odot-\phi)\Bigg]
\end{aligned}
\tag{2.98}
$$

$$
\begin{aligned}
0 = &\frac{3}{4}\varepsilon_\odot e\sqrt{1-e^2}\cos^2(\phi_\odot-\phi) + \frac{15}{4}\varepsilon_\odot e\sqrt{1-e^2}\sin^2(\phi_\odot-\phi) \\
&+\frac{3}{2}\varepsilon_p e\frac{\cos^2\phi}{(1-e^2)^2} - \frac{3}{2}\varepsilon_\odot e\sqrt{1-e^2} + \frac{3}{4}\varepsilon_p e\frac{1-e^2-5(1-e^2)\cos^2\phi}{(1-e^2)^3} \\
&-\frac{75}{64}\varepsilon_\odot\varepsilon_\otimes\Bigg[2e^2\cos^3(\phi_\odot-\phi) - 2e^2\cos(\phi_\odot-\phi)\sin^2(\phi_\odot-\phi)\sqrt{1-e^2} \\
&+14e^2\sqrt{1-e^2}\cos(\phi_\odot-\phi)\sin^2(\phi_\odot-\phi) + 2(1-e^2)^{\frac{3}{2}}\cos(\phi_\odot-\phi)\sin^2(\phi_\odot-\phi) \\
&-2e^2\sqrt{1-e^2}\cos(\phi_\odot-\phi)\sin^2(\phi_\odot-\phi) + 7e^2\sqrt{1-e^2}\cos(\phi_\odot-\phi)\sin^2(\phi_\odot-\phi) \\
&-(1-e^2)^{\frac{3}{2}}\cos^3(\phi_\odot-\phi) - \frac{8}{5}e^2\sqrt{1-e^2}\cos(\phi_\odot-\phi) + \frac{1}{5}\sqrt{1-e^2}\cos(\phi_\odot-\phi) \\
&-\frac{16}{5}e^2\sqrt{1-e^2}\cos(\phi_\odot-\phi)\Bigg]
\end{aligned}
\tag{2.99}
$$

Gathering our terms we get:

$$0 = \frac{3}{4}\varepsilon_p(1-e^2)^{-\frac{3}{2}}\sin(2\phi) - \frac{3}{8}\varepsilon_\odot(1+4e^2)\sin 2(\phi_\odot - \phi)$$
$$-\frac{75}{64}\varepsilon_\odot\varepsilon_\otimes e \left[-\frac{7}{2}(1+e^2)\cos(\phi_\odot - \phi)\sin 2(\phi_\odot - \phi) \right.$$
$$\left. + (2+5e^2)\sin^3(\phi_\odot - \phi) + \frac{1}{5}(1-8e^2)\sin(\phi_\odot - \phi) \right] \quad (2.100)$$

$$0 = \frac{3}{4}\varepsilon_p e(1-e^2)^{-2}(1-3\cos^2\phi) - \frac{3}{4}\varepsilon_\odot e(1-e^2)^{\frac{1}{2}}(1-4\sin^2(\phi_\odot - \phi))$$
$$-\frac{75}{64}\varepsilon_\odot\varepsilon_\otimes(1-e^2)^{\frac{1}{2}} \left[(3e^2-1)\cos^3(\phi_\odot - \phi) \right.$$
$$+ (\frac{1}{5} - \frac{24}{5}e^2)\cos(\phi_\odot - \phi)$$
$$\left. + (1+\frac{15}{2}e^2)\sin(\phi_\odot - \phi)\sin 2(\phi_\odot - \phi) \right] \quad (2.101)$$

It's trivial here also to see that the introduction of the octupole term into the dynamics has broken some symmetries in the system, specifically the invariance under $\mathbf{e} \to -\mathbf{e}$ transition, or going from the aligned case in configuration (a) to the anti-aligned case in configuration (b). On the other hand, going from (a) to (c) results in no change in the equations and thus the same solutions will satisfy both configurations.

The equations are non-symmetric in going from (a) to (d), but a transition of $\phi \to \pi - \phi$ restores them. So that's equivalent as we said earlier to a shift in the nodes and position of the pericenter by π. Hence we keep our focus on configuration (a), apsidally aligned with the external perturber, and configuration (b), apsidally anti-aligned with the external perturber.

2.4.4 Generalization into Full Spatial Dynamics

We are now able to solve our equations of motion resembling our particles' fixed orbits while being perturbed by the inner quadrupole and the outer octupole, and study their stability to perturbations in eccentricity and angular momentum.

But we are only able to to solve for coplanar-coplanar configurations, in which all of the vectors are in the same plane. However, we would like to complete the machinery in generalizing our scope to extended spatial configurations by producing the equations in orbital elements. Moreover, of more interest to us than looking for new equilibria is to study the variations of the coplanar-coplanar equilibria when changing the orientation of the perturbations; and this can also be done via the orbital elements description.

Equations of Motion in Orbital Elements

The Hamiltonians written in vectorial elements earlier can be written in terms of orbital elements by writing the cartesian components of the vectors $\mathbf{j}$ and $\mathbf{e}$ in terms of eccentricity e, argument of the pericenter ω, inclination i, and longitude of the ascending node Ω as in (17):

$$\mathbf{j} = \sqrt{1 - e^2} \begin{pmatrix} \sin i \sin \Omega \\ -\sin i \cos \Omega \\ \cos i \end{pmatrix} \tag{2.102}$$

$$\mathbf{e} = e \begin{pmatrix} \cos \omega \cos \Omega - \sin \omega \cos i \sin \Omega \\ \cos \omega \sin \Omega + \sin \omega \cos i \cos \Omega \\ \sin \omega \sin i \end{pmatrix} \tag{2.103}$$

We consider the outer binary orbit as our fixed reference frame. For now, we set $\Omega_\odot = 0$ and $\omega_\odot = \pi/2$, and we define the mutual inclination between the tested orbit and the inner quadrupole as J_p:

$$\cos J_p = \sin i \sin i_p \cos(\Omega - \Omega_p) + \cos i \cos i_p \tag{2.104}$$

Upon this transformation, the inner quadrupole can be written as:

$$\Psi_p = -\frac{\varepsilon_p}{4(1 - e^2)^{\frac{3}{2}}} \left(1 - 3 \cos^2 J_p \right) \tag{2.105}$$

The outer potentials upon transformation are equivalent to those in (22), hence:

$$\Psi_{quad} = -\frac{3}{8} \varepsilon_\odot \left(-\frac{1}{3} - \frac{e^2}{2} + (1 + \frac{3}{2} e^2) \cos^2 i + \frac{5}{2} e^2 (1 - \cos^2 i) \cos 2\omega \right) \tag{2.106}$$

$$\Psi_{oct} = \frac{75}{64}\varepsilon_\odot\varepsilon_\otimes\times$$

$$\left(\left(\left(e + \frac{3}{4}e^3\right) \times \left(\left[3\cos^3 i - \frac{11}{5}\cos i\right]\cos\Omega\sin\omega\right.\right.\right.$$

$$\left.+ \left[\cos^2 i - \frac{1}{5}\right]\sin\Omega\cos\omega\right)$$

$$+ \frac{7}{4}e^3 \times \left(\left[-\cos^3 i + \cos i\right]\cos\Omega\sin 3\omega\right.$$

$$\left.\left.\left[-\cos^2 i + 1\right]\sin\Omega\cos 3\omega\right)\right) \qquad (2.107)$$

Thus we define $\Psi = \Psi_p + \Psi_{quad} + \Psi_{oct}$. And to produce the equations of motion, known a Lagrange equations of motion (17), we need the following differentials:

$$\frac{\partial\Psi}{\partial e} = -\frac{3}{4}\varepsilon_p\frac{e}{(1-e^2)^{\frac{5}{2}}}\left[1 - 3\cos^2 J_p\right]$$

$$+ \frac{3}{8}\varepsilon_\odot e\left(1 - 3\cos^2 i - 5(1 - \cos^2 i)\cos 2\omega\right)$$

$$+ \frac{75}{64}\varepsilon_\odot\varepsilon_\otimes \times \left(\left(1 + \frac{9}{4}e^2\right) \times \left(\left[3\cos^3 i - \frac{11}{5}\cos i\right]\cos\Omega\sin\omega\right.\right.$$

$$\left.+ \left[\cos^2 i - \frac{1}{5}\right]\sin\Omega\cos\omega\right)$$

$$+ \frac{21}{4}e^2 \times \left(\left[-\cos^3 i + \cos i\right]\cos\Omega\sin 3\omega\right.$$

$$\left.\left.+ \left[-\cos^2 i + 1\right]\sin\Omega\cos 3\omega\right)\right)$$

27

$$\frac{\partial \Psi}{\partial i} = \frac{3}{2}\varepsilon_p \frac{1}{(1-e^2)^{\frac{3}{2}}} \big[\cos i \sin i_p \cos(\Omega - \Omega_p) - \sin i \cos i_p\big] \times \cos J_p$$

$$+ \frac{3}{8}\varepsilon_\odot \big[\cos i \sin i\big] \times \big[2 + 3e^2 - 5e^2 \cos 2\omega\big]$$

$$- \frac{75}{64}\varepsilon_\odot \varepsilon_\otimes \sin i \times \left(\left(e + \frac{3}{4}e^3\right)\left(\big[9\cos^2 i - \frac{11}{5}\big]\cos\Omega\sin\omega\right.\right.$$

$$+ \big[2\cos i\big]\sin\Omega\cos\omega\Big)$$

$$+ \frac{7}{4}e^3\Big(\big[-3\cos^2 i + 1\big]\cos\Omega\sin 3\omega$$

$$\left.\left.+ \big[-2\cos i\big]\sin\Omega\cos 3\omega\right)\right)$$

$$\frac{\partial \Psi}{\partial \Omega} = -\frac{3}{2}\varepsilon_p \frac{1}{(1-e^2)^{\frac{3}{2}}}\big[\sin i \sin i_p \sin(\Omega - \Omega_p)\big] \times \cos J_p$$

$$+ \frac{75}{64}\varepsilon_\odot\varepsilon_\otimes \times \left(\left(e + \frac{3}{4}e^3\right)\left(\big[-3\cos^3 i + \frac{11}{5}\cos i\big]\sin\Omega\sin\omega\right.\right.$$

$$+ \big[\cos^2 i - \frac{1}{5}\big]\cos\Omega\cos\omega\Big)$$

$$+ \frac{7}{4}e^3\Big(\big[+\cos^3 i - \cos i\big]\sin\Omega\sin 3\omega$$

$$\left.\left.+ \big[-\cos^2 i + 1\big]\cos\Omega\cos 3\omega\right)\right)$$

$$\frac{\partial \Psi}{\partial \omega} = \frac{15}{8}\varepsilon_\odot e^2 \sin^2 i \sin(2\omega)$$

$$+ \frac{75}{64}\varepsilon_\odot \varepsilon_\otimes \times \left(\left(e + \frac{3}{4}e^3\right) \times \left(\left[3\cos^3 i - \frac{11}{5}\cos i\right]\cos\Omega\cos\omega\right.\right.$$

$$\left. + \left[-\cos^2 i + \frac{1}{5}\right]\sin\Omega\sin\omega\right)$$

$$+ \frac{21}{4}e^3 \times \left(\left[-\cos^3 i + \cos i\right]\cos\Omega\cos 3\omega\right.$$

$$\left.\left. + \left[\cos^2 i + 1\right]\sin\Omega\sin 3\omega\right)\right)$$

These differentials allow us to write equations of variation for the orbital elements, namely Lagrange equations (17)

$$\frac{\mathrm{d}e}{\mathrm{d}t} = -\frac{\sqrt{1-e^2}}{na^2 e}\frac{\partial \Psi}{\partial \omega} \tag{2.108}$$

$$\frac{\mathrm{d}i}{\mathrm{d}t} = \frac{1}{na^2\sqrt{1-e^2}\sin i}\left(\cos i \frac{\partial \Psi}{\partial \omega} - \frac{\partial \Psi}{\partial \Omega}\right) \tag{2.109}$$

$$\frac{\mathrm{d}\Omega}{\mathrm{d}t} = \frac{1}{na^2\sqrt{1-e^2}\sin i}\frac{\partial \Psi}{\partial i} \tag{2.110}$$

$$\frac{\mathrm{d}\omega}{\mathrm{d}t} = \frac{\sqrt{1-e^2}}{na^2 e}\frac{\partial \Psi}{\partial e} - \frac{\cot i}{na^2\sqrt{1-e^2}}\frac{\partial \Psi}{\partial i} \tag{2.111}$$

This equations are of significance to us: First we can verify the solutions we get from the vectorial equations; an independent confirmation that is deemed essential as we are producing results that are unique to the literature. Also, as we mentioned earlier, these equations can describe non-symmetric configurations, allowing us to complete the picture provided by the vectorial equations. Moreover, these equations allow us to create surface of section for our particles.

Chapter 3

Multipoles in Action

3.1 Satellite-Earth-Sun Analogue System

With the machinery of the previous chapter, we are now able to produce and analyze results. We take the results of TTN (9) as a reference, and we first try to reproduce and verify thoser results, which are based on inner and outer quadrupolar contributions, to check our analytic and computational tools. Then we would introduce the effect of the octupole and check its impact.

3.1.1 Quadrupolar Description

Circular Coplanar-Coplanar

We first consider the case of circular orbits ($\mathbf{e} = 0$). In this case the second of our coplanar-coplanar equations of motion is trivially satisfied, and the first equation yields:

$$0 = 2\varepsilon_p \sin(2\phi) - \varepsilon_\odot \sin 2(\phi_\odot - \phi) \tag{3.1}$$

$$or \qquad \tan 2\phi = \frac{\varepsilon_\odot \sin 2\phi_\odot}{\varepsilon_\odot \cos 2\phi_\odot - 2\varepsilon_p} = \frac{\sin 2\phi_\odot}{\cos 2\phi_\odot - 2r_L^5/a^5} \tag{3.2}$$

If this equation has ϕ as a solution, then obviously $\phi \pm 1/2\pi$ and $\phi + \pi$ are also solutions. Also the Laplace radius is defined as r_L:

$$r_L^5 = J_2' R^2 a_\odot^3 (1 - e_\odot^2)^{3/2} \frac{M}{M_\odot} = a^5 \frac{\varepsilon_p}{\varepsilon_\odot} \tag{3.3}$$

Stability analysis for the circular coplanar-coplanar case is trivial, as the two linearized equations are decoupled between the dynamical vectors, and we can find the eigenvalues of the linearization matrix and consequently the associated stability for each one separately.

This analysis produces the results shown in the following figures. Two circular equilibria appear at each semi-major axis; they are separated by $\pi/2$ creating two families of equilibria as we sweep the full range of distance; of course that's what we expected because for ϕ being a solution, $\phi + \pi/2$ is also a solution. The latter family is unstable to perturbations in eccentricity and angular momentum vectors; while the former is stable as long as the obliquity of the planet is less that $67°$. These results do verify those of TTN that are themselves consistent with the so-called classical *Laplace Surface* defined by fixed circular orbits residing in the plane of the inner quadrupole (the equator of the planet) at short distances, and transitions upon passing through the Laplace radius defined earlier to reside in the orbit of the planet at longer distances.
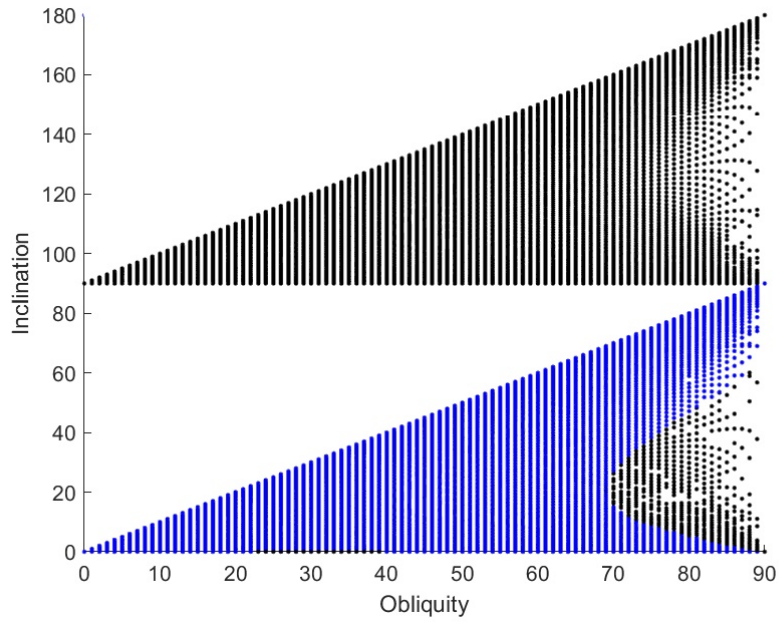
Figure 3.1: Circular Coplanar Coplanar solutions describing the classical Laplace Surface. Both equilibria and their stability(blue) are consistent with TTN. Stability is considered for perturbations in both eccentricity and angular momentum vectors. Circular equilibria turn unstable for $\phi_\odot > 67°$, proven later to be in favor of eccentric coplanar-coplanar equilibria.
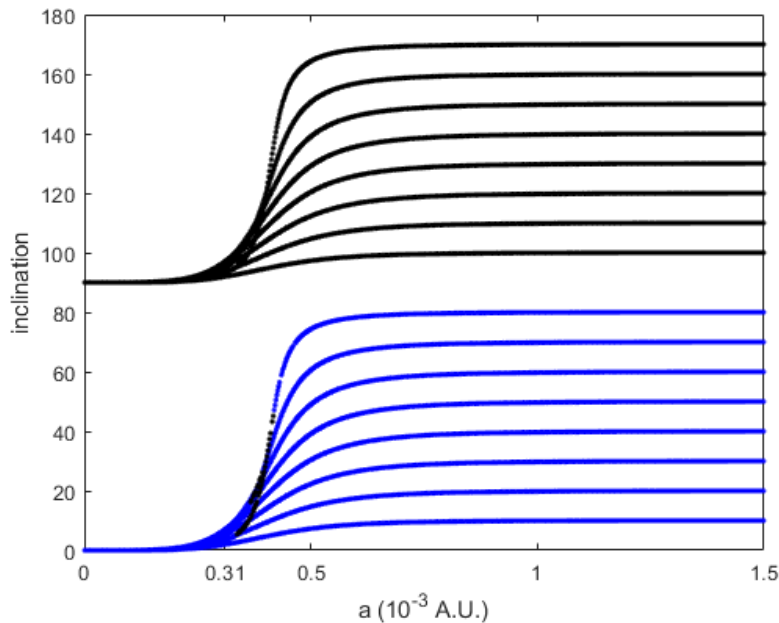
Figure 3.2: Classical Laplace Equilibria as a function of distance from the planet. Orbits are in the plane of the planet's equator at short distances, thus called planet dominated, and cross to the sun dominated regime beyond the Laplace radius.
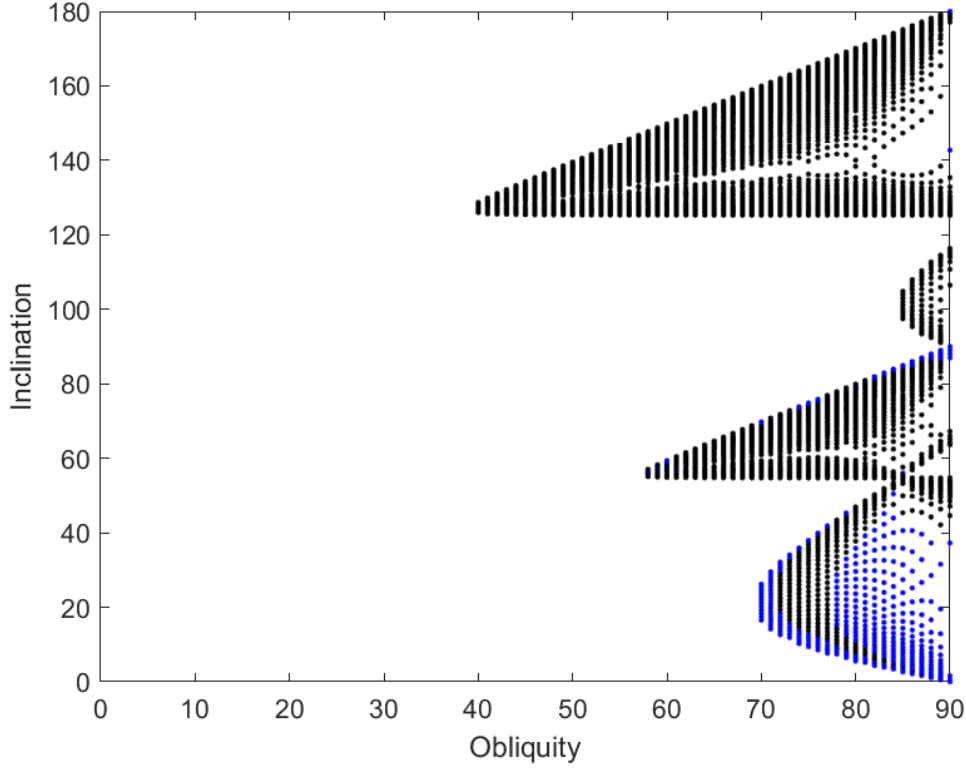
Figure 3.3: Eccentric coplanar-coplanar solutions and their associated stability in blue.

Eccentric Coplanar-Coplanar:

If we allow for arbitrary eccentricity solutions, at the quadrupolar description, we have the following equilibrium conditions:

$$2\varepsilon_p \sin 2\phi = \varepsilon_\odot (1 - e^2)^{3/2}(1 + 4e^2) \sin 2(\phi_\odot - \phi)$$
$$\varepsilon_p (1 - 3\cos^2 \phi) = \varepsilon_\odot (1 - e^2)^{5/2}(1 - 4\sin^2(\phi_\odot - \phi)) \tag{3.4}$$

Regions in which these equilibria exist are bounded by the lines $\phi = \phi_\odot$, $\phi = \phi_\odot + \frac{1}{2}\pi$, and $\phi = \pm\cos^-(1\sqrt{3})$. Eccentric coplanar–coplanar equilibria appear to be bifurcating from the circular coplanar equilibria at the point where the circular coplanar equilibrium becomes unstable.

3.1.2   The Effect of the Octupole:

We first check the effect of the octupole term on the circular equilibria defining the Laplace Surface. We note again that when we impose ($e = 0$) on the equations of motion at the level of the quadrupoles, the first equation describes the Laplace Surface, while the second (the eccentricity vector equation) is satisfied trivially. However, when we add the octupole, the added terms vanish in the angular momentum vector equation, leaving us with the quadrupolar terms only; but we note the survival of terms in the eccentricity vector equation. Hence we are left with two conditions to be satisfied when looking for circular equilibria:

$$0 = 2\varepsilon_p \sin(2\phi) - \varepsilon_\odot \sin 2(\phi_\odot - \phi) \tag{3.5}$$

$$0 = \varepsilon_\odot \varepsilon_\otimes \cos(\phi_\odot - \phi)\left(-3\cos^2(\phi_\odot - \phi) + \frac{11}{5}\right) \tag{3.6}$$

The octupole, if non-vanishing ($e_\odot > 0$) i.e. the outer perturber is on an eccentric orbit, imposes a constraint on circular equilibria, namely equation 3.6. This condition does not depend on the value of the outer eccentricity as long as it is non-zero. Solutions of the this condition are given by:

$$\cos(\phi_\odot - \phi) = 0 \qquad or \qquad \cos(\phi_\odot - \phi) = \pm\sqrt{\frac{11}{15}} \tag{3.7}$$

Hence out of the classical circular Laplace equilibria presented in fig.3.1, only those satisfying these conditions survive the octupole addition. The three families of solutions to equation 3.6 are shown in figure 3.4; only one family (shown in red) is associated with the classical Laplace equilibria, and thus the rest of the Laplace circular equilibria do not pertain as solutions to both conditions. Thus we can say that the octupole added a constraint that almost destroyed the whole Laplace Surface structure as a surface of circular equilibria planes.

Concerning the eccentric equilibria, we have seen that even for a fairly eccentric outer binary ($e_\odot = 0.6$), and for its full range of inclinations, the octupole could not introduce a significant change to the equilibria already described at the quadrupolar level. This is definitely due to the very small semi-major axes ratio. We took things far and extended the analysis up to Hill's radius, which is interpreted as the planet's radius of influence, and roughly after which the particle is dominated by the solar tide rather than the planet, and will mostly be unbound to the planet. It is defined by:

$$r_H = a_\odot \left(\frac{M}{3M_\odot}\right)^{1/3} \tag{3.8}$$

This takes the value of $0.01AU$ for the moon around the Earth.
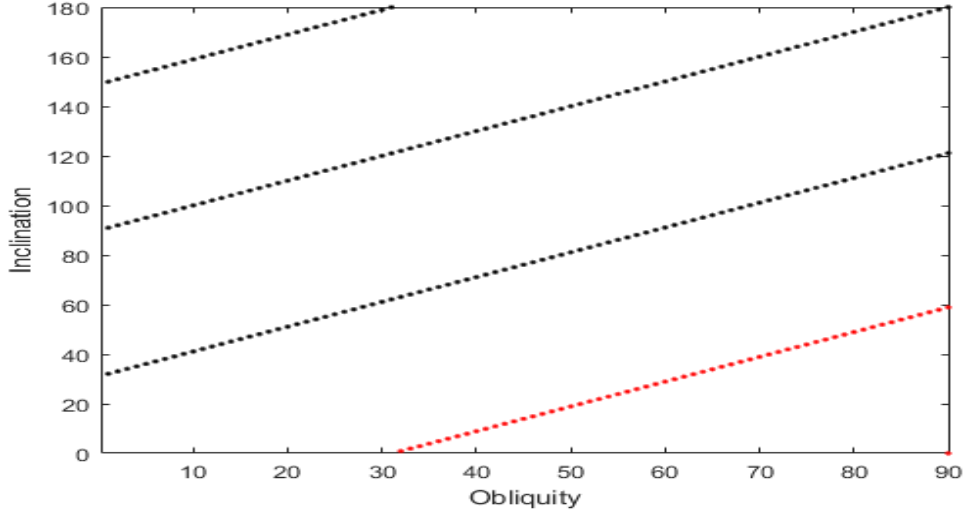
Figure 3.4: Inclination solutions of equation 3.6. These solutions are only function of the obliquity $\phi_\odot$. They are presented in equation 3.7, specifically they're: $(\phi_\odot - \phi) = \pi/2, (\phi_\odot - \phi) = 31.09°$, or $(\phi_\odot - \phi) = 180 - 31.09°$. Only one family, shown in red, also satisfies equation 3.5 (the classical Laplace equilibria).

Although our use of the orbit averaged solar potential requires that $r << r_H$, we took r_H as our distance limit in order to allow the octupole to be of strongest effect. However, even there, the ratio of semi-major axes is 1/100, thus the strength of the quadrupole is roughly hundred times the strength of the octupole. And our results show that the octupole could not alter the quadrupole results, neither in structure, nor in stability, and figure 3.3 still holds at this level. We see that the structure of eccentric equilibria there is fine tuned, and in order to generate variations by a stronger octupole we had to allow the outer binary to be of extremely high eccentricity and shorter distance. We were able then to generate highly eccentric equilibira at lower obliquities than the quadrupolar description, but as a corollary, r_H decreased and our particles then would be on parts of the orbits beyond it.

Thus we can safely conclude regarding this satellite-Earth-Sun analogue system that:

- The addition of the octupole induces a constraint on circular equilibria. A constraint that mostly destroys the whole structure of the Laplace Surface.

- The structure of eccentric equilibria, for a fairly eccentric earth, is described by the quadrupole, as the octupole is relatively very weak because of the small semi-major axes ratio.

NASA Exoplanet Archive

Fri Jun 7 10:06:18 2019
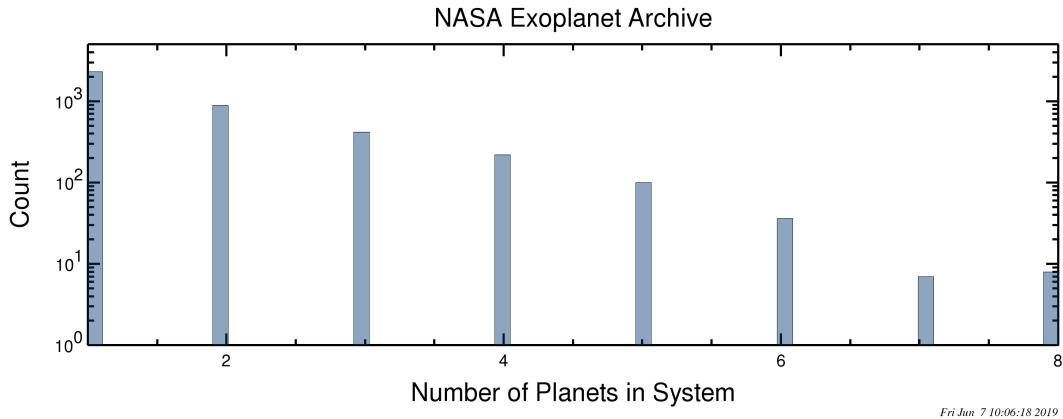
Figure 3.5: Frequency of confirmed exoplanets in planetary systems. The count is on a logarithmic scale. Nearly half (2298) of the planets are in single planetary systems, while the rest reside in multiplanetary systems. Source of data: NASA Exolplanet Archive, June 2019.

3.2 An Exoplanetary Case Study: Kepler-108

To analyze the effect of the octupole further, we study an exoplanetary system, and the applicability of our formalism will become more convenient as we proceed.

Around four thousand exo-planets have been confirmed (NASA Exolplanet Archive), and nearly half of them reside in a multi-planetary system (fig.3.5). The catalogue of the *Kepler* mission is particularly important because it contains multiplanetray systems roughly eight times as many as all radial velocity surveys combined (23; 24). An advantage of multiplanetary systems is that they allow us to constrain the mutual inclinations of the planets, either by comparing relative transit durations and orbital periods (25), or by comparing the frequencies of systems with different multiplicities in the *Kepler* survey to those in radial-velocity surveys because the chance that multiple planets in a single system will transit is much higher if they are near coplanarity (26).

Such studies showed that the vast majority of observed exoplanet systems are statistically consistent with having low mutual inclinations ($< 5°$) (25). However, out of those systems, only three are observed to have significant mutual inclinations: Kepler-419 b and c planets are observed to have a mutual inclination of $9^{\circ}{}^{+8}_{-6}$ from TTV constraints; Upsilon Andromeda c and d are reported to have a mutual inclination around $30°$ from the astrometric measurements using the Hubble Space Telescope; and the system of interest to us Kepler-108.

36

Based on a comprehensive analysis of *Kepler* light curves, the planetary system Kepler-108 was verified in 2014 (27). The system is composed of a stellar binary: Kepler-108 A and Kepler 108-B; the latter being orbited by two giant planets: Kepler-108 b and Kepler-108 c (the inner and outer planets respectively, with the inner being more massive). A photodynamics analysis of the system estimated a high mutual inclination between the planets ($24^{\circ+11}_{-8}$) (28).

Recently, Xu and Fabrycky (29) attempted to explain this mutual inclination by a novel secular-orbital resonance that they study in multiplanet systems perturbed by binary companions. They call it "Ivection" resonance, and they claim that it happens when the nodal precession rate of the planet matches a multiple of the orbital frequency of the binary, and its physical nature is similar to the previously-studied evection resonance (30).

In another attempt to explain this mutual inclination, along with the moderate eccentricity, we model the system with our formalism: The outer perturber being the stellar companion Kepler-108 A, the inner quadrupole provided by the inner planet, and we solve for equilibria of the outer planet in this dynamical system.

We do not know the period or the eccentricity of the outer star, only its sky projected distance being approximately 327 AU (31). We use the masses of the system components, their separations, and eccentricities (28; 29), while solving for the parameters of the outer planet, as the following:

Component	Kepler-108 A	Kepler-108 B	Kepler-108 b	Kepler-108 c
Mass	$1.3 M_{\odot}$	$0.96 M_{\odot}$	$0.31 M_J$	$0.17 M_J$
Separation	projected:327 AU, used $a = 170 AU$		$0.292 AU$	$0.721 AU$
Eccentricity	used $e = 0.95$		0.135	0.128

Although the mass of the inner planet is nearly twice that of the outer one, for a full consistent treatment we should not regard the outer planet as a test particle, but rather as a massive object that would have its effect on the inner planet; then we have to consider the inner planet as live as the outer planet and study the dynamics of both i.e. solve for equilibria for both planets. But for the sake of our study of the octupole here, specifically in looking for modifications of the Laplace Surface, we will proceed with the test particle approximation.

Also, since we only the projected separation between the stellar companions, we have a margin of freedom for the corresponding semi-major axis and eccentricity, constrained by keeping the apoapse larger than 327 AU, and the periapse not too close to the planetary system. With the aim of understanding the effect of the octupole, we choose a semi-major axis ($a = 170 AU$) and an eccentricity ($e = 0.95$). Thus the apoapse of the stellar binary is $b = 170(1+0.95) = 331.5 AU$, and the periapse $q = 170(1 - 0.95) = 8.5 AU$.

At the quadrupolar level, as expected, we produce the same results produced

in (9) and in our previous section. What we are more interested in here, is how would the octupole modify the classical Laplace Surface for a highly eccentric outer binary.

In fig 3.6, we show the modification of the classical Laplace Surface shown in fig 3.1 and fig 3.2. The octupole in this system is stronger than that presented in the previously studied analogue of Satellite-Earth-Sun system. When we speak of the strength of the octupole, what we actually mean is its relative strength with respect to the quadrupole. The octupole in the previous system has $\varepsilon_\otimes$ in the order of 10^{-2}, where as here it has $\varepsilon_\otimes$ in the order of 10^{-1}. Thus unlike the previous case, the octupole terms here were able to significantly change the eccentric equilibria present at the quadrupolar description.

Hence with the octupole here, we observe the emergence of nonlinear bifurcations of equilibria that were not present at the quadrupolar description. We leave the analysis of these new equilibria to the next chapters, and we concentrate for now on the Laplace Surface itself. The classical Laplace Surface as we know by now has two main features: The circular feature of the equilibira, and their alignment with the inner quadrupole at short distances from it, and with the outer quadrupole at larger distances. In the modified Laplace equilibria we present here, the alignment feature is preserved. However, the Laplace Surface is now modified such that the circular equilibria are pumped with eccentricity as we see in the figure. Thus the octupole, which was able to destroy the circular Laplace equilibria defining the classical Laplace Surface by the condition it added on circular equilibria, was also able here to generate an Eccentric Laplace Surface, which has the same behavior of angular momentum alignment as the classical one.

In figure 3.6, we first distinguish between the two regions that we are familiar with in the classical description: The stable circular region, and the region of unstable circular equilibria that bifurcate into eccentric ones.

The first region grows in eccentricity as a function of distance from the inner quadrupole, or equivalently, as a function of inclination from the inner quadrupole. This is somehow intuitive: The inner quadrupole forces the circularization of the equilibria, and the outer eccentric octupole drives the orbits eccentric. The eccentricity grows gradually to around 0.3 in the outer perturber dominated regime. The other region which emerges at mutual inclinations $> 68°$ features higher eccentricities as indicated by the color map.

Although this needs further work, but we succeeded in generating families of equilibria of moderate inclinations and eccentricities matching the observed parameters of Kepler-108 planets.
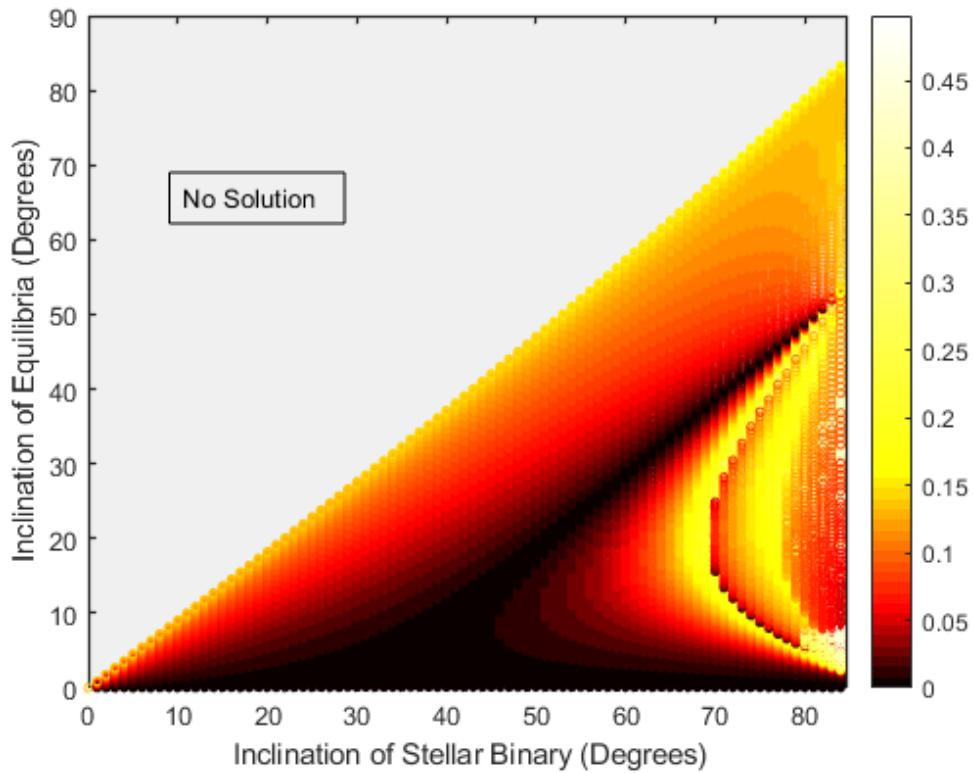
Figure 3.6: The modified Laplace Surface as a function of the mutual inclination between the two perturbations. The inclinations on the axes are measured with respect to the inner quadrupole. The colormap shows the eccentricity of the equilibria. At each stellar binary inclination, we create a surface of equilibria that features the same inclination behavior as the classical one, however it is not composed of circular orbits; the darkest points are of very small, but non-zero, eccentricity.

3.3 Dynamics Beyond Neptune:

The dynamical structure of the Solar System as it is observed now is represented schematically in fig 3.7. The trajectories of the planets and of the Main Belt asteroids are quite circular, so the scale gives an idea of their mutual distances. On the contrary, the orbits of the trans-Neptunian objects and of the comets can be very eccentric, so their trajectories in the physical space span a very large range of distances (from the Sun to very remote regions). In the figure, objects as Centaurs and Halley-type comets are not represented as "populations", since they are usually considered as unstable transitional orbital states.

Bodies of the Oort Cloud have so large semi-major axes that they are affected by galactic tides (that is, an acceleration from the whole Galaxy which is slightly different that the one felt by the barycenter of the Solar System). Passing stars can also have a strong influence on them, creating sporadic "comets showers" toward the planetary region if they pass close enough. As a result of these perturbations, the Oort Cloud is thought to be quite spherical, at least beyond 104 AU. Oort Cloud comets that have a perihelion inside the planetary region spend almost all their orbital period away, near their apocenters.

The shape of the Kuiper Belt component is quite well explained by the admitted formation scenario of the Solar System, however, the overall dynamics and past evolution of the trans-Neptunian region is still poorly understood. This holds, especially at high-perihelion distances, where it connects the Oort Cloud. This is firstly due to the lack of observational data (since it is very difficult to observe such distant objects), but also because the few observed objects have orbits which are incompatible with the formation scenario of the Solar System. Indeed, objects as Sedna or 2012VP113 have very eccentric orbits but also very high perihelion distances (76 and 80 AU), which indicates that: i) they cannot have been formed in their current state, otherwise their orbits would be quite circular; ii) they are too far to have been scattered in their current position by the planets; iii) they are not far enough to be substantially affected by the galactic tides. Various numerical experiments showed that mean-motion resonances are also unlikely to be able to produce such orbits(32). However, it is known from a long time by numerical ways that the secular dynamics in a mean motion resonance can produce high-amplitude oscillations of the perihelion distance and of the inclination (see for example (33)). So we appeal to the secular non-resonant approach. In 2016, the authors of (34) put together a hypothesis of a still undiscovered planet orbiting in the far trans-Neptunian region. Indeed, some of the most distant objects known appear to have roughly aligned orbits, and numerical simulations show that a distant Neptune-mass planet could produce such an accumulation. This would also explain their unexpectedly distant and eccentric orbits, though now we have a problem questioning the formation of the planet itself!
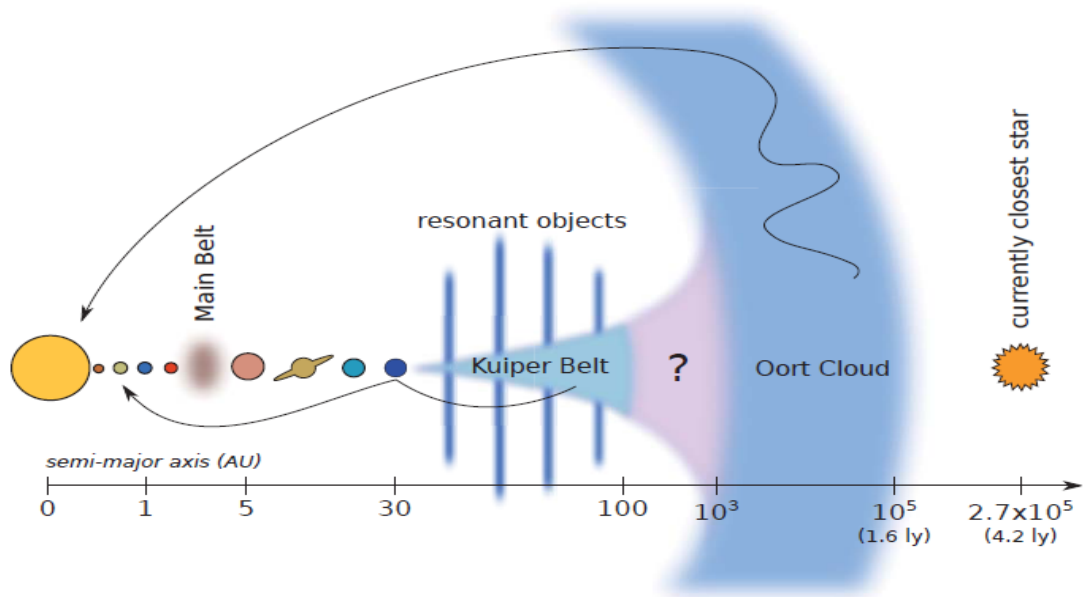
Figure 3.7: Current dynamical structure of the Solar System as it is considered today. The bodies sizes are not to scale. The horizontal axis represents the semi-major axes of the orbits, and the vertical placement gives an idea of the inclinations. Credits to "Institute for Celestial Mechanics and Computation of Ephemerides (IMCCE)".

The suggestion of Planet IX caused a great bustle in the planetary science community. Tens of articles about it were published, dealing with its formation or capture, its effects on the known planets, its orbital stability, its current probable position, its physical characteristics, its observability... Only a few tried to suggest an alternative, and the unique work of Touma and Sefilian in 2019 (35) stood out to re-question the need of the suggested planet, by suggesting that the same effects such a planet can cause can be induced by the self-gravitating disk of the TNOs themselves. This work will be discussed in details and built upon in Chapter 5, but for now we study the Planet IX hypothesis.

In this section, we use the machinery of multipoles developed earlier to look for results that could match the moderately inclined and highly eccentric eTNOs presented in table 3.1. We look for orbital solutions that are fixed in space while being perturbed internally by a quadrupole provided by the giant planets, and externally by the suggested Planet IX, with parameters suggested by the authors of (34), namely: $a_9 = 700AU, e_9 = 0.6, i_9 = 30°$. To look for equilibria we have used both our vectorial and orbital elements equations. Results were consistent and representative samples are presented in the figures below with corresponding stability classified based on the values of the nodes.

Figure 3.8: Eccentricity and Inclination profiles for equilibira generated by solving the equations of motion up to the octupolar order. Reference frame is the frame of P9. Plotted above the equilibria are the observed eTNOs; we can say we have a decent matching as this eTNOs follow a rend of a family which is stable and anti-aligned with the perturber.
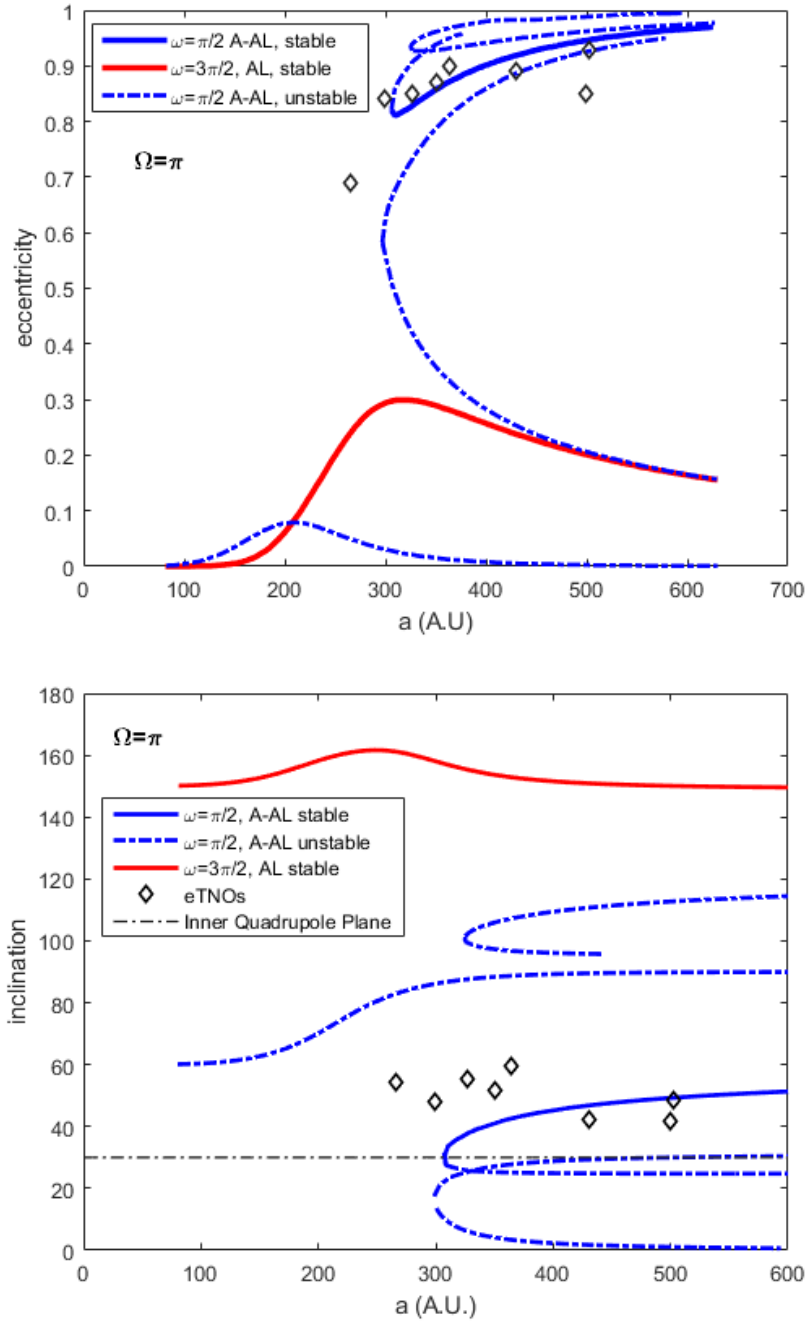
Table 3.1: Orbital parameters of observed clustered extreme TNOs of semi-major axis> $250 AU$ and pericenters beyond Neptune. Data from Minor Planet Center

TNO	a (a.u)	e	i (°)	ω (°)	Ω (°)
2012 VP113	258.27	0.69	24.1	293.5	90.7
2014 SR349	302.23	0.84	18.0	340.9	34.8
2004 VN112	318.97	0.85	25.6	326.8	66.0
2013 RF98	357.63	0.90	29.6	311.6	67.6
2010 GB174	350.59	0.86	21.6	347.45	130.8
2010 GB174	468.98	0.92	18.6	285.6	112.9
SEDNA	478.88	0.84	11.9	311.5	144.3

Figure 3.9: Eccentricity profiles for equilibria with nodes different than $(0, \pi)$. Clearly, equilibira with arbitrary nodes and apse alignments bifurcate from equilbiria with symmetric configurations.

43

The equilibria profiles we generated in fig.3.9 via the multipolar expansion truncated at the octupolar level are interesting and unique with respect to the literature. In the coplanar-coplanar configuration, if we used the quadrupole only, we would have no eccentric solutions with the used mutual inclination between the binaries ($\phi_\odot = 30°$) as eccentric, though unstable, solutions only emerge around $\phi_\odot = 38°$ and are of very high retrograde inclinations. However, the octupole allowed for eccentric solutions at ($\phi_\odot = 30°$), and we note the following:

- The eccentricity profile we generated in fig 3.9 represents both $\Omega = [0, \pi]$ configurations. We presented in the figure the ($\Omega = \pi$) solutions; shifting to ($\Omega = 0$) renders each anti-aligned family an aligned one and vice versa, and shifts the inclinations by $i \rightarrow \pi - i$

- The classical Laplace Surface, again, refers to a family of stable circular equilibiria that starts in the plane of the inner quadrupole, and transitions with increasing semi-major axis to the plane of the outer perturber. When we introduced the octupole, as we've seen in the previous studied cases, the circular equilibria do not pertain, but they grow in eccentricity from minimal values at short semi-major axis values. The growth is especially significant beyond the Laplace radius, where the eccentricity reaches moderate values ($e = 0.2, 0.3$). This feature of eccentricity has been seen in the previous cases; yet the interesting feature appears in the inclination profile: rather than transitioning between the planes of the perturbations as we've seen in the created eccentric Laplace Surface in Kepler-108, the surface was modified so that after going off the inner plane, and before residing in the outer plane, it then declines and resides in the inner plane again. This modification occurs around a radius that witnesses the emergence of the nonlinear bifurcations we have. Thus we can say that upon the introduction of the very strong octupole in this case, (and we note again that our quantification of the strength of the octupole is actually based upon its relative strength with respect to the quadrupole), the Laplace Surface was modified by being pumped with eccentricity, and by compromising the equilibira residing in the outer orbit in favor of new non-linear bifurcations.

- The classical Laplace Surface is always accompanied with another unstable family of inclinations shifted by $\pi/2$. This family was also present in the inclinations profile upon the introduction of the octupole; however, it gains some eccentricity (reaching $e = 0.1$) at exactly the Laplace radius.

- The weird feature of inclination present here and not in Kepler 108 could only be because the octupole is much stronger with respect to the quadrupole than in Kepler 108 because of the much higher semi-major axis ratio. Thus we questioned the convergence of the series in this case, and it turned out the series diverges, and this structure of equilibra, although very interesting, is not valid. The complete analysis of the convergence follows.
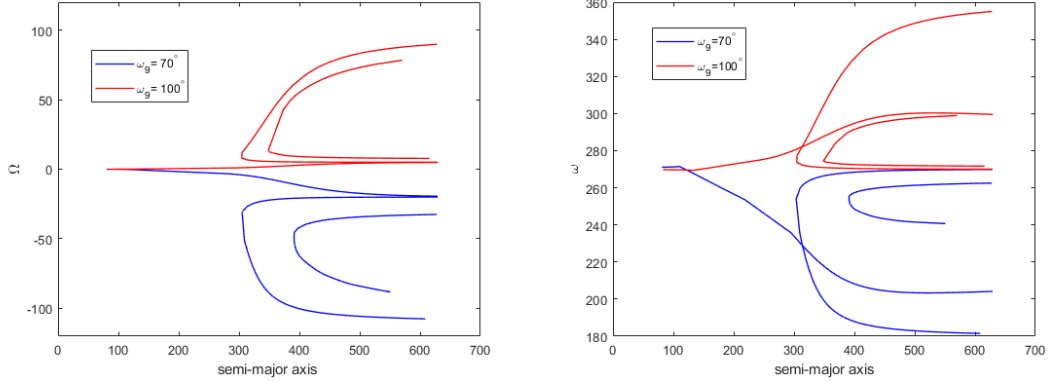
Figure 3.10: Variations in the orbital elements of $\Omega = 0, \omega = 3\pi/2$ solutions when we vary the apse of Planet IX for $\omega_\odot = 90°$ to $70°$ and $100°$. *Left*: Variation in the node. *Right*: Variation in the apse.

Robustness to Perturbation Variation

As we explained earlier, the significance of the octupole is that it broke the symmetry in the orientation of the orbit. This orientation is nonetheless dependent on the orientation of the perturber. The results we presented were for a specific orientation of the perturber, and although they're invalid because of the series divergence, but we can still check weather these octupole solutions are robust if we change the orientation of the perturber, or if they are fine tuned to its symmetric configuration and they would get wiped out upon that change. We did two variations, one in the apse of the outer perturber changing it from $\omega_\odot = \pi/2$, and the other in the node of the inner quadrupole, changing it from $\Omega_p = 0$.

Our analysis on variations showed us that the solutions are robust, and rather than being wiped out they are smoothly dragged upon the change in the perturbations' orientations. We present an example in which we slightly deviated the apse of Planet IX from $\omega_\odot = 90°$. The figures show the coplanar-coplanar families that were fixed with $\Omega = 0, \omega = 3\pi/2$, are deviating smoothly in the apse and the node from those values, parallel to the deviation of the planet, while maintaining the same eccentricity profile. Similar variations were observed when we varied the node of the inner quadrupole.

What we lose in these variations is the notion of the solutions being aligned or anti-aligned with the perturber. However, we maintain the clustering of the solutions in a single orientation especially that the observed eTNOs as we've seen follow the trend of one family of equilibria.

45

Solar Binary: Toy Model

After analyzing the variations in the solutions due to variations in the orientation of the perturbations, we now study variations due the strength of the perturbation, which for Planet XI is dependent on its mass, semi-major axis, and eccentricity, where the latter is of significance because it encodes the strength of the octupole specifically. Thus we replace P9 mass with a solar mass, and we regenerate equilibria for different eccentricities of this binary. The increase in mass increases the quadrupole and octupole strength by increasing $\varepsilon_\odot$, and this decreases r_L, while the increase in eccentricity increases more the strength of the octupole through $\varepsilon_\otimes$. We proceed blindly, yet aware that a solar mass instead of P9 could perturb the solar system: it may destabilize it by affecting the total angular momentum through perturbing the solar spin or the planets configuration. In fig.**??** below, we see as a function of the eccentricity of P9, how one family that was circular at the quadrupolar description for axisymmetric outer perturber, is turning eccentric. Consequently, nonlinear bifurcations that emerged for P9 case emerge in this case of a solar companion. The semi-major axis at which these bifurcations emerge is directly proportional to the eccentricity, typically because the octupole is stronger as $e_\odot$ increaese, and thus the particle will feel its effect at lower distances. The effect of the mass was also obvious as we see that for the same eccentricity of p9, the bifurcations are at lower distances.

Figure 3.11: Eccentricities of $\Omega = 0$ equilibria for the solar binary with $e_\odot$ going from 0.1 to 0.9.
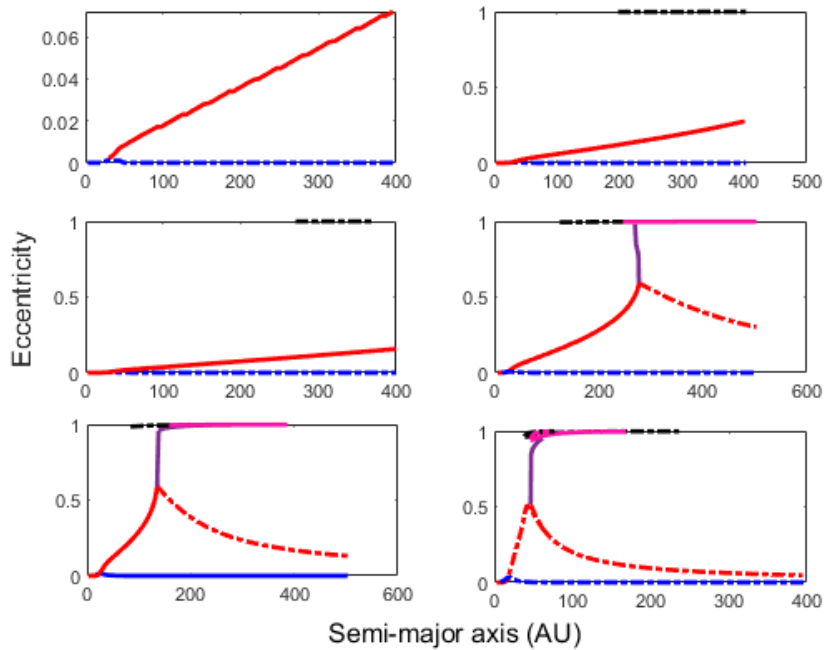
Questioning Convergence

These results, proven robust and analyzed extensively, were quite promising at first. We were able to produce anti-aligned highly eccentric stable equilibria for the suggested parameters, decently matching the eTNOs. But as we said, we realized that the multipoles diverge for the region of our interest. To realize that, we had to test the structure of equilibria as we add higher order terms and see their effect.

Defining $(\mathbf{e} \cdot \hat{\boldsymbol{u}}_\odot)$ as e_u, and so on for the rest of the vector products, the full construction of the hexadecapole is done in the Appendix, and it gives:

$$\langle\langle \Phi_{hex} \rangle\rangle = -\frac{315}{512}\varepsilon_\odot \Bigg[\varepsilon_\otimes^2 \Big(\frac{21}{2} e_n^4 + (16e^2 - 10)e_u^2 - 42e_n^2 e_u^2 + (6e^2 - 9)e_n^2$$

$$+ 14e_u^2 j_n^2 + (\frac{-72}{7}e^2 + \frac{2}{7})j_u^2 + 14e_n^2 j_u^2 + \frac{1}{2}j_n^4$$

$$+ (\frac{-62}{7}e^2 - \frac{1}{7})j_n^2 - 2j_n^2 j_u^2 - \frac{68}{7}e^4 + \frac{66}{7}e^2 - \frac{1}{70} \Big)$$

$$\frac{\varepsilon_\otimes^2}{e_\odot^2} \Big(21e_n^4 + (-20e^2 + 2)e_n^2 + (\frac{20}{7}e^2 - \frac{6}{7})j_n^2 + j_n^4$$

$$+ \frac{16}{7}e^4 - \frac{4}{7}e^2 + \frac{3}{35} \Big) \Bigg] \quad (3.9)$$

For the parameters used for the test on the solar binary in fig 3.12, orbit crossing occurs at $r = 280$A.U. As expected, at $\phi_\odot = 30°$, there are no eccentric solutions at the quadrupolar level, while they're present at $\phi_\odot = 70°$. Some of the solutions, specifically those emerging at low a, are not altered by higher orders, while others are disrupted as we impose higher order effects. Of course we have seen that the structure of equilibria is similar in the case of P9 to that of the solar binary, and the only difference is that the interesting equilibria bifurcate at a shorter distance in the case of the solar binary because of its stronger effect.

Hence the addition higher of order terms was destructive to our desirable structure of equilibria as we see in fig.3.12, and so we questioned the convergence of the multipoles expansion for such a setting. We have extensively studied the convergence in the Appendix by measuring the numerical magnitudes of the orders. Our results were very clear that the series converge for semi-major axis below 280 AU, which is the orbits crossing radius, and diverge for higher radii (The condition of convergence is discussed in details in the following chapter). We present a sample of the analysis here in fig. 3.13, and leave the completion of the discussion for the following chapters. This leaves us with no choice but to say that this approach of multipoles fails to describe the dynamics beyond Neptune for $a > 280AU$, and we are in need of an alternative approach that avoids the limitation of the parametric expansion. Thus in the next chapters, we appeal
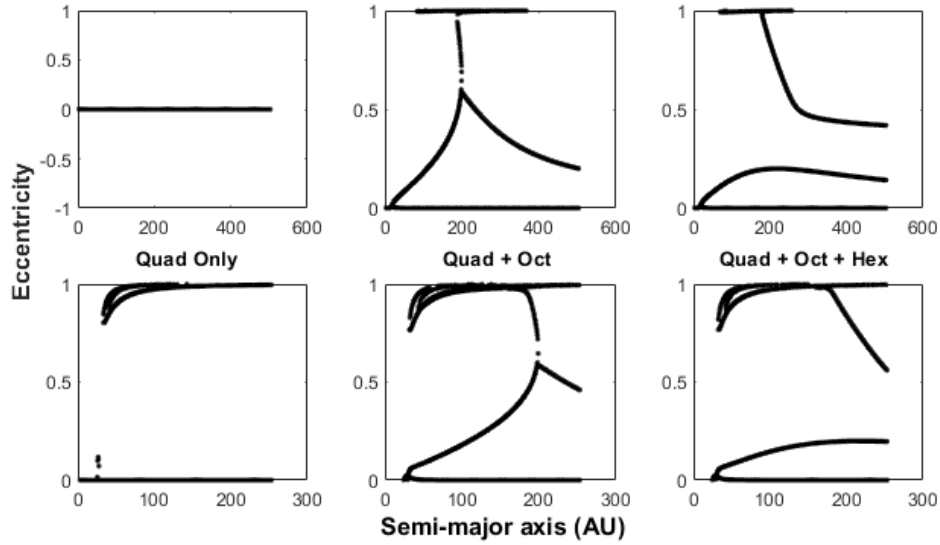
Figure 3.12: The effect of higher orders in the outer potential of the solar binary at 700 A.U, $e_\odot = 0.6$. The top panel is for and inclination of the binary of $30°$, the bottom is for $70°$. As expected, for quadrupoles only, we have no circular solutions in the top panel. Upon the introduction of the octupole, eccentric solutions emerge at such a mutual inclination. The effect of the hexadecapole is very clear in the disruption of equilibria generated by the octupole.

to a quasi-analytical quasi-numerical method to solve our problem; we explain further why the multipoles diverge, the condition of divergence, and how we can avoid that.
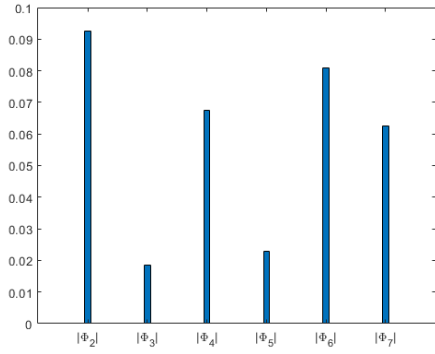
(a) e=0.1, a=400au
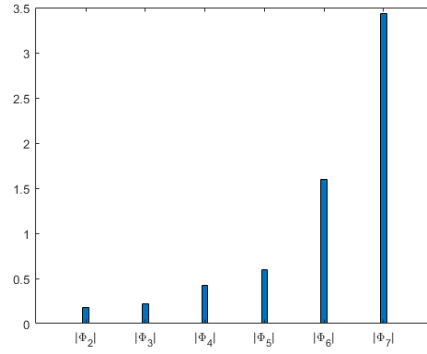
(b) e=0.8, a=400au
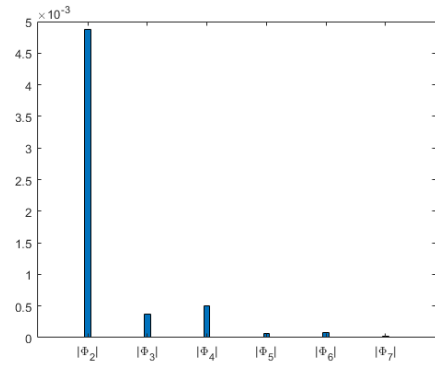
(c) e=0.1, a=150au
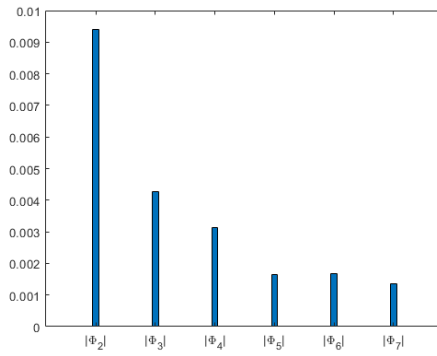
(d) e=0.8, a=150au

Figure 3.13: Numerical values of the orders in the potential expanded up to the 7th order in the planar case for different parameters of the solar binary setting at $a_\odot = 700\text{a.u.}$ and $e_\odot = 0.6$. As we can see, the magnitudes of the orders decay at a small semi-major axis ($a = 150a.u$), and grow for higher a semi-major axis ($a = 400a.u$). We studied the planar case because it was easier for us to expand into higher orders than the three-dimensional case, allowing us to see the trend more clearly. But a convergence analysis for a three-dimensional setting is also discussed in the appendix.

49

Chapter 4

Planet IX in Harmonics

4.1 The Gravitational Potential in Spherical Harmonics

As the parametric expansion failed for the Planet IX setting due to convergence issues, we try to recover the three-dimensional gravitational potential generated by the planet numerically by constructing the representative spherical harmonics and their associated modes. In general, a real function can be represented in terms of spherical harmonics

$$
f(\theta, \phi) = \sum_{l=0}^{\infty} \left[A_l^0(r) Y_l^0(\theta) + \sum_{m=1}^{m=l} A_l^m(r) \sqrt{\frac{2l+1}{4\pi} \frac{(l-m)!}{(l+m)!}} P_l^m(\cos\theta) \cos(m\phi + \Phi_l^m(r)) \right]
$$

(4.1)

where A_l^m's are the associated modes functions of the radii, and Φ_l^m's are the associated phase angles. Considering the orbit of the planet as a ring, and setting its plane as the reference plane, we numerically compute the modes, functions of the radius, of the gravitational potential of this ring, then we identify the most dominant of the them.

The first impression towards this approach is would be questioning why would this expansion work, while the multipoles expansion fails, although both expansions come down eventually to an expansion in Legendre Polynomials. This is true in certain ranges of radii, but the discrepancy arises in a specific range, and this range turns out to be our spatial region of interest.

The actual difference comes down to how each method deals with the distribution of mass in the ring of the perturber. For a certain ring of the particle, the multipoles expansion would be considering all the mass of the perturbation ring either outside or inside that ring. Thus for our test particles in question, if all are within or without the perturber's ring i.e. if $r_i < r_j$ or $r_i > r_j$ is maintained, for the radii corresponding to the particles and the perturber rings respectively, then the multipoles and the spherical harmonics expansion would
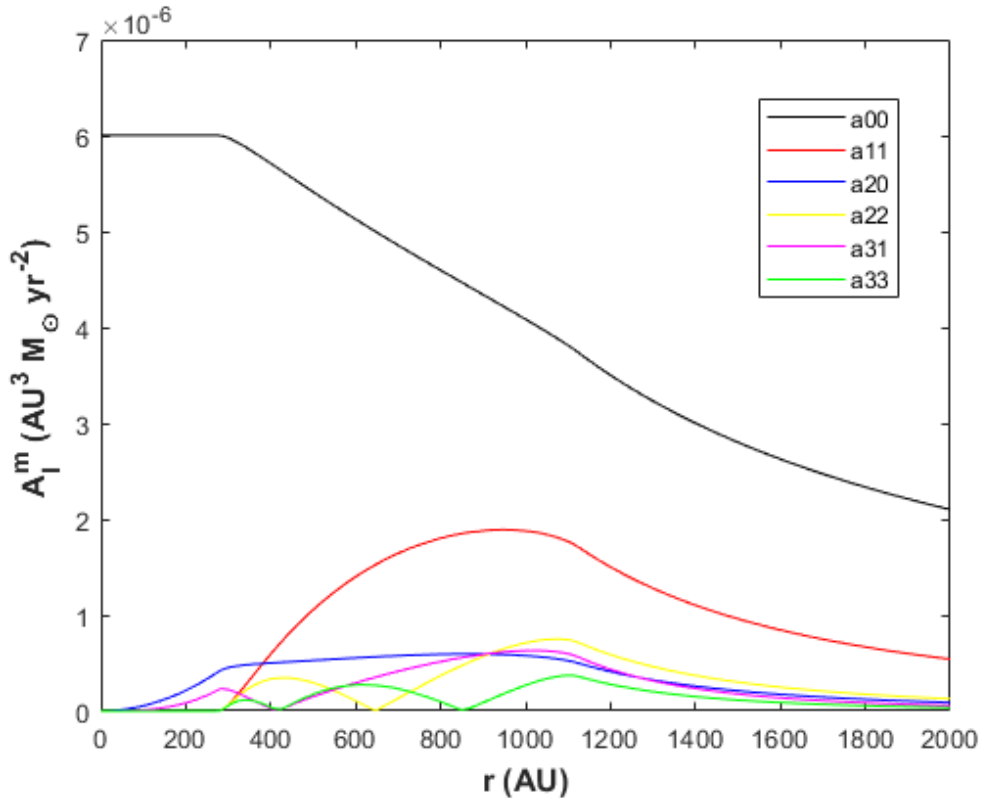
Figure 4.1: Relative absolute amplitudes of the dominant modes. We can clearing see the decaying trend of the modes as we increase their order.

yield an identical description of the interaction. This condition is clear in concentric circles, however considering an eccentric perturber, the particles' orbits have to be always within its periapse, or always outside its apoapse for a correct multipolar description. However in our case for P9, we're considering eccentric particles with semi-major axes in the intermediate range between the periapse and the apoapse, with orbital radii such that the mass distribution of the planet is sometimes within, othertimes outside, so the planet has contribution from within and without. The multipoles fails to account for such a distribution, in fact it is precisely within this range of interest where the orbit averaged multipoles series diverges, while the numerical computing of the harmonics series converges, yielding results that approach exact quadrature (fig 4.2), and we can see the modes decaying in magnitude as we increase the order (fig 4.1), hence this expansion succeeds in accounting for such a distribution.

We will study more the convergence of the harmonics in the following section when we compute our equilibria while truncating the expansion at different orders and observing the differences. We will also discuss more the difference between the multipoles and the harmonics.
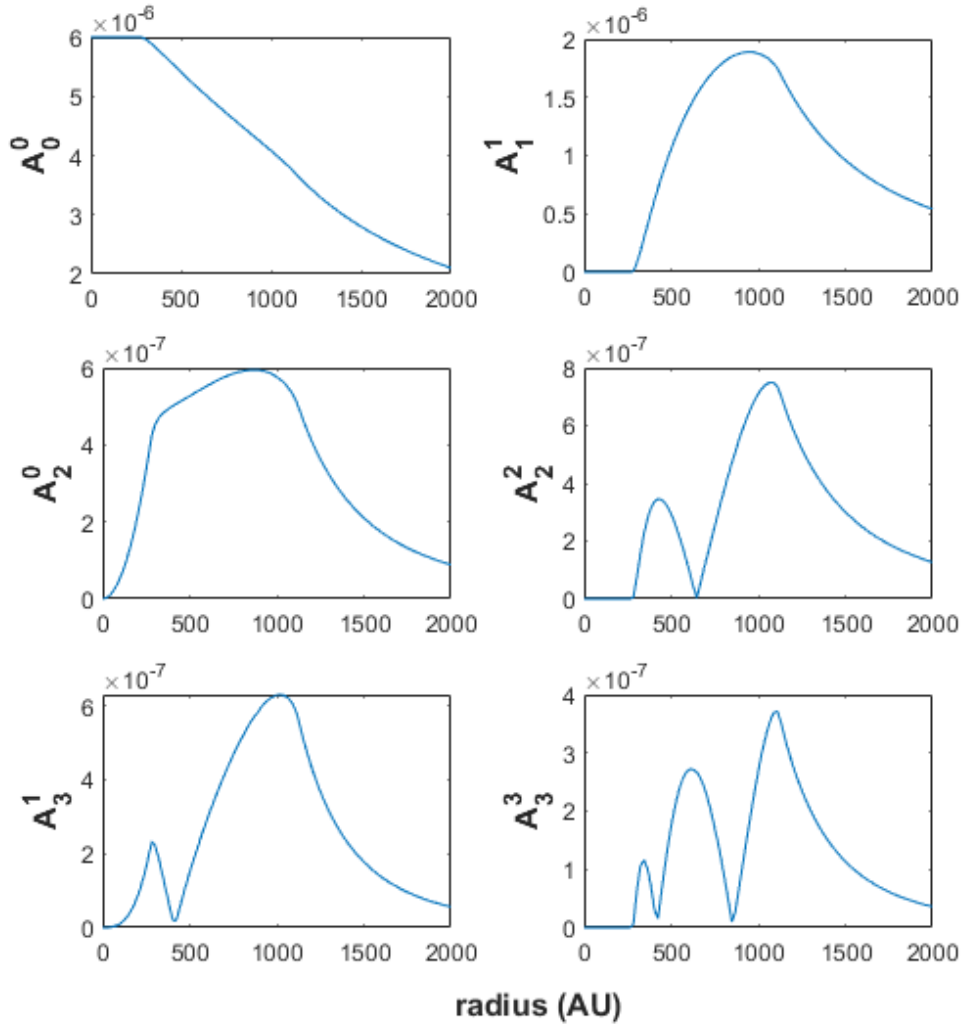
Figure 4.2: Absolute value amplitudes of the computed dominant modes. Some modes are negative over certain ranges of the radius. The behavior of higher order harmonics feature exact quadratures.

Identifying the dominant modes in the expansion, we get the following potential, where all the modes and phases are functions of the radius r:

$$
\begin{aligned}
\Phi_{p9}(r, \theta, \phi) ={}& A_0^0 Y_0^0 \cos \Phi_0^0 + A_1^1 Y_1^1 \cos \Phi_1^1 + A_2^0 Y_2^0 \cos \Phi_2^0 + A_2^2 Y_2^2 \cos \Phi_2^2 \\
& + A_3^1 Y_3^1 \cos \Phi_3^1 + A_3^3 Y_3^3 \cos \Phi_3^3 \quad\quad\quad\quad\quad\quad\quad (4.2)
\end{aligned}
$$

$$
\begin{aligned}
={}& -\frac{1}{\sqrt{4\pi}} A_0^0 - \sqrt{\frac{3}{8\pi}} \sin\theta \cos\phi A_1^1 + \sqrt{\frac{5}{16\pi}} (3\cos^2\theta - 1) A_2^0 \\
& + \sqrt{\frac{15}{32\pi}} \sin^2\theta \cos 2\phi \cos \Phi_2^2 A_2^2 - \sqrt{\frac{21}{64\pi}} \sin\theta (5\cos^2\theta - 1) \cos\phi \cos \Phi_3^1 A_3^1 \\
& + \sqrt{\frac{35}{64\pi}} \sin^3\theta \cos 3\phi \cos \Phi_3^3 A_3^3 \quad\quad\quad\quad\quad\quad\quad (4.3)
\end{aligned}
$$

where the phases $\Phi_2^2, \Phi_3^1, \Phi_3^3$ change over the range of r.

This potential is then to be averaged over the fast angle. Now to write our potential in vecotrial form we start by the transformation from the used spherical coordinates to the orbital elements:

$$
\begin{aligned}
x &= r\sin\theta\cos\phi = r\big[\cos(\Omega - \varpi_{p9})\cos(\omega + f) - \sin(\Omega - \varpi_{p9})\sin(\omega + f)\cos(i)\big] \\
y &= r\sin\theta\sin\phi = r\big[\sin(\Omega - \varpi_{p9})\cos(\omega + f) + \cos(\Omega - \varpi_{p9})\sin(\omega + f)\cos(i)\big] \\
z &= r\cos\theta = r\sin(\omega + f)\sin(i) \quad\quad\quad\quad\quad\quad\quad\quad\quad\quad\quad (4.4)
\end{aligned}
$$

Picking up the functions of the fast angle (the true anomaly f in this case) to be averaged, we define:

$$
f_{l,m,n}(a, e) = \langle A_l^m(r) \cos(nf) \rangle \quad\quad\quad\quad\quad\quad (4.5)
$$

We then transform from orbital elements to vector notation using the definition of the angular momentum and eccentricity vectors as:

$$
\mathbf{j} = \sqrt{1 - e^2} \begin{pmatrix} \sin i \sin \Omega \\ -\sin i \cos \Omega \\ \cos i \end{pmatrix} \quad\quad\quad\quad\quad\quad (4.6)
$$

$$
\mathbf{e} = e \begin{pmatrix} \cos\omega \cos\Omega - \sin\omega \cos i \sin\Omega \\ \cos\omega \sin\Omega + \sin\omega \cos i \cos\Omega \\ \sin\omega \sin i \end{pmatrix} \quad\quad\quad\quad\quad\quad (4.7)
$$

we get:

$$
\bar{\Phi}_{p9} = -\frac{1}{\sqrt{4\pi}} f_{0,0,0} + \sqrt{\frac{3}{8\pi}} f_{1,1,1}(\hat{\boldsymbol{u}} \cdot \hat{\boldsymbol{u}}_\odot)
$$

$$
+ \sqrt{\frac{5}{16\pi}} \Big[f_{2,0,0}\big(\tfrac{1}{2} - \tfrac{3}{2}(\hat{\boldsymbol{n}} \cdot \hat{\boldsymbol{n}}_\odot)^2\big) - \tfrac{3}{2} f_{2,0,2}\big(1 - (\hat{\boldsymbol{n}} \cdot \hat{\boldsymbol{n}}_\odot)^2 - 2(\hat{\boldsymbol{u}} \cdot \hat{\boldsymbol{n}}_\odot)^2\big) \Big]
$$

$$
+ \sqrt{\frac{15}{32\pi}} \Big[f_{2,2,0}\big(\tfrac{1}{2} - (\hat{\boldsymbol{n}} \cdot \hat{\boldsymbol{u}}_\odot)^2 - \tfrac{1}{2}(\hat{\boldsymbol{n}} \cdot \hat{\boldsymbol{n}}_\odot)^2\big)
$$

$$
+ f_{2,2,2}\big(-\tfrac{3}{2} + 2(\hat{\boldsymbol{u}} \cdot \hat{\boldsymbol{u}}_\odot)^2 + (\hat{\boldsymbol{n}} \cdot \hat{\boldsymbol{u}}_\odot)^2 + (\hat{\boldsymbol{u}} \cdot \hat{\boldsymbol{n}}_\odot)^2 + \tfrac{1}{2}(\hat{\boldsymbol{n}} \cdot \hat{\boldsymbol{n}}_\odot)^2\big) \Big]
$$

$$
+ \sqrt{\frac{21}{64\pi}} \Big[f_{3,1,1}\Big((\hat{\boldsymbol{u}} \cdot \hat{\boldsymbol{u}}_\odot) - \tfrac{5}{4}\big((\hat{\boldsymbol{u}} \cdot \hat{\boldsymbol{u}}_\odot)(1 - (\hat{\boldsymbol{n}} \cdot \hat{\boldsymbol{n}}_\odot)^2) - 2(\hat{\boldsymbol{n}} \cdot \hat{\boldsymbol{u}}_\odot)(\hat{\boldsymbol{u}} \cdot \hat{\boldsymbol{n}}_\odot)(\hat{\boldsymbol{n}} \cdot \hat{\boldsymbol{n}}_\odot)\big)\Big)
$$

$$
- \tfrac{5}{4} f_{3,1,3}\Big((\hat{\boldsymbol{u}} \cdot \hat{\boldsymbol{u}}_\odot)(4(\hat{\boldsymbol{u}} \cdot \hat{\boldsymbol{n}}_\odot)^2 + (\hat{\boldsymbol{n}} \cdot \hat{\boldsymbol{n}}_\odot)^2 - 1) + 2(\hat{\boldsymbol{n}} \cdot \hat{\boldsymbol{u}}_\odot)(\hat{\boldsymbol{u}} \cdot \hat{\boldsymbol{n}}_\odot)(\hat{\boldsymbol{n}} \cdot \hat{\boldsymbol{n}}_\odot)\Big) \Big]
$$

$$
+ \tfrac{3}{4}\sqrt{\frac{35}{64\pi}} \Big[f_{3,3,1}\Big((\hat{\boldsymbol{u}} \cdot \hat{\boldsymbol{u}}_\odot)(-4(\hat{\boldsymbol{n}} \cdot \hat{\boldsymbol{u}}_\odot)^2 - (\hat{\boldsymbol{n}} \cdot \hat{\boldsymbol{n}}_\odot)^2 + 1) - 2(\hat{\boldsymbol{n}} \cdot \hat{\boldsymbol{u}}_\odot)(\hat{\boldsymbol{u}} \cdot \hat{\boldsymbol{n}}_\odot)(\hat{\boldsymbol{n}} \cdot \hat{\boldsymbol{n}}_\odot)\Big)
$$

$$
+ f_{3,3,3}\Big(+\tfrac{16}{3}(\hat{\boldsymbol{u}} \cdot \hat{\boldsymbol{u}}_\odot)^3 + (\hat{\boldsymbol{u}} \cdot \hat{\boldsymbol{u}}_\odot)(4(\hat{\boldsymbol{n}} \cdot \hat{\boldsymbol{u}}_\odot)^2 + 4(\hat{\boldsymbol{u}} \cdot \hat{\boldsymbol{n}}_\odot)^2 + (\hat{\boldsymbol{n}} \cdot \hat{\boldsymbol{n}}_\odot)^2 - 5)
$$

$$
- 2(\hat{\boldsymbol{n}} \cdot \hat{\boldsymbol{u}}_\odot)(\hat{\boldsymbol{u}} \cdot \hat{\boldsymbol{n}}_\odot)(\hat{\boldsymbol{n}} \cdot \hat{\boldsymbol{n}}_\odot)\Big) \Big] \tag{4.8}
$$

Using $\mathbf{e} = e\hat{\mathbf{u}}$, and $\mathbf{j} = \sqrt{1 - e^2}\hat{\mathbf{n}}$ we can write:

$$
\begin{aligned}
\bar{\Phi}_{p9} =& \Phi_0(e) + \Phi_1(e)(\mathbf{e} \cdot \hat{\mathbf{u}}_\odot) + \Phi_2(e)(\mathbf{j} \cdot \hat{\mathbf{n}}_\odot)^2 + \Phi_3(e)(\mathbf{e} \cdot \hat{\mathbf{n}}_\odot)^2 + \Phi_4(e)(\mathbf{j} \cdot \hat{\mathbf{u}}_\odot)^2 \\
&+ \Phi_5(e)(\mathbf{e} \cdot \hat{\mathbf{u}}_\odot)^2 + \Phi_6(e)(\mathbf{e} \cdot \hat{\mathbf{u}}_\odot)(\mathbf{j} \cdot \hat{\mathbf{n}}_\odot)^2 + \Phi_7(e)(\mathbf{e} \cdot \hat{\mathbf{n}}_\odot)(\mathbf{j} \cdot \hat{\mathbf{u}}_\odot)(\mathbf{j} \cdot \hat{\mathbf{n}}_\odot) \\
&+ \Phi_8(e)(\mathbf{e} \cdot \hat{\mathbf{u}}_\odot)(\mathbf{e} \cdot \hat{\mathbf{n}}_\odot)^2 + \Phi_9(e)(\mathbf{e} \cdot \hat{\mathbf{u}}_\odot)(\mathbf{j} \cdot \hat{\mathbf{u}}_\odot)^2 + \Phi_{10}(e)(\mathbf{e} \cdot \hat{\mathbf{u}}_\odot)^3 \quad (4.9)
\end{aligned}
$$

with the functions $\Phi_i(e)$ defined:

$$
\Phi_0(e) = -\frac{1}{\sqrt{4\pi}} f_{0,0,0} + \frac{1}{2}\sqrt{\frac{5}{16\pi}}[f_{2,0,0} - 3f_{2,0,2}] + \frac{1}{2}\sqrt{\frac{15}{32\pi}}\Big[f_{2,2,0} - 3f_{2,2,2}\Big]
$$

$$
\Phi_1(e) = \frac{1}{e}\bigg[\sqrt{\frac{3}{8\pi}}f_{1,1,1} + \frac{1}{4}\sqrt{\frac{21}{64\pi}}\Big[-f_{3,1,1} + 5f_{3,1,3}\Big] + \frac{3}{4}\sqrt{\frac{35}{64\pi}}\Big[f_{3,3,1} - 5f_{3,3,3}\Big]\bigg]
$$

$$
\Phi_2(e) = \frac{1}{1-e^2}\bigg[\frac{3}{2}\sqrt{\frac{5}{16\pi}}\Big[-f_{2,0,0} + f_{2,0,2}\Big] + \frac{1}{2}\sqrt{\frac{15}{32\pi}}\Big[-f_{2,2,0} + f_{2,2,2}\Big]\bigg]
$$

$$
\Phi_3(e) = \frac{1}{e^2}\bigg[3\sqrt{\frac{5}{16\pi}}f_{2,0,2} + \sqrt{\frac{15}{32\pi}}f_{2,2,2}\bigg]
$$

$$
\Phi_4(e) = \frac{1}{1-e^2}\bigg[\sqrt{\frac{15}{32\pi}}\Big[-f_{2,2,0} + 2f_{2,2,2}\Big]\bigg]
$$

$$
\Phi_5(e) = \frac{1}{e^2}\bigg[2\sqrt{\frac{15}{32\pi}}f_{2,2,2}\bigg]
$$

$$
\Phi_6(e) = \frac{1}{e(1-e^2)}\bigg[\frac{5}{4}\sqrt{\frac{21}{64\pi}}\Big[f_{3,1,1} - f_{3,1,3}\Big] + \frac{3}{4}\sqrt{\frac{35}{64\pi}}\Big[-f_{3,3,1} + f_{3,3,3}\Big]\bigg]
$$

$$
\Phi_7(e) = \frac{1}{e(1-e^2)}\bigg[\frac{5}{2}\sqrt{\frac{21}{64\pi}}\Big[f_{3,1,1} - f_{3,1,3}\Big] + \frac{3}{2}\sqrt{\frac{35}{64\pi}}\Big[-f_{3,3,1} + f_{3,3,3}\Big]\bigg]
$$

$$
\Phi_8(e) = \frac{1}{e^3}\bigg[-5\sqrt{\frac{21}{64\pi}}f_{3,1,3} + 3\sqrt{\frac{35}{64\pi}}f_{3,3,3}\bigg]
$$

$$
\Phi_9(e) = \frac{1}{e(1-e^2)}\bigg[3\sqrt{\frac{35}{64\pi}}\Big[-f_{3,3,1} + f_{3,3,3}\Big]\bigg]
$$

$$
\Phi_{10}(e) = \frac{1}{e^3}\bigg[4\sqrt{\frac{35}{64\pi}}f_{3,3,3}\bigg]
$$

From here on, the analysis will be basically based on studying the contributions of the modes: $A_0^0, A_1^1, A_2^0, A_3^1$ then trying to see how the contribution of the higher order modes: A_2^2, A_3^3 change results.
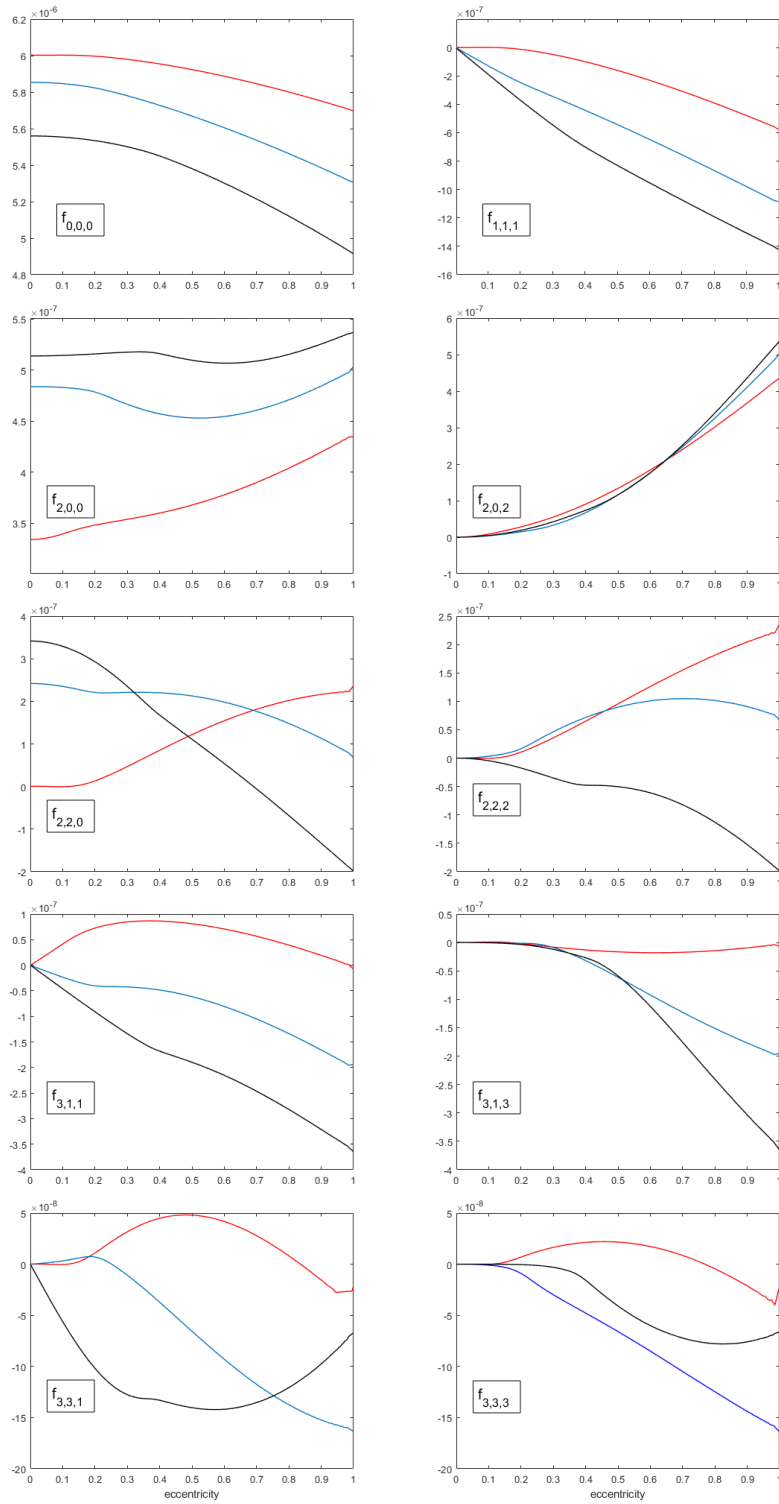
Figure 4.3: Averaged functions $f_{l,m,n}$(a,e) defined by eq4.5. Plots are for semi-major axes: 250 AU (Red), 350 AU (Blue), 450 AU (Black)

4.1.1 Comparison Against Multipoles Expansion

As we have seen earlier, the multipoles expansion is invalid for our study because the series diverges fast enough without allowing us to maintain a picture of fixed orbits over our desired wide range of semi-major axes. To see where things go wrong, we compare the potentials produced by the multipolar expansion (up to the octupole), with that produced by harmonics. As we see in figure 4.4, the two expansions agree up to a certain semi-major axis in each case. The semi-major axis at which the discrepancy starts emerging depends on the eccentricity of the orbit. As the eccentricity increases, the range over which agreement is established shrinks.

The agreement region, which we will call the convergence region of the multipoles series, that we observe in this analysis is in fact consistent with an extensive study of the convergence region in the expansion of the averaged direct part of the disturbing function (36)(37). In this work, the authors show that although the role of the formal parameter in the power series expansion is played by

$$X_{i,j} = \frac{a_i}{a_j(1 - e_j^2)} \tag{4.10}$$

for an interaction between two bodies i, j orbiting a third body, and that it is a requirement for the series to converge that $X_{i,j}$ be less than 1, they claim that divergence flows from a different source: the convergence limit of the expansion is simply interpreted as the condition for the collision line. Hence the "anti-collision line" defined as

$$a_j(1 - e_j) = a_i(1 + e_i) \tag{4.11}$$

The series diverges above this line and the positions of equilibria are strongly distorted. Hence in our case we expect convergence of the multipoles expansion when the apocenter of the inner orbit is inside the pericenter of the outer orbit, i.e for P9 case:

$$\tag{4.12}$$

$$a(1 + e) < 700AU(1 - 0.6)$$
$$< 280AU \tag{4.13}$$

This condition was clearly manifested in our convergence analysis in the previous chapter and in the Appendix, and is also clear in the following figures of comparison between the analytic expansion in multipoles and the numerical expansion in spherical harmonics. As we said earlier also, the Harmonics expansion avoids this limitation by correctly modelling the distribution of mass in the outer ring in a region where the rings cross.
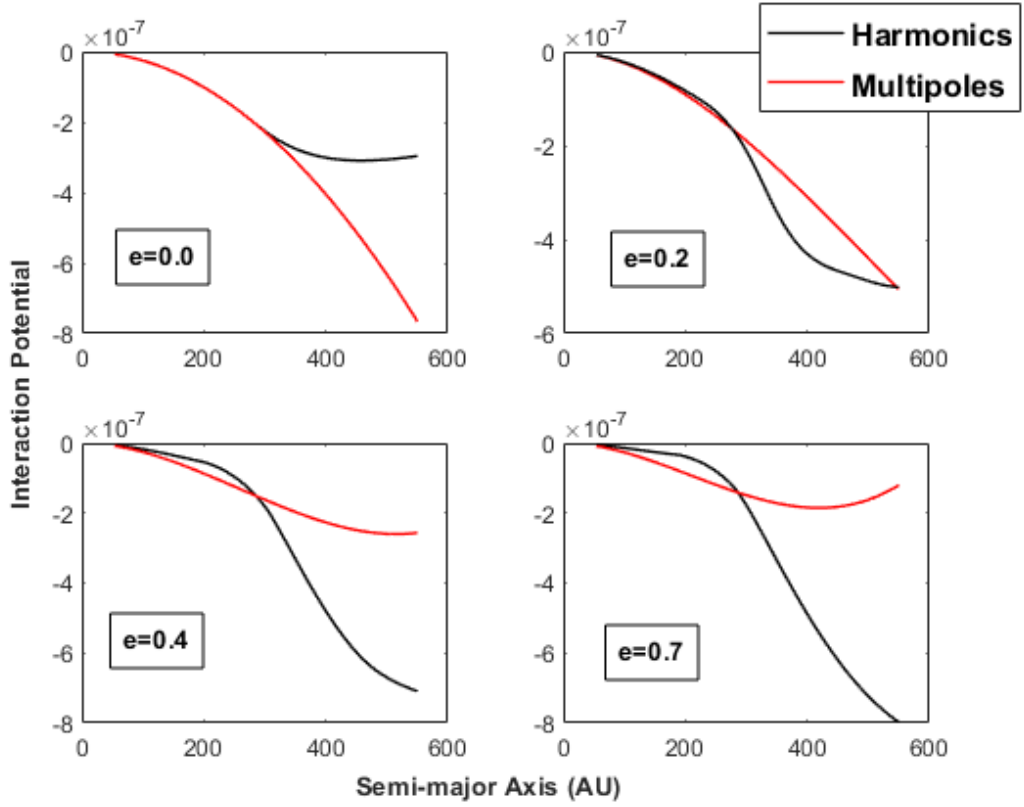
Figure 4.4: Comparison between Planet IX potentials generated by multipolar expansion up to the octupole, and numerical harmonics expansion. The eccentricities are for our particle. We see the agreement of both potentials in the region abiding by the condition we discussed in the previous section i.e. when the particle's orbit is totally inside the ring of the perturber. When the particle occurs on radii at which the ring contributes from within and without, the multipoles expansion fails, while the numerical expansion succeeds. Thus we see the agreement between the potentials clearly up to 280 AU (the periapse of Planet IX.

4.1.2 Equations of Motion

Using the Milankovich vector equations defined earlier, we produce the contribution of P9 in the dynamical equations of motion, added to the contribution of the inner quadrupole generated by the outer massive planets. Let $\mathbf{j} \cdot \hat{\boldsymbol{n}}_\odot = j_n$, $\mathbf{e} \cdot \hat{\boldsymbol{u}}_\odot = e_u$ and so on, we have:

$$
\begin{aligned}
L\frac{d\mathbf{j}}{dt} = & +\Gamma\frac{\mathbf{j}\cdot\hat{\boldsymbol{n}}_{\boldsymbol{p}}}{(1-e^2)^{\frac{5}{2}}}(\mathbf{j}\times\hat{\boldsymbol{n}}_{\boldsymbol{p}}) \\
& -\Big[2\Phi_2(e)j_n + 2\Phi_6(e)j_n e_u + \Phi_7(e)e_n j_u\Big](\mathbf{j}\times\hat{\boldsymbol{n}}_\odot) \\
& -\Big[\Phi_7(e)e_n j_n + 2\Phi_4(e)j_u + 2\Phi_9(e)e_u j_u\Big](\mathbf{j}\times\hat{\boldsymbol{u}}_\odot) \\
& -\Big[\Phi_1(e) + \Phi_6(e)j_n^2 + \Phi_8(e)e_n^2 + 2\Phi_5(e)e_u + 3\Phi_{10}(e)e_u^2\Big](\mathbf{e}\times\hat{\boldsymbol{u}}_\odot) \\
& -\Big[2\Phi_3(e)e_n + 2\Phi_8(e)e_u e_n + \Phi_7(e)j_u j_n\Big](\mathbf{e}\times\hat{\boldsymbol{n}}_\odot) \quad\quad (4.14)
\end{aligned}
$$

$$
\begin{aligned}
L\frac{d\mathbf{e}}{dt} = & +\Gamma\frac{\mathbf{j}\cdot\hat{\boldsymbol{n}}_{\boldsymbol{p}}}{(1-e^2)^{\frac{5}{2}}}(\mathbf{e}\times\hat{\boldsymbol{n}}_{\boldsymbol{p}}) - \frac{\Gamma}{2}\frac{1-e^2-5(\mathbf{j}\cdot\hat{\boldsymbol{n}}_{\boldsymbol{p}})^2}{(1-e^2)^{\frac{7}{2}}}(\mathbf{j}\times\mathbf{e}) \\
& -\Big[2\Phi_2(e)j_n + 2\Phi_6(e)j_n e_u + \Phi_7(e)e_n j_u\Big](\mathbf{e}\times\hat{\boldsymbol{n}}_{\boldsymbol{d}}) \\
& -\Big[\Phi_7(e)e_n j_n + 2\Phi_4(e)j_u + 2\Phi_9(e)e_u j_u\Big](\mathbf{e}\times\hat{\boldsymbol{u}}_{\boldsymbol{d}}) \\
& -\Big[\Phi_1(e) + \Phi_6(e)j_n^2 + \Phi_8(e)e_n^2 + 2\Phi_5(e)e_u + 3\Phi_{10}(e)e_u^2\Big](\mathbf{j}\times\hat{\boldsymbol{u}}_{\boldsymbol{d}}) \\
& -\Big[2\Phi_3(e)e_n + 2\Phi_8(e)e_u e_n + \Phi_7(e)j_u j_n\Big](\mathbf{j}\times\hat{\boldsymbol{n}}_{\boldsymbol{d}}) \\
& -\Big[D_0 + D_1 e_u + D_2 j_n^2 + D_3 e_n^2 + D_4 j_u^2 + D_5 e_u^2 + D_6 e_u j_n^2 \\
& \quad\quad + D_7 e_n j_u j_n + D_8 e_u e_n^2 + D_9 e_u j_u^2\Big](\mathbf{j}\times\mathbf{e}) \quad\quad (4.15)
\end{aligned}
$$

Where we have defined, for $i = 1..4$ corresponding to the outer massive planets:

$$
\Gamma = \frac{3}{4}\frac{GM_\odot}{a}\sum_{i=1}^{i=4}\frac{m_i a_i^2}{M_\odot a^2} \quad\quad (4.16)
$$

and we used the notation:

$$
\frac{1}{e}\frac{d\Phi_i}{de} = D_i(e) \quad\quad (4.17)
$$

4.2 Precession Rates

4.2.1 Inner Quadrupole Action

Before looking for stationary orbits we study rates of apse precession over ranges of orbital parameters. Apsidal precession of test particles is dictated by troques from the inner massive planets and from the P9 itself. Given the contribution of the inner quadrupole as:

$$\Psi_p = \frac{\Gamma}{6(1-e^2)^{3/2}}[3\cos^2 i - 1]$$

$$= \frac{\Gamma}{6l^3}[3\cos^2 i - 1] \tag{4.18}$$

for $l = \sqrt{1-e^2}$.

$$L\dot{\varpi} = \frac{\sqrt{1-e^2}}{e}\frac{\partial \Psi_p}{\partial e} + \frac{\tan \frac{i}{2}}{\sqrt{1-e^2}}\frac{\partial \Psi_p}{\partial i}$$

$$= -\frac{\partial \Psi_p}{\partial l} + \frac{1}{l}\tan\frac{i}{2}\frac{\partial \Psi_p}{\partial i}$$

$$= \frac{\Gamma}{2l^4}[5\cos^2 i - 2\cos i - 1] \tag{4.19}$$

for $L = na^2 = \sqrt{GM_{\odot}a}$ the constant angular momentum conjugate to the mean anomaly, with mean motion n. In the case of the solar system, the inner quadrupole is defined in Table 4.1:

Table 4.1: Properties of outer planets

Planet	a	m	$a^2m/M_{\odot}$
	(AU)	$(10^{24}Kg)$	AU^2
Jupiter	5.203	1898	0.0258
Saturn	9.537	568	0.0260
Uranus	19.191	86.8	0.0161
Neptune	30.069	102	0.0464

Thus for the planets contribution:

$$\dot{\varpi}\Big|_{planets} = \frac{1}{l^4}[5\cos^2 i - 2\cos i - 1]\frac{0.2692AU^{7/2}}{a^{7/2}}yr^- \tag{4.20}$$

Thus for coplanar $(i = 0°)$, circular equilibria, we have an apsidal precession rate ranging between $1.3 \times 10^{-8}yr^-$ and $1.4 \times 10^{-10}yr^-$ for a between 150 and $550AU$. More elaborate analysis is shown in the following figures.

Figure 4.5: Apsidal precession rates driven by the effect of the massive planets for coplanar orbits at different eccentricities over a range of semi-major axes. As the inner quadrupole is axisymmetric these rates do not differ between different apse alignment configurations of the orbits. Orbits of higher eccentricity have higher rates, reaching $3.5 \times 10^{-7} yr^{-}$ for $e = 0.9$
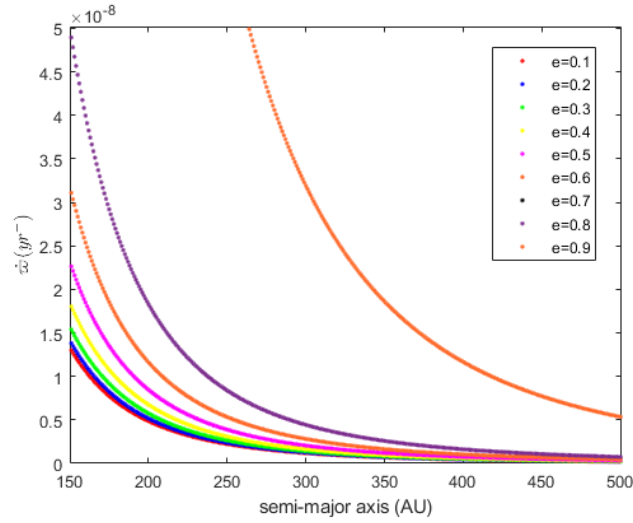
Figure 4.6: Apsidal precession at different orbit inclinations for $e = 0.3, e = 0.9$. As expected, this prograde precession is attenuated as the inclination increases.
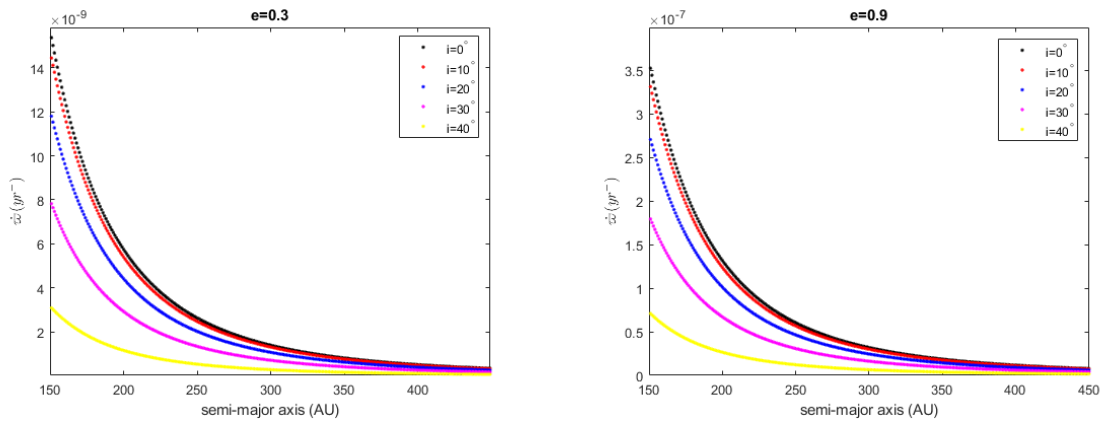
4.2.2 P9 Action

Planet IX contribution is again, written in vector notation up to most dominant lower order modes:

$$\bar{\Phi}_{p9} = \Phi_0(e) + \Phi_1(e)(\mathbf{e} \cdot \hat{\boldsymbol{u}}_\odot) + \Phi_2(e)(\mathbf{j} \cdot \hat{\boldsymbol{n}}_\odot)^2 + \Phi_3(e)(\mathbf{e} \cdot \hat{\boldsymbol{n}}_\odot)^2 + \Phi_6(e)(\mathbf{e} \cdot \hat{\boldsymbol{u}}_\odot)(\mathbf{j} \cdot \hat{\boldsymbol{n}}_\odot)^2$$
$$+ \Phi_7(e)(\mathbf{e} \cdot \hat{\boldsymbol{n}}_\odot)(\mathbf{j} \cdot \hat{\boldsymbol{u}}_\odot)(\mathbf{j} \cdot \hat{\boldsymbol{n}}_\odot) + \Phi_8(e)(\mathbf{e} \cdot \hat{\boldsymbol{u}}_\odot)(\mathbf{e} \cdot \hat{\boldsymbol{n}}_\odot)^2$$

with the functions $\Phi_i(e)$ defined earlier. This can be written in coplanar-coplanar configuration as:

$$\bar{\Phi}_{p9} = \cos\alpha\left[\Psi_1(e) + \frac{3}{4}\Psi_3(e)\right] + \cos 2\alpha\left[\frac{1}{2}\Psi_2(e)\right] + \cos 3\alpha\left[\frac{1}{4}\Psi_3(e)\right] + \frac{1}{2}\Psi_2(e) + \Psi_4(e) \tag{4.21}$$

for $\alpha = (i - i_9)$ for the functions $\Psi_i(e)$ defined in terms of $\Phi_i(e)$ for aligned and anti-aligned configurations as:

$$\Psi_1(e) = \left[\pm \Phi_8(e) \pm \Phi_7(e)\right]e^3 + \left[\pm \Phi_1(e) \mp \Phi_7(e)\right]e$$
$$\Psi_2(e) = \left[-\Phi_2(e) - \Phi_3(e)\right]e^2 + \Phi_2(e)$$
$$\Psi_3(e) = \left[\mp \Phi_8(e) \mp \Phi_7(e) \mp \Phi_6(e)\right]e^3 + \left[\pm \Phi_6(e) \pm \Phi_7(e)\right]e$$
$$\Psi_6(e) = \Phi_0(e) + \Phi_3(e)e^2 \tag{4.22}$$

To find the apsidal precession contribution of the planet, we find first:

$$\frac{\partial \bar{\Phi}_{p9}}{\partial e} = \cos\alpha\left[\frac{\partial \Psi_1(e)}{\partial e} + \frac{3}{4}\frac{\partial \Psi_3(e)}{\partial e}\right] + \cos 2\alpha\left[\frac{1}{2}\frac{\partial \Psi_2(e)}{\partial e}\right] + \cos 3\alpha\left[\frac{1}{4}\frac{\partial \Psi_3(e)}{\partial e}\right]$$
$$+ \frac{1}{2}\frac{\partial \Psi_2(e)}{\partial e} + \frac{\partial \Psi_4(e)}{\partial e} \tag{4.23}$$

$$\frac{\partial \bar{\Phi}_{p9}}{\partial i} = -\left[\Psi_1(e) + \frac{3}{4}\Psi_3(e)\right]\sin\alpha - 2\sin 2\alpha\,\Psi_2(e) - \frac{3}{4}\Psi_3(e)\sin 3\alpha \tag{4.24}$$

Thus we can calculate:

$$L\dot{\varpi}_{p9} = \frac{\sqrt{1-e^2}}{e}\frac{\partial \Psi_p}{\partial e} + \frac{\tan\frac{i}{2}}{\sqrt{1-e^2}}\frac{\partial \Psi_p}{\partial i} \tag{4.25}$$

After computing the precession rates driven by Planet IX, we add these rates to those driven by the inner quadrupole and check for for different eccentricities if we can freeze the orbits in space. We did the analysis for planar and inclined configurations. Planar total rates are shown in the figure below.
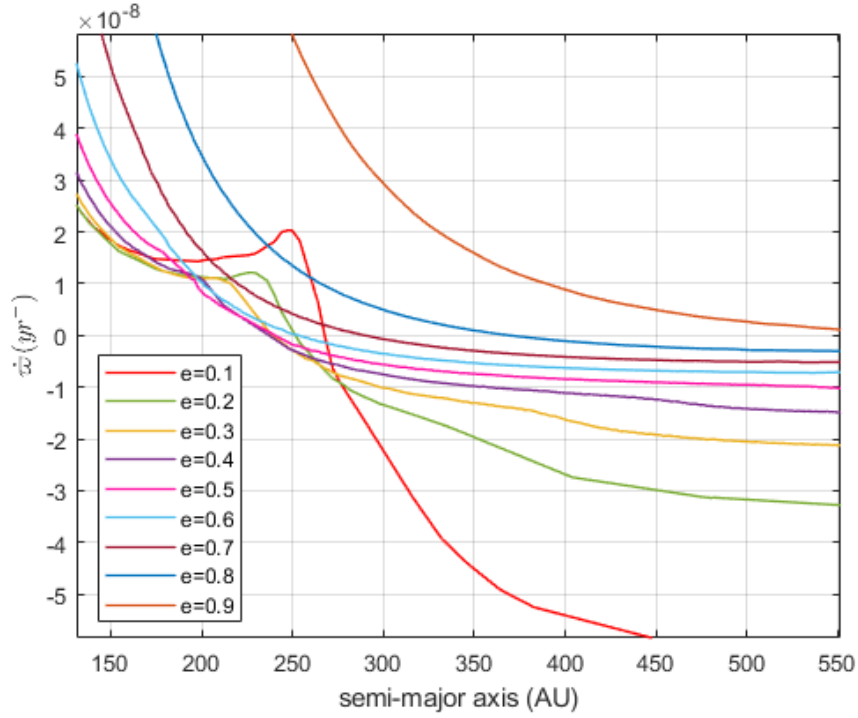
Figure 4.7: Total apsidal precession rates for orbits anti-aligned with Planet IX driven by the sum of the effects of the massive planets and Planet IX for coplanar orbits at different eccentricities over a range of semi-major axes.

Clearly, Planet IX can cancel the prograde precession driven by the inner quadrupole for all eccentricities. The figure predicts that anti-aligned highly eccentric equilbira can be reached over moderate distances (e=0.7 at 290 AU, e=0.8 at 370 AU). The figure also indicates that we start seeing stationary anti-aligned orbits after $a = 230 AU$.

4.3 Equilibria

4.3.1 Planar Case

We first inspect the existence of equilibria in a coplanar configuration i.e. where Planet IX and the inner quadrupole reside in the same plane. This case has been extensively studied, with different approaches of modelling the potential. In (34), the phase portraits of the planar Hamiltonian that retains the perturbation of Planet IX up to the octupole order showed only a libration island that is apsidally aligned with the perturber, and is of increasing eccentricity as a function of distance. The secular phase portraits of the un-truncated planar Hamiltonian computed exactly in (38), with the same conditions of the perturber as (34), show an extra stable anti-aligned family that emerges after a=250 AU.

The apsidal precession rates plotted in show that we have orbits anti-aligned with the perturber with zero precession with eccentricities up to e=0.9. So we have managed to produce with the spherical harmonics expansion the anti-aligned family that is not present in the multipoles expansion of (34), but is present in (38).

In the planar case, our Hamiltonian reduces to:

$$\bar{\Phi}_{planar} = -\frac{\Gamma}{3j^3} + \Phi_0(e) + \Phi_1(e)e\cos\Delta\varpi + \Phi_2(e)j^2 + \Phi_5(e)e^2\cos^2\Delta\varpi$$
$$+ \Phi_6(e)j^2 e\cos\Delta\varpi + \Phi_{10}(e)e^3\cos^3\Delta\varpi \tag{4.26}$$

while the equations of motion reduce to one equation of motion as the angular momentum equation is trivially satisfied:

$$L\frac{d\mathbf{e}}{dt} = \left[\Gamma\frac{e}{(1-e^2)^2} \mp \Phi_1(e)j + 2\Phi_2(e)ej - 2\Phi_5(e)ej \pm \Phi_6(e)j(3e^2-1) \mp 3\Phi_{10}(e)e^2 j \right.$$
$$\left. - D_0(e)je \mp D_1(e)e^2 j - D_2(e)j^3 e - D_5(e)e^3 j \mp D_6(e)e^2 j^3 \mp D_{10}(e)e^4 j \right]\hat{v}_{\odot} \tag{4.27}$$

With these we investigate the phase space and associated equilibria. As we mentioned earlier, our analysis will be based on lower order terms, then we add higher order terms to see their effect.
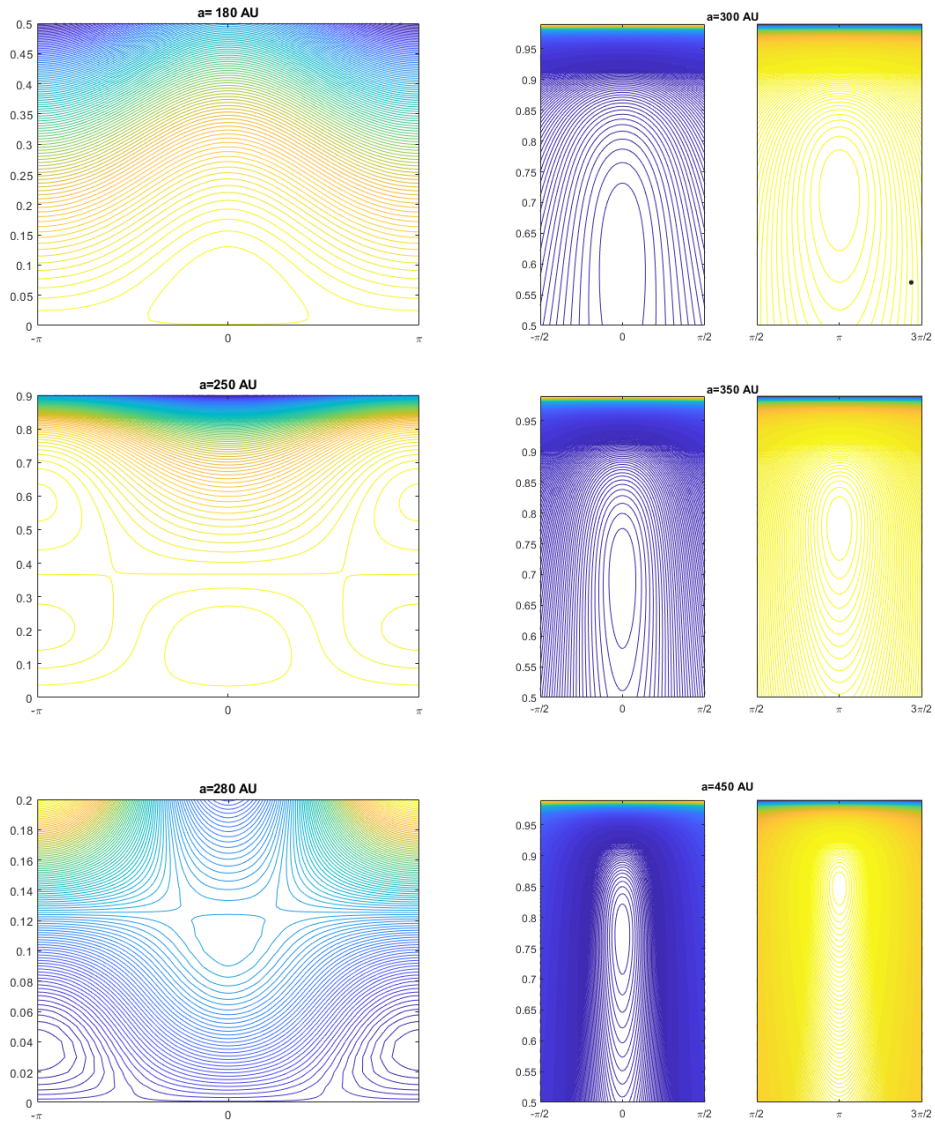
Figure 4.8: Phase Portraits of the lower order planar Hamiltonian.
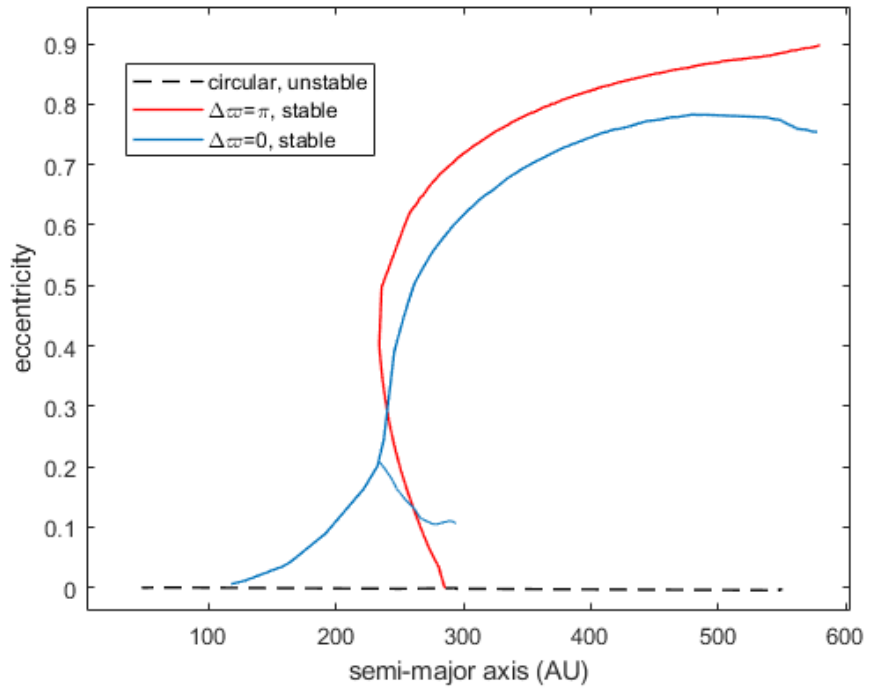
Figure 4.9: Equilibria in (a,e) space for the lower orders Hamiltonian.
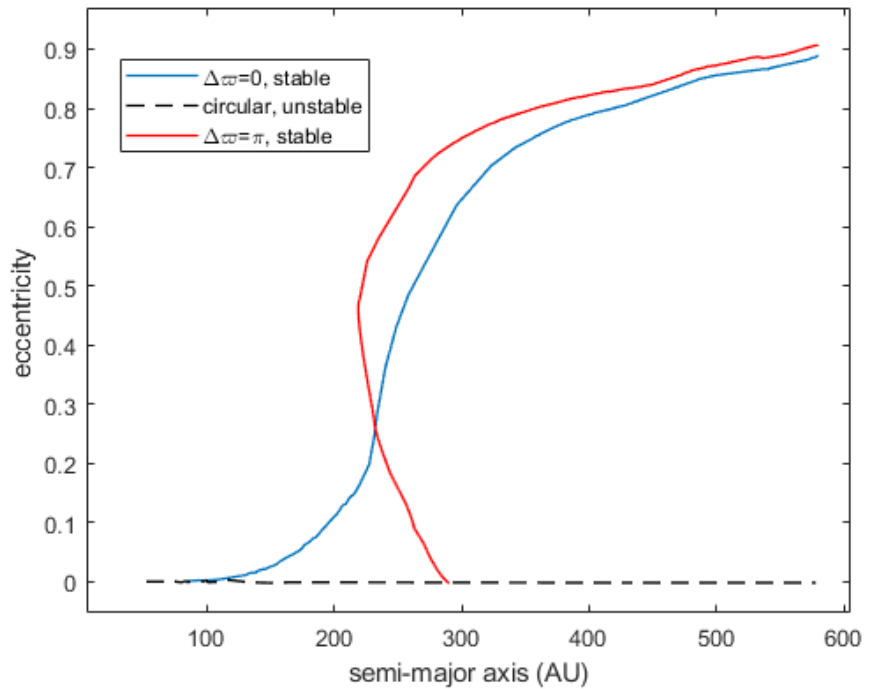
Figure 4.10: Equilibria in (a,e) space for the all orders Hamiltonian.

Our phase portraits for the lower orders Hamiltonian in figure 4.8 are consistent with the equilibria generated by solving the planar equation of motion. We have the aligned libration family of increasing eccentricity present in almost all of the literature. However, we were able to recover a stable anti-aligned family that was not present in (34), but appeared in (38) as the author computed the interaction potential exactly. The consistency is also in the radius at which this family appears; it appears in our analysis around 230 AU and in (38) around 250 AU. This anti-aligned family is consistent with the phase portraits and the apsidal precession freezing observed earlier. However, what differs for this family is that over a short range of semi-major axes (230-280 AU) it has two equilibria branches, one with low eccentricity and the other with increasing eccentricity. That is not consistent with (38) as no anti-aligned branch with low eccentricity is present.

In the lower orders Hamiltonian, the aligned family gives rise at 250 AU into a low eccentricity branch that appears in the phase portraits to be holding unstable non-aligned equilibria. This low eccentricity aligned branch does not persist when we add the higher order terms, indicating that this family, which does not appear in the literature, is structurally unstable to orders addition.

Other than that, we can say that the addition of the higher orders did not impact the whole equilibria structure much, so based on this convergence that we observe, we proceed to investigate full 3D dynamics where we impose mutual inclination between the inner and outer perturbers.

4.3.2 Full Spatial Dynamics:

We attempt solving the system of equations 4.14 in a coplanar coplanar configuration. Thus this reduces to:

$$L\frac{d\mathbf{j}}{dt} = 0 = \frac{\Gamma}{2}\frac{\sin 2\phi}{(1-e^2)^{\frac{3}{2}}}$$
$$- \sin\alpha\Bigg[2\cos\alpha\Big(\Phi_2(e)j^2 - \Phi_3(e)e^2 - \Phi_4(e)j^2 + \Phi_5(e)e^2\Big)$$
$$+ 3\cos^2\alpha\Big(\pm\Phi_6(e)ej^2 \pm \Phi_7(e)ej^2 \mp \Phi_8(e)e^3 \mp \Phi_9(e)ej^2 \pm \Phi_{10}(e)e^3\Big)$$
$$\pm \Phi_1(e) \mp \Phi_7(e)ej^2 \pm \Phi_8(e)e^3 \pm \Phi_9(e)ej^2 \Bigg] \tag{4.28}$$

$$L\frac{d\mathbf{e}}{dt} = 0 = \mp\frac{\Gamma}{2}\frac{e}{(1-e^2)^2}(1 - 3\cos^2\phi)$$
$$- j\Bigg[\cos^2\alpha\Big(\mp 2\Phi_2(e)e \mp 2\Phi_3(e)e \pm 2\Phi_4(e)e \pm 2\Phi_5(e)e$$
$$\pm D_2ej^2 \mp D_3e^3 \mp D_4j^2e \pm D_5e^3\Big)$$
$$+ \cos^3\alpha\Big(\Phi_6(e)(1 - 3e^2) - \Phi_7(e)(3e^2 - 1) - 3\Phi_8(e)e^2 - \Phi_9(e)(1 - 3e^2) + 3\Phi_{10}e^2$$
$$+ D_6j^2e^2 + D_7e^2j^2 - D_8e^4 - D_9j^2e^2 + D_{10}e^4\Big)$$
$$+ \cos\alpha\Big(\Phi_1(e) + \Phi_7(e)(3e^2 - 1) + 3\Phi_8(e)e^2 + \Phi_9(e)(1 - 3e^2)$$
$$+ D_1e^2 - D_7e^2j^2 + D_8e^4 + D_9j^2e^2\Big)$$
$$\pm 2\Phi_3(e)e \mp 2\Phi_4(e)e \pm D_0e \pm D_3e^3 \pm D_4ej^2 \Bigg] \tag{4.29}$$

for inclination ϕ, and for $\alpha = \phi - \phi_9$.

4.3.3 Linear Stability Analysis:

We go through the same procedure of linearizing our equations of motion to lower order terms to find the eigenvalues of the linearization matrix. By construction zeroth order terms are cancelled as they satisfy the equation, and we are left with:

$$
\begin{aligned}
L\frac{d\mathbf{j}_1}{dt} &= (\mathbf{j}_0 \times \hat{\boldsymbol{n}}_{\boldsymbol{p}})\Big[5\Gamma\frac{j_{np}}{(1-e_0)^{\frac{7}{2}}}(\mathbf{e}_0 \cdot \mathbf{e}_1) + \Gamma\frac{1}{(1-e_0^2)^{\frac{5}{2}}}j_{1_{np}}\Big] \\
&+ (\mathbf{j}_1 \times \hat{\boldsymbol{n}}_{\boldsymbol{p}})\Big[\Gamma\frac{1}{(1-e_0^2)^{\frac{5}{2}}}j_{np}\Big] \\
&- (\mathbf{j}_1 \times \hat{\boldsymbol{n}}_{\boldsymbol{d}})\Big[2\Phi_2(e_0)j_n + 2\Phi_6(e_0)e_u j_n + \Phi_7(e_0)e_n j_u\Big] \\
&- (\mathbf{j}_0 \times \hat{\boldsymbol{n}}_{\boldsymbol{d}})\Big[2\Phi_2(e_0)j_{1n} + 2\Phi_6(e_0)[e_{1u}j_n + e_u j_{1n}] + \Phi_7(e_0)[e_{1n}j_u + e_n j_{1u}] \\
&\qquad\qquad + (\mathbf{e}_0 \cdot \mathbf{e}_1)K_1\Big] \\
&- (\mathbf{j}_1 \times \hat{\boldsymbol{u}}_{\boldsymbol{d}})\Big[\Phi_7(e_0)e_n j_n\Big] \\
&- (\mathbf{j}_0 \times \hat{\boldsymbol{u}}_{\boldsymbol{d}})\Big[\Phi_7(e_0)[e_{1n}j_n + e_n j_{1n}] + (\mathbf{e}_0 \cdot \mathbf{e}_1)D_7 e_n j_n\Big] \\
&- (\mathbf{e}_1 \times \hat{\boldsymbol{u}}_{\boldsymbol{d}})\Big[\Phi_1(e_0) + \Phi_6(e_0)j_n^2 + \Phi_8(e_0)e_n^2\Big] \\
&- (\mathbf{e}_0 \times \hat{\boldsymbol{u}}_{\boldsymbol{d}})\Big[2\Phi_6(e_0)j_n j_{1n} + 2\Phi_8(e_0)e_n e_{1n} + (\mathbf{e}_0 \cdot \mathbf{e}_1)K_2\Big] \\
&- (\mathbf{e}_0 \times \hat{\boldsymbol{n}}_{\boldsymbol{d}})\Big[2\Phi_3(e_0)e_{1n} + 2\Phi_8(e_0)[e_{1u}e_n + e_u e_{1n}] + \Phi_7(e_0)[j_{1u}j_n + j_{1n}j_u] \\
&\qquad\qquad + (\mathbf{e}_0 \cdot \mathbf{e}_1)K_3\Big] \\
&- (\mathbf{e}_1 \times \hat{\boldsymbol{n}}_{\boldsymbol{d}})\Big[2\Phi_3(e_0)e_n + 2\Phi_8(e_0)e_u e_n + \Phi_7(e_0)j_u j_n\Big] \qquad (4.30)
\end{aligned}
$$

where we have defined the following:

$$
\begin{aligned}
K_1 &= 2D_2 j_n + 2D_6 e_u j_n + D_7 e_n j_u \\
K_2 &= D_1 + D_6 j_n^2 + D_8 e_n^2 \\
K_3 &= 2D_3 e_n + 2D_8 e_u e_n + D_7 j_u j_n \\
K_4 &= D_0 + D_1 e_u + D_3 e_n^2 + D_2 j_n^2 + D_6 e_u j_n^2 + D_8 e_u e_n^2 + D_7 j_u j_n e_n \\
K_5 &= D_0' + e_u D_1' + e_n^2 D_3' + j_n^2 D_2' + e_u j_n^2 D_6' + e_u e_n^2 D_8' + j_u j_n e_n D_7' \\
T &= -\frac{\Gamma}{2}\Big[(1-e_0^2)^{-\frac{5}{2}} - 5j_{n_p}^2(1-e_0^2)^{-\frac{7}{2}}\Big] \qquad (4.31)
\end{aligned}
$$

for $D_i' = \frac{dD_i}{de}$

$$L\frac{d\mathbf{e}_1}{dt} = (\mathbf{e}_0 \times \hat{\boldsymbol{n}_p})\Big[5\Gamma\frac{j_{np}}{(1-e_0)^{\frac{7}{2}}}(\mathbf{e}_0 \cdot \mathbf{e}_1) + \Gamma\frac{1}{(1-e_0^2)^{\frac{5}{2}}}j_{1_{np}}\Big]$$
$$+ (\mathbf{e}_1 \times \hat{\boldsymbol{n}_p})\Big[\Gamma\frac{1}{(1-e_0^2)^{\frac{5}{2}}}j_{np}\Big]$$
$$- (\mathbf{e}_1 \times \hat{\boldsymbol{n}_d})\Big[2\Phi_2(e_0)j_n + 2\Phi_6(e_0)e_u j_n + \Phi_7(e_0)e_n j_u\Big]$$
$$- (\mathbf{e}_0 \times \hat{\boldsymbol{n}_d})\Big[2\Phi_2(e_0)j_{1n} + 2\Phi_6(e_0)[e_{1u}j_n + e_u j_{1n}] + \Phi_7(e_0)[e_{1n}j_u + e_n j_{1u}]$$
$$+ (\mathbf{e}_0 \cdot \mathbf{e}_1)K_1\Big]$$
$$- (\mathbf{e}_1 \times \hat{\boldsymbol{u}_d})\Big[\Phi_7(e_0)e_n j_n\Big]$$
$$- (\mathbf{e}_0 \times \hat{\boldsymbol{u}_d})\Big[\Phi_7(e_0)[e_{1n}j_n + e_n j_{1n}] + (\mathbf{e}_0 \cdot \mathbf{e}_1)D_7 e_n j_n\Big]$$
$$- (\mathbf{j}_1 \times \hat{\boldsymbol{u}_d})\Big[\Phi_1(e_0) + \Phi_6(e_0)j_n^2 + \Phi_8(e_0)e_n^2\Big]$$
$$- (\mathbf{j}_0 \times \hat{\boldsymbol{u}_d})\Big[2\Phi_6(e_0)j_n j_{1n} + 2\Phi_8(e_0)e_n e_{1n} + (\mathbf{e}_0 \cdot \mathbf{e}_1)K_2\Big]$$
$$- (\mathbf{j}_0 \times \hat{\boldsymbol{n}_d})\Big[2\Phi_3(e_0)e_{1n} + 2\Phi_8(e_0)[e_{1u}e_n + e_u e_{1n}] + \Phi_7(e_0)[j_{1u}j_n + j_{1n}j_u]$$
$$+ (\mathbf{e}_0 \cdot \mathbf{e}_1)K_3\Big]$$
$$- (\mathbf{j}_1 \times \hat{\boldsymbol{n}_d})\Big[2\Phi_3(e_0)e_n + 2\Phi_8(e_0)e_u e_n + \Phi_7(e_0)j_u j_n\Big]$$
$$- (\mathbf{j}_0 \times \mathbf{e}_0)\Big[\frac{1}{e_0}(\mathbf{e}_0 \cdot \mathbf{e}_1)K_5 + e_{1u}K_2 + e_{1n}K_3 + j_{1n}K_1 + j_{1u}e_n j_n D_7$$
$$+ \frac{5\Gamma}{2}\Big(\frac{(\mathbf{e}_0 \cdot \mathbf{e}_1)}{(1-e_0^2)^{\frac{7}{2}}} - 7\frac{j_{np}^2(\mathbf{e}_0 \cdot \mathbf{e}_1)}{(1-e_0^2)^{\frac{9}{2}}} - 2\frac{j_{np}j_{1np}}{(1-e_0^2)^{\frac{7}{2}}}\Big)\Big]$$
$$- \big[(\mathbf{j}_0 \times \mathbf{e}_1) + (\mathbf{j}_1 \times \mathbf{e}_0)\big]\Big[K_4 + T\Big] \qquad (4.32)$$

We resolve these two coupled three dimentional equations intro their components as we did earlier in order to find the linearization matrix and proceed to eigenvalues analysis.

Figure 4.11: Equilibria families aligned and anti-aligned with the perturber in (a,e) and (a,i) space.
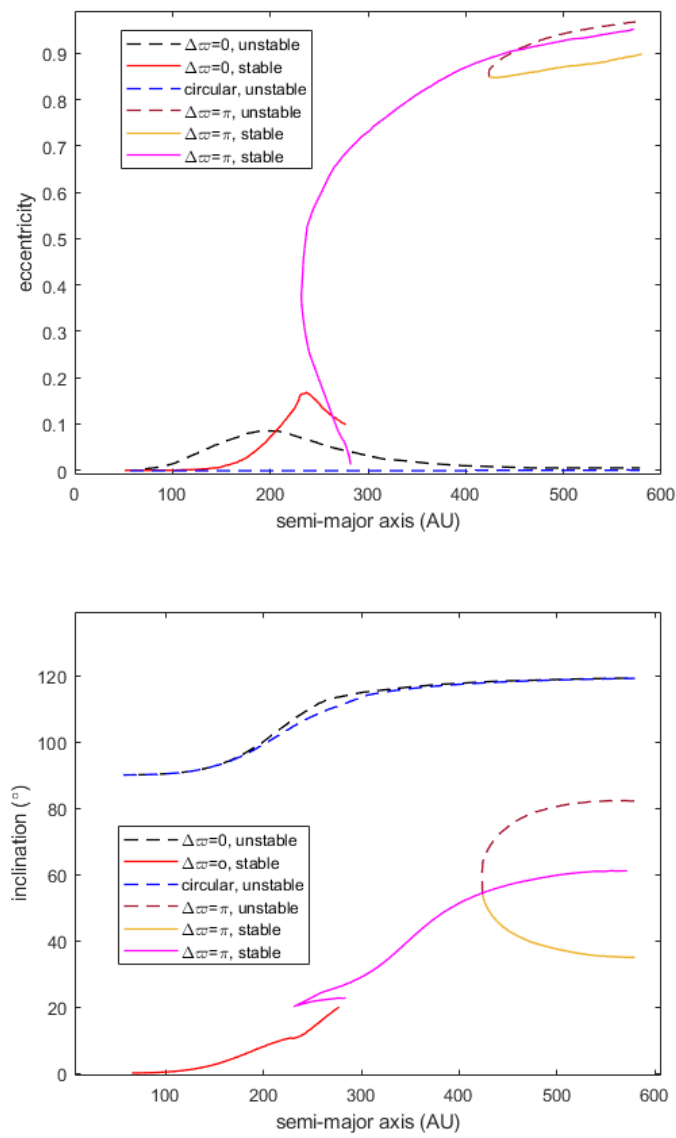
In 3D dynamics, we were able to produce a very rich parameter space of solutions when accounting for Planet IX in harmonics. The problem faced with multipoles was avoided here by the computation of the numerical potential of the planet ring. The harmonics modes decay in magnitude as a function of order. Thus we are more confident of our results here.
On the equilibria presented in fig.4.11 we note the following:

- First, in comparison with the knowm results, which we repeat: they constituted of two families of equilibria, the stable one referred to the classical Laplace Surface, which was circular and transitioned in inclination between the inner plane and the outer plane. This family, which we've seen to be modified under the action of multipoles: it was pumped in eccentricity, and after taking off the inner plane reaches an inclination where it goes back to inner plane; here we see this family also being pumped in eccentricity around the Laplace radius, but it does not go back to the inner plane; it actually does not persist, but rather is wiped out in favor of of a new bifurcation that we have also seen an analogous for in the multipoles description.

- Second, the eccentric antialigned family that takes on when the aligned family dies, continues to increase in inclination, but instead of residing in the outer plane, it exceeds it in inclination and resides eventually in a plane with double its inclination ($60°$).

- Third, the unstable family that accompanies the Laplace Surface at every description is also present here, but in comparison to the multipoles, it has two branches here, one gets eccentric around the Laplace radius, then circularizes again, and that's present in the multipoles, while another remains circular.

- Fourth, similar to multipoles, very highly eccentric nonlinear bifurcations also emerge here, except that here they do at higher semi-major axes.

- We can say in general, the region of agreement which we observed at the level of the potentials comparison earlier, which is the region of convergence of the multipoles ($a < 280AU$), is rendered a region of agreement in the solutions also.

Our study of the modes was useful. We note that the aligned family increasing in eccentricity to very high values disappeared when we went from the planar case to full spatial case, leaving us with the desirable anti-aligned family of increasing eccentricity and moderate inclinations. A combination of both families generates a surface that starts in the inner plane, gets pumped in eccentricity and inclination until it resides in a plane inclined by double the inclination of P9. Thus we also conclude here as in the previous cases, an eccentric perturber, if correctly accounted for, destroys the classical Laplace Surface, and creates another surface of

eccentric equilibria with increasing inclination. This surface includes a family of equilibria that anti-aligned with the Planet IX, highly eccentric, and moderately inclined, matching the observed eTNOs.

Chapter 5

The Self-Gravitating Disk: Planet IX Alternative?

We have seen in the previous section that accounting for the proposed Planet IX can explain the clustered highly eccentric eTNOs. However, we followup on the recent work we discussed earlier (35), in which the authors try to explain these observations using self-gravity by modelling a moderately eccentric ($e \approx 0.7$) shepherding disk extending between 40 and 750 AU with a mass of $10 M_\oplus$. Indeed, the authors succeed in creating a stable, apsidally anti-aligned secular equilibrium at high eccentricity by freezing the longitudes of perihelion through a cancellation of effects between the giant planets and the disk itself. What the authors could not generate in that work were inclined frozen equilibria as they considered dynamics to be planar, and considering both perturbers in the same plane cannot fix the nodes for inclined equilibria. Our aim in this section is to try to generate precisely such equilibria by exploring various complementary channels.

5.1 Disk Potential

Starting with the mass and eccentricity distributions of DM1 (Disk Model 1) presented and used in (35), we compute the full spatial potential of the self-gravitating disk formed of coplanar and eccentric rings. The potential is expanded in spherical harmonics by recovering the dominant modes in the expansion, as we did previously for Planet IX. In this case dominant modes are up to ($l = 3, m = 1$), namely $a_{0,0}, a_{1,1}, a_{2,0}, a_{3,1}$. So we end up with:

$$\bar{\Phi}_d = -\sqrt{\frac{1}{4\pi}}\langle a_{0,0}(r)\rangle + \sqrt{\frac{5}{4\pi}}\langle a_{2,0}(r)P_2^0(\cos\theta)\rangle - \sqrt{\frac{3}{8\pi}}\langle a_{1,1}(r)P_1^1(\cos\theta)\cos\phi\rangle$$

$$+ \sqrt{\frac{7}{48\pi}}\langle a_{3,1}(r)P_3^1(\cos\theta)\cos\phi\rangle \tag{5.1}$$

Substituting the required Legendre polynomials and transforming the spherical angles into orbital elements, then picking up the functions of the fast angle (the true anomaly f in this case) to be averaged we get:

$$\bar{\Phi}_d = F(e) + G(e)[\cos(\Omega - \varpi_d)\cos\omega - \cos i \sin(\Omega - \varpi_d)\sin\omega]$$

$$+ \frac{3}{4}\sqrt{\frac{5}{4\pi}}\sin^2 i[f_{2,0,0} - \cos 2\omega f_{2,0,2}]$$

$$- \frac{15}{8}\sqrt{\frac{7}{48\pi}}\sin^2 i[f_{3,1,1}(\cos(\Omega - \varpi_d)\cos\omega - 3\sin(\Omega - \varpi_d)\cos i \sin\omega)$$

$$+ f_{3,1,3}(\sin(\Omega - \varpi_d)\cos i \sin 3\omega - \cos(\Omega - \varpi_d)\cos 3\omega)] \quad (5.2)$$

$$F(e) = -\sqrt{\frac{1}{4\pi}}f_{0,0,0} - \frac{1}{2}\sqrt{\frac{5}{4\pi}}f_{2,0,0} \quad ; \quad G(e) = \sqrt{\frac{3}{8\pi}}f_{1,1,1} + \frac{3}{2}\sqrt{\frac{7}{48\pi}}f_{3,1,1} \quad (5.3)$$

Now we transform into the vectorial variables using $\hat{\boldsymbol{n}}, \hat{\boldsymbol{n}}_d$ as the non-dimensional angular momentum unit vectors for the particle and the disk respectively, and $\hat{\boldsymbol{u}}, \hat{\boldsymbol{u}}_d$ as the eccentricity unit vectors. Again, using $\mathbf{e} = e\hat{\boldsymbol{u}}$, and $\mathbf{j} = \sqrt{1 - e^2}\hat{\boldsymbol{n}}$ we can write:

$$\bar{\Phi}_d = \Phi_0(e) + \Phi_1(e)(\mathbf{e} \cdot \hat{\boldsymbol{u}}_d) + \Phi_2(e)(\mathbf{e} \cdot \hat{\boldsymbol{n}}_d)^2 + \Phi_3(e)(\mathbf{j} \cdot \hat{\boldsymbol{n}}_d)^2 + \Phi_4(e)(\mathbf{e} \cdot \hat{\boldsymbol{u}}_d)(\mathbf{j} \cdot \hat{\boldsymbol{n}}_d)^2$$

$$+ \Phi_5(e)(\mathbf{e} \cdot \hat{\boldsymbol{u}}_d)(\mathbf{e} \cdot \hat{\boldsymbol{n}}_d)^2 + \Phi_6(e)(\mathbf{j} \cdot \hat{\boldsymbol{u}}_d)(\mathbf{e} \cdot \hat{\boldsymbol{n}}_d)(\mathbf{j} \cdot \hat{\boldsymbol{n}}_d) \quad (5.4)$$

with the functions $\Phi_i(e)$ defined:

$$\Phi_0(e) = F(e) + \frac{3}{4}\sqrt{\frac{5}{4\pi}}[f_{2,0,0} - f_{2,0,2}]$$

$$\Phi_1(e) = \frac{1}{e}\left[G(e) - \frac{15}{8}\sqrt{\frac{7}{48\pi}}[f_{3,1,1} + 2f_{3,1,3}]\right]$$

$$\Phi_2(e) = \frac{3}{2}\sqrt{\frac{5}{4\pi}}\frac{f_{2,0,2}}{e^2}$$

$$\Phi_3(e) = -\frac{3}{4}\sqrt{\frac{5}{4\pi}}\left[\frac{f_{2,0,0} - f_{2,0,2}}{1 - e^2}\right]$$

$$\Phi_4(e) = -\frac{15}{8}\sqrt{\frac{7}{48\pi}}\left[\frac{f_{3,1,1} - 2f_{3,1,3}}{e(1 - e^2)}\right]$$

$$\Phi_5(e) = -\frac{15}{8}\sqrt{\frac{7}{48\pi}}\frac{f_{3,1,3}}{e^3}$$

$$\Phi_6(e) = -\frac{15}{4}\sqrt{\frac{7}{48\pi}}\left[\frac{-f_{3,1,1} + f_{3,1,3}}{e(1 - e^2)}\right]$$

75

5.1.1 Equations of Motion

To describe the dynamics of a particle orbiting the Sun in the trans-Neptunian region while being perturbed by the disk we modelled and the giant planets, we construct the particle's Hamiltonian as the sum of both secular contributions:

$$H = \bar{\Phi}_d - \Psi_p \tag{5.5}$$

where Ψ_p is defined in equation 4.18. Going through the same procedure we used earlier, and using Milankovich equations vectorial variables, we get the following equations of motion:

$$
\begin{aligned}
L\frac{d\mathbf{j}}{dt} = & +\Gamma \frac{\mathbf{j} \cdot \hat{\boldsymbol{n}}_{\boldsymbol{p}}}{(1-e^2)^{\frac{5}{2}}}(\mathbf{j} \times \hat{\boldsymbol{n}}_{\boldsymbol{p}}) \\
& - \left[2\Phi_3(e)j_n + 2\Phi_4(e)j_n e_u + \Phi_6(e)e_n j_u\right](\mathbf{j} \times \hat{\boldsymbol{n}}_{\boldsymbol{d}}) \\
& - \left[\Phi_6(e)e_n j_n\right](\mathbf{j} \times \hat{\boldsymbol{u}}_{\boldsymbol{d}}) \\
& - \left[\Phi_1(e) + \Phi_4(e)j_n^2 + \Phi_5(e)e_n^2\right](\mathbf{e} \times \hat{\boldsymbol{u}}_{\boldsymbol{d}}) \\
& - \left[2\Phi_2(e)e_n + 2\Phi_5(e)e_u e_n + \Phi_6(e)j_u j_n\right](\mathbf{e} \times \hat{\boldsymbol{n}}_{\boldsymbol{d}})
\end{aligned}
\tag{5.6}
$$

$$
\begin{aligned}
L\frac{d\mathbf{e}}{dt} = & +\Gamma \frac{\mathbf{j} \cdot \hat{\boldsymbol{n}}_{\boldsymbol{p}}}{(1-e^2)^{\frac{5}{2}}}(\mathbf{e} \times \hat{\boldsymbol{n}}_{\boldsymbol{p}}) - \frac{\Gamma}{2}\frac{1 - e^2 - 5(\mathbf{j} \cdot \hat{\boldsymbol{n}}_{\boldsymbol{p}})^2}{(1-e^2)^{\frac{7}{2}}}(\mathbf{j} \times \mathbf{e}) \\
& - \left[2\Phi_3(e)j_n + 2\Phi_4(e)j_n e_u + \Phi_6(e)e_n j_u\right](\mathbf{e} \times \hat{\boldsymbol{n}}_{\boldsymbol{d}}) \\
& - \left[\Phi_6(e)e_n j_n\right](\mathbf{e} \times \hat{\boldsymbol{u}}_{\boldsymbol{d}}) \\
& - \left[\Phi_1(e) + \Phi_4(e)j_n^2 + \Phi_5(e)e_n^2\right](\mathbf{j} \times \hat{\boldsymbol{u}}_{\boldsymbol{d}}) \\
& - \left[2\Phi_2(e)e_n + 2\Phi_5(e)e_u e_n + \Phi_6(e)j_u j_n\right](\mathbf{j} \times \hat{\boldsymbol{n}}_{\boldsymbol{d}}) \\
& - \left[D_0 + D_1 e_u + D_2 e_n^2 + D_3 j_n^2 + D_4 e_u j_n^2 + D_5 e_u e_n^2 + D_6 j_u e_n j_n\right](\mathbf{j} \times \mathbf{e})
\end{aligned}
\tag{5.7}
$$

Where we have defined, for $i = 1..4$ corresponding to the outer massive planets:

$$\Gamma = \frac{3}{4}\frac{GM_\odot}{a}\sum_{i=1}^{i=4}\frac{m_i a_i^2}{M_\odot a^2} \tag{5.8}$$

and we used the notation:

$$\frac{1}{e}\frac{d\Phi_i}{de} = D_i(e) \tag{5.9}$$

5.1.2 Precession Rates

We first inspect if we can freeze our particle's orbit by checking if the contributions from the inner quadrupole and the disk can cancel out each resulting in a fixed configuration in the apse and the node. We do this for the planad and 3D case, and we present a sample of results.

• Disk Action

The disk contribution is again, written in vector notation as:

$$\bar{\bar{\Phi}}_d = \Phi_0(e) + \Phi_1(e)(\mathbf{e} \cdot \hat{\boldsymbol{u}}_d) + \Phi_2(e)(\mathbf{e} \cdot \hat{\boldsymbol{n}}_d)^2 + \Phi_3(e)(\mathbf{j} \cdot \hat{\boldsymbol{n}}_d)^2 + \Phi_4(e)(\mathbf{e} \cdot \hat{\boldsymbol{u}}_d)(\mathbf{j} \cdot \hat{\boldsymbol{n}}_d)^2$$
$$+ \Phi_5(e)(\mathbf{e} \cdot \hat{\boldsymbol{u}}_d)(\mathbf{e} \cdot \hat{\boldsymbol{n}}_d)^2 + \Phi_6(e)(\mathbf{j} \cdot \hat{\boldsymbol{u}}_d)(\mathbf{e} \cdot \hat{\boldsymbol{n}}_d)(\mathbf{j} \cdot \hat{\boldsymbol{n}}_d) \tag{5.10}$$

with the functions $\Phi_i(e)$ defined earlier. This can be written in coplanar-coplanar configuration as:

$$\bar{\bar{\Phi}}_d = \cos\alpha\left[\Psi_1(e) + \frac{3}{4}\Psi_3(e)\right] + \cos 2\alpha\left[\frac{1}{2}\Psi_2(e)\right] + \cos 3\alpha\left[\frac{1}{4}\Psi_3(e)\right] + \frac{1}{2}\Psi_2(e) + \Psi_4(e) \tag{5.11}$$

for $\alpha = (i - i_d)$, where i is the inclination of the particle and i_d being the inclination of the disk, both with respect to the reference frame being the plane of the inner quadrupole; and for the functions $\Psi_i(e)$ defined in terms of $\Phi_i(e)$ for aligned and anti-aligned configurations as:

$$\Psi_1(e) = \left[\pm\Phi_5(e) \pm \Phi_6(e)\right]e^3 + \left[\pm\Phi_1(e) \mp \Phi_6(e)\right]e$$

$$\Psi_2(e) = \left[-\Phi_3(e) - \Phi_2(e)\right]e^2 + \Phi_3(e)$$

$$\Psi_3(e) = \left[\mp\Phi_5(e) \mp \Phi_6(e) \mp \Phi_4(e)\right]e^3 + \left[\pm\Phi_4(e) \pm \Phi_6(e)\right]e$$

$$\Psi_4(e) = \Phi_0(e) + \Phi_2(e)e^2 \tag{5.12}$$

Obviously, if we are to consider an axisymmetric disk, this will leave us with axisymmetric contributions from $\Psi_2(e), \Psi_4(e)$ only, while other functions should vanish. To find the apsidal precession contribution of the disk, we find first:

$$\frac{\partial \bar{\bar{\Phi}}_d}{\partial e} = \cos\alpha\left[\frac{\partial \Psi_1(e)}{\partial e} + \frac{3}{4}\frac{\partial \Psi_3(e)}{\partial e}\right] + \cos 2\alpha\left[\frac{1}{2}\frac{\partial \Psi_2(e)}{\partial e}\right] + \cos 3\alpha\left[\frac{1}{4}\frac{\partial \Psi_3(e)}{\partial e}\right]$$
$$+ \frac{1}{2}\frac{\partial \Psi_2(e)}{\partial e} + \frac{\partial \Psi_4(e)}{\partial e} \tag{5.13}$$

$$\frac{\partial \bar{\bar{\Phi}}_d}{\partial i} = -\left[\Psi_1(e) + \frac{3}{4}\Psi_3(e)\right]\sin\alpha - 2\sin 2\alpha\,\Psi_2(e) - \frac{3}{4}\Psi_3(e)\sin 3\alpha \tag{5.14}$$

After computing the precession rates of the disk, we add these rates to those driven by the inner quadrupole computed in the previous section and check for for different eccentricities if we can freeze the orbits in space. We did the analysis for planar and inclined configurations. Planar total rates are shown in figure 5.1 below. However, as expcted, we could not fix the nodes for eccentric families in inclined configurations.
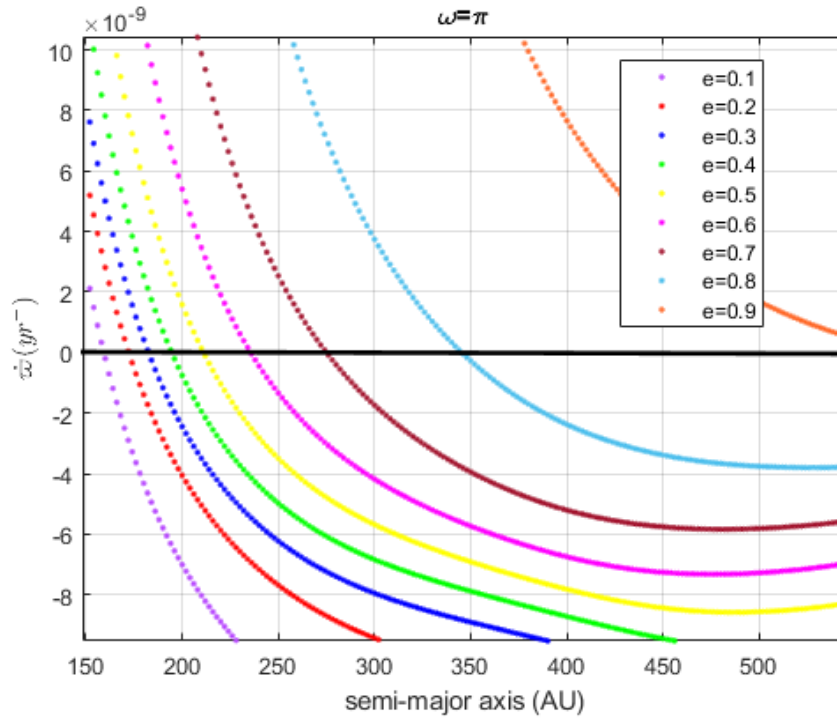
Figure 5.1: Total apsidal precession rates for orbits anti-aligned with the disk driven by the sum of the effects of the massive planets and the disk for coplanar orbits at different eccentricities over a range of semi-major axes.

5.1.3 Equilibria

If we consider the disk to be in the plane of the massive planets, meaning $\hat{\boldsymbol{n}}_d \cdot \hat{\boldsymbol{n}}_p = 1$, and we look for planar aligned and anti-aligned equilibria, where $\mathbf{e} \cdot \hat{\boldsymbol{u}}_d = \pm 1$ respectively; then $\frac{d\mathbf{j}}{dt} = 0$ is trivially satisfied, and we are left with:

$$L\frac{d\mathbf{e}}{dt} = 0 = \pm\Gamma\frac{e}{(1-e^2)^2} + 2\Phi_3(e)je \mp 2\Phi_4(e)e^2j \mp \Phi_1(e)j \mp \Phi_4(e)j^3$$
$$- \left[D_0je \pm D_1je^2 + D_3j^3e \pm D_4e^2j^3 \right] \tag{5.15}$$

Solutions that satisfy this equation are consistent with planar solutions produced in (35), but as we said, we are more interested in off-plane solutions, so we proceed to consider an inclination between the perturbers, baring in mind that we still have no physical reasons to maintain such a configuration.

Looking for coplanar-coplanar equilibria in the case of an inclined disk, we define $\alpha = \phi - \phi_d$, where ϕ is the inclination of the particle with respect to the inner quadrupole and ϕ_d is the inclination of the disk. Thus we have:

$$L\frac{d\mathbf{j}}{dt} = 0 = \frac{\Gamma}{2}\frac{\sin 2\phi}{(1-e^2)^{\frac{3}{2}}}$$
$$- \sin\alpha\left[\cos\alpha\left(2\Phi_3(e)j^2 - 2\Phi_2(e)e^2 \right)\right.$$
$$+ \cos^2\alpha\left(\pm 3\Phi_4(e)ej^2 \pm 3\Phi_6(e)ej^2 \mp 3\Phi_5(e)e^3 \right)$$
$$\left.\pm \Phi_1(e) \mp \Phi_6(e)ej^2 \pm \Phi_5(e)e^3 \right] \tag{5.16}$$

$$L\frac{d\mathbf{e}}{dt} = 0 = \mp\frac{\Gamma}{2}\frac{e}{(1-e^2)^2}(1 - 3\cos^2\phi)$$
$$- j\left[\cos^2\alpha\left(\mp 2\Phi_3(e)e \pm D_3ej^2 \right)\right.$$
$$+ \cos^3\alpha\left(\Phi_4(e)(1 - 3e^2) + D_4j^2e^2 \right)$$
$$+ \sin^2\alpha\cos\alpha\left(\Phi_6(e)(3e^2 - 1) + 3\Phi_5(e)e^2 + D_5e^4 - D_6e^2j^2 \right)$$
$$+ \cos\alpha\left(\Phi_1(e) + D_1e^2 \right)$$
$$\left.+ \sin^2\alpha\left(\pm 2\Phi_2(e)e \pm D_2e^3 \right) \pm D_0e \right] \tag{5.17}$$

79

5.1.4 Fixed Disk

Disk in Plane:

We start by showing aligned and anti-aligned equilbira sustained by the mutual cancellation of effects of the inner quadrupole and the non-inclined non-precessing disk ($\phi_d = 0, \alpha = \phi$). The equilibria and their associated stabilities we produce are identical to those presented in the work of (35), expect we add an unstable circular and polar family that is not present in the referenced work as the authors solved for eccentric equilibria only. This family will turn out to be of huge significance later on.

Figure 5.2: Equilibria and associated stability for $\phi_d = 0°$. Profile is identical to that of the referenced work.
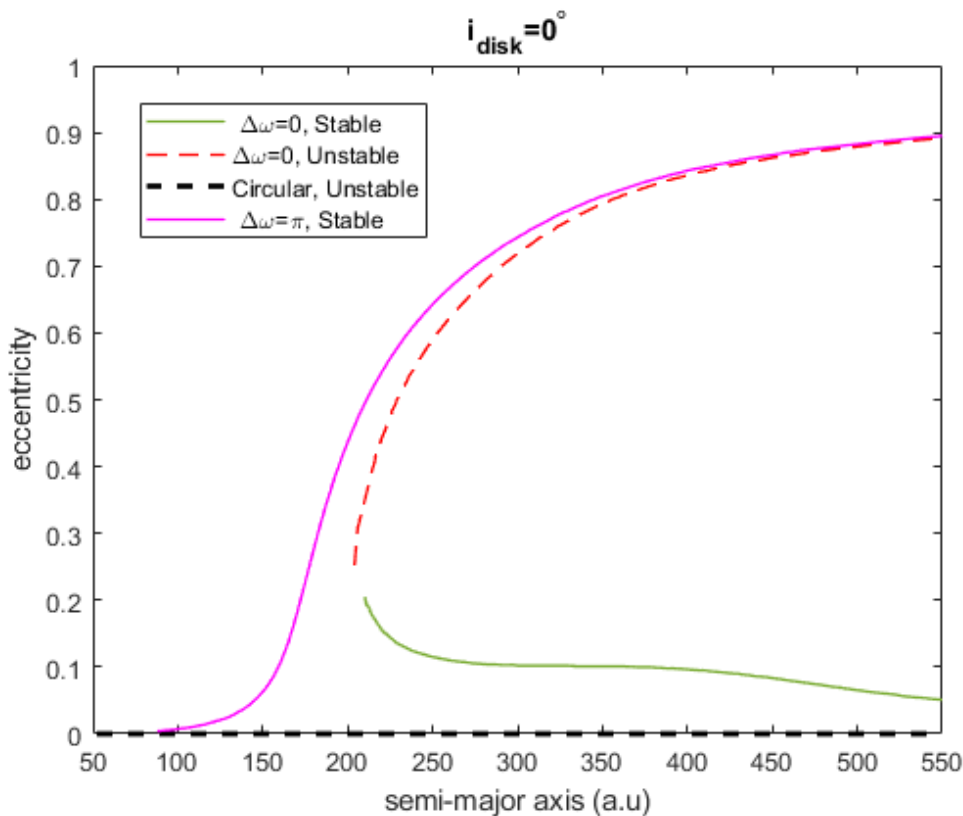
The stability analysis for this configuration is promising. Some of the families of equilibria, both aligned and anti-aligned with the disk's apse, are stable to perturbations in eccentricity and inclination; meaning planar equilibria can go off plane with a small perturbation in inclination and still maintain their orbits.

Although for the planar disk we have off-plane equilibria that are unstable circular-polar orbits, but we are interested in generating equilibria of moderate inclinations. So we appeal to two variations on the planar model.

Inclined Disk: A Toy Model

As we mentioned earlier, we have no physical reason to maintain an inclined disk. Driven by the fact that the observed TNO's are held in inclined orbits, we proceed with this assumption to see the behavior of inclination of solutions, hoping we can match the observation in such a configuration. We study equilibria and their stability with the disk at different inclinations. As we start increasing ϕ_d, we maintain aligned and anti-aligned solutions with the same eccentricity trend. However, equilibria start growing in inclination in parallel with the increasing inclination of the disk.

An eccentric Laplace-Surface-like structure emerges in the case of an inclined disk. Eccentric, aligned and anti-aligned equilibria, follow the behavior of classical Laplace Surface objects i.e are in the plane of the inner quadrupole at low semi-major axis, and transition in inclination as a function of a until they reside in the plane of the disk at high enough a ($\phi \to 0$ as $a \to 0$ and $\phi \to \phi_d$ as $a \to \infty$), although the inner quadrupole dominated regime is anti-aligned, while the disk dominated regime is aligned.

For $\Phi_d = 30°$, we plotted the data of the observed extreme TNOs. The figure shows that the objects follow quite closely the same profile, in both eccentricity and inclination, as the obtained equilbira, especially the stable anti aligned ones.

Table 5.1: Orbital parameters of observed clustered extreme TNOs.

TNO	a (a.u)	e	i (°)	ω (°)	Ω (°)
2012 VP113	258.27	0.69	24.1	293.5	90.7
2014 SR349	302.23	0.84	18.0	340.9	34.8
2004 VN112	318.97	0.85	25.6	326.8	66.0
2013 RF98	357.63	0.90	29.6	311.6	67.6
2010 GB174	350.59	0.86	21.6	347.45	130.8
2010 GB174	468.98	0.92	18.6	285.6	112.9
SEDNA	478.88	0.84	11.9	311.5	144.3

Figure 5.3: Eccentricity and inclination profiles of equilibria and their associated stability for $\phi_d = 30°$, along with the clustered TNOs
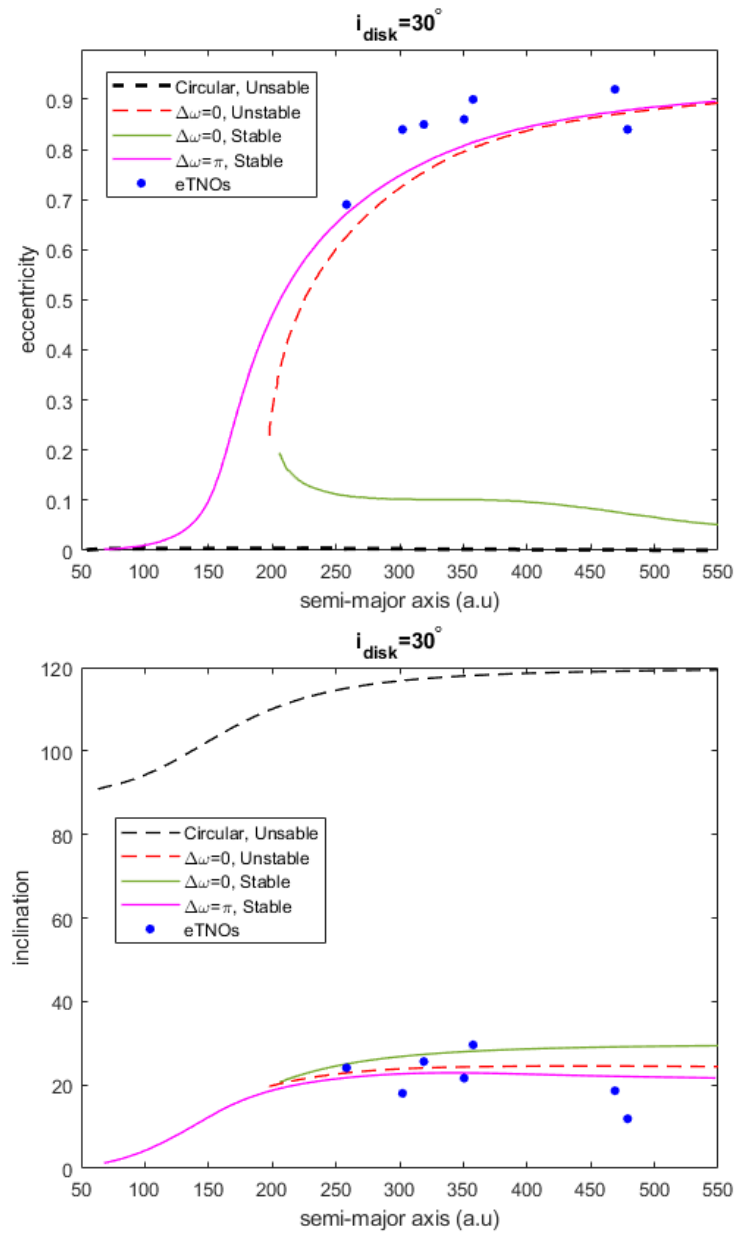
The stability behavior of eccentric families is also retained when the disk is inclined ($\phi_d > 0°$), until we reach $\phi_d \approx 35°$, where the anti-aligend branch starts losing stability at a certain semi-major axis in favor of a newly formed highly eccentric, near-polar family.

Figure 5.4: Eccentricity and inclination profiles of equilibria and their associated stability for $\phi_d = 35°, 40°$
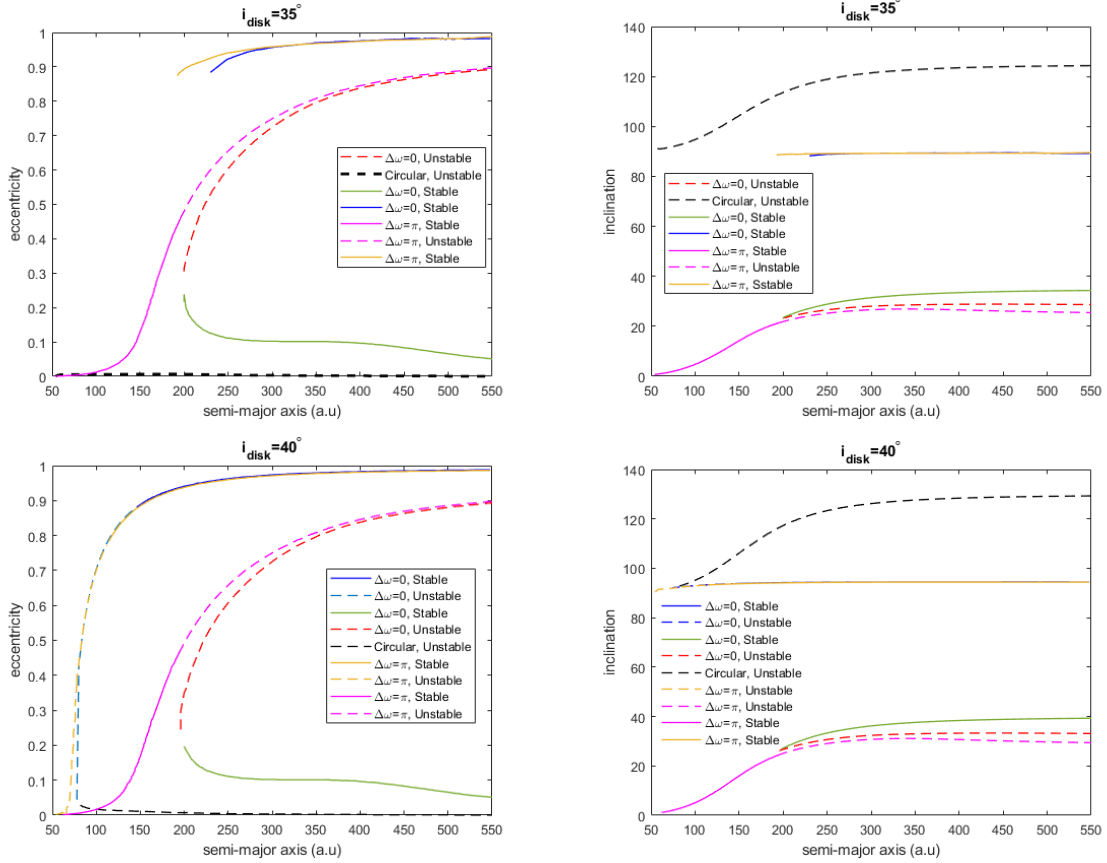
The β-Pictoris Picture:

To apply the tools we have developed for a mutual inclination between the disk and the quadrupole, we study the β-Pictoris system, β-Pic from now on. This system accumulated interest after Smith and Terrile (39) looked into a prominent Infrared Astronomical Satellite (IRAS) infrared excess detection and imaged an edge-on circumstellar disk in dust scattered light. After that, many observational and theoretical studies helped assemble a picture of a dynamically active system that contains a directly imaged planet, β-Pic planet-b (40), a debris disk (41), multiple planetesimal belts (42), and a circling gas cloud that indicates a recent collision between planetesimals (43).
A couple of peculiarities are of interest in the β-Pic system:

- The disk has a warped inner part extending till 80 AU, with an inclination of $3.5 - 4.6°$ between the warped component and the main disk (the outer part) (44).

- The asymmetries observed in the main disk, mainly the non-axisymmetric distribution of the orbiting dust particles between 150 and 800 AU (41).

- A very massive planet $\beta - Pic - b$, with mass estimations ranging between 10 and $16 M_J$ (45) (46) orbits $\beta - Pic$ and is located within the warped component with a semi-major axis ranging between 8 and 13 AU (most probably 9 AU)(44)(47).

Thus we model this system using DM1 we already used, with the inclined inner quadrupole served by $\beta - pic - b$, and the incentive is to study as a function of the mass of the disk, the behavior of the inner part i.e. what mass of DM1, which is used earlier with $10 M_\oplus$, is needed to keep the inner part within the plane of the inner quadrupole. Thus we scale the strength of the disk by a factor "f" i.e $f = 0.2$ resembles a disk of mass $2 M_\oplus$.
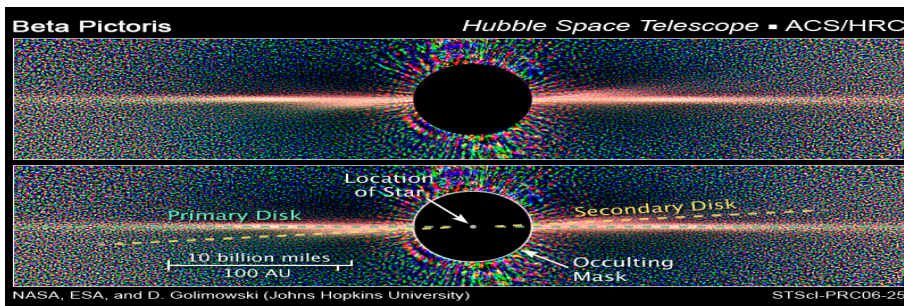
Figure 5.5: Hubble Space Telescope view of Beta Pictoris clearly shows a primary dust disk and a much fainter secondary dust disk. The secondary disk extends at least 24 billion miles from the star and is tilted roughly 4 to 5 degrees from the primary disk.Image from NASA website.

Figure 5.6: Inclinations of equilibria for the $\beta - pic$ setting for different masses of the disk. $Left$: Inclinations of full aligned and anti-aligned equilibira. $Right$: Inclinations of the nearly-axisymmetric part.
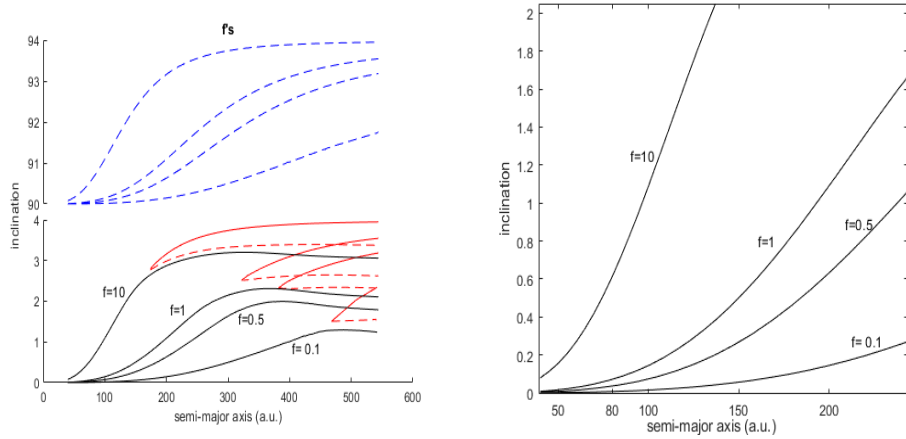
Clearly, the inner quadrupole is strong enough to force an inner disk to reside in its plane for different disk masses. Of course that is due to the huge mass of the planet (we used $13M_J$), and its semi-major axis (we used $a_b = 9AU$), making it a stronger quadrupole than that in the solar system. But it is clear that to let the inner component of the disk and the quadrupole reside in the same plane up till 80 AU, a less massive disk ($f = 0.1$ i.e $1M_\oplus$) would be more appropriate.
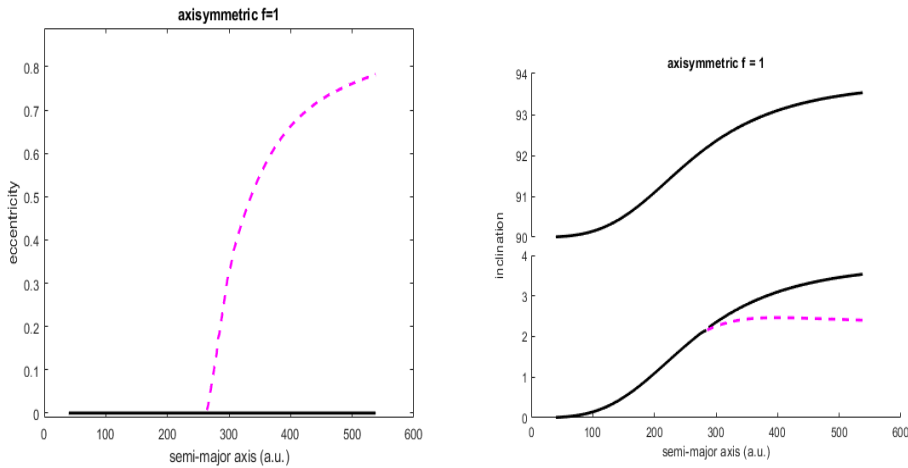
Figure 5.7: Equilibria for the $\beta - pic$ setting for an axisymmetric disk. $Left$: Eccentricity profile. $Right$: Inclinations profile.

5.1.5 Effect of Planetary Embryos:

Recent work of Silsbee and Tremaine (48) suggested via a set of N-Body simulations the existence of multiple bodies with masses between that of Mars and Earth in the outer planetesimal disk of our solar system. The results of the simulations i.e. the survival of those objects, is constrained by the condition of maintaining the current configurations of Uranus and Neptune, thus the parameter space of the results of the simulations is constrained to a narrow region of moderately inclined, low eccentric solutions with semi-major axis $< 200AU$. In the planar disk model presented earlier, we failed to maintain inclined eccentric stationary orbits because nodal precession cannot be frozen for inclined configurations. In fact the net effect of the perturbers generates continuous regression in the node for inclined equilibira.
Our plan is first to check if the suggested planetary embryos can be maintained in inclined configuration under the effect of the disk and inner quadrupole. We have seen earlier that for the disk in the plane of the planets, the only inclined solutions are circular polar ones. But we now need moderately inclined objects. Hence to reach that, we allow the disk to be apsidally moving in a retrograde orientation, and we look for circular inclined equilibria that are moving with the disk, but are not affecting the disk because of their small mass. If we can maintain these inclined circular orbits, we then study their effect as quadrupoles on our test particles.

Precessing Disk:

Because our aim is to take the eccentric equilibria we generated off plane, but at the same time maintain their high eccentricity, and since we're allowing the disk to precess now, we study first the effect of this precession on our already established planar equilibria to see the magnitude of the distortion.
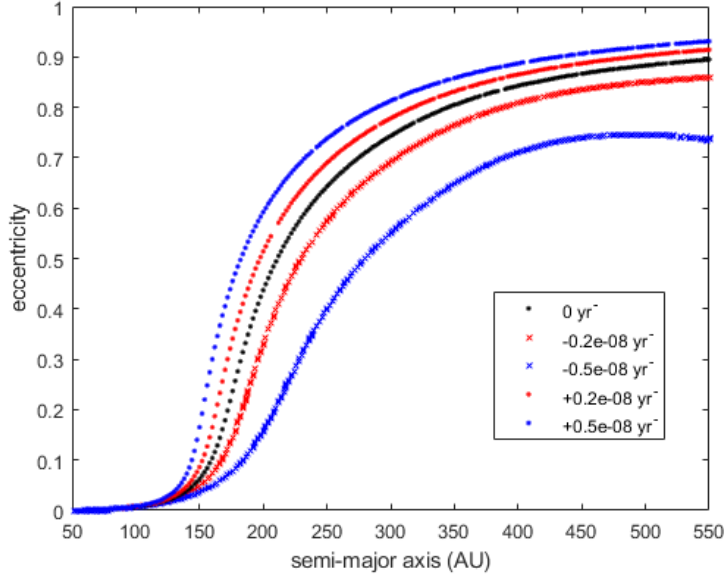
Figure 5.8: The effect of disk precession for different rates on the family of equilibria anti-aligned with the disk.

We do that assuming that the timescale associated with the secular effect of the inner quadrupole is less than that associated with the exchange of angular momentum with the disk, hence an adiabatic interaction. Thus we model the apse of the disk precessing with time, with a precession rate $\dot{\varpi}_d$, so that:

$$\varpi_d = \dot{\varpi}_d t \tag{5.18}$$

To get rid of time dependence, we transfer to the frame co-precessing with the apsidal line of the disk through a canonical transformation using a Type-2 generating function, to end up with a precession contribution to the Hamiltonian:

$$L\dot{\varpi}_d(1 - \sqrt{1 - e^2})\cos i \qquad i.e. - \dot{\varpi}_d H = -L\dot{\varpi}_d(\mathbf{j} \cdot \hat{\boldsymbol{n}}_{\boldsymbol{d}}) \tag{5.19}$$

After adding the effect of this contribution to the equations of motion, we see the results in figure 5.8 for prograde and retrograde disk precession. Clearly, for a precessing disk, the Anti-Aligned family decreases in eccentricity for retrograde precession of the disk, and increases for prograde precession. The opposite effect is observed for the low eccentricity aligned family. Because the total nodal precession of inclined equilibria for a non-precessing disk was retrograde, we are interested in a retrograde regime of the disk. We now proceed to look for circular inclined equilibiria.

If we impose the circular condition on our equations of motion 5.6 and 5.7, the second equation is satisfied trivially, and we are left with one equation to be

solved for the inclination as a function of the semi-major axis and the precession rate:

$$L\frac{d\mathbf{j}}{dt} = \Gamma\frac{\mathbf{j}\cdot\hat{\boldsymbol{n}}_p}{(1-e^2)^{5/2}}\mathbf{j}\times\hat{\boldsymbol{n}}_p - (\mathbf{j}\times\hat{\boldsymbol{n}}_d)\Big[2\Phi_3(0)\mathbf{j}\cdot\hat{\boldsymbol{n}}_d - L\dot{\varpi}_d\Big] \qquad (5.20)$$

which reduces as a condition of coplanar-coplanar circular equilibria to:

$$0 = \frac{\Gamma}{2}\sin 2\phi - j\sin\phi\big(2\Phi_3(0)\cos\phi - L\dot{\varpi}_d\big) \qquad (5.21)$$

Obviously, the planar prograde and retrograde orientations remain as equilibria, but we would be altering the polar circular family that we have seen in the non-precessing configuration. Results for different disk retrograde precession rates are presented in the following figure.

Figure 5.9: Inclinations of circular equilibria for different disk retrograde precessions; From right to left: $0, -0.1, -0, 3, -0.5$, and $-0.7\times 10^{-8} yr^-$. Blue represents orbits that are unstable to angular momentum and eccentricity perturbations. Red are stable orbits.
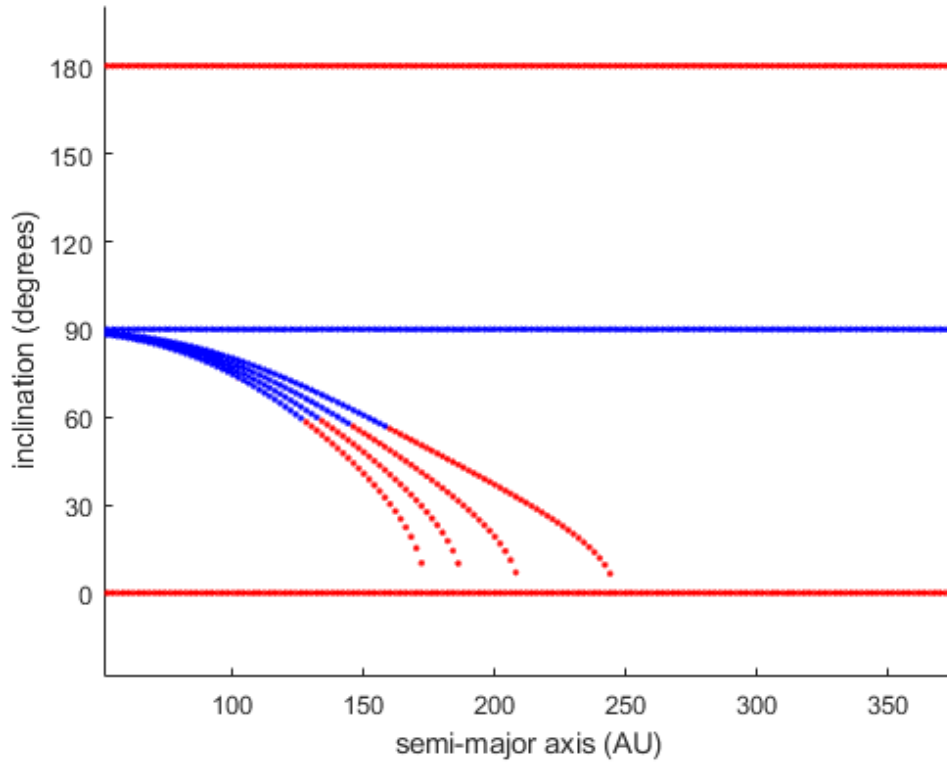
As we predicted, the precession is altering the circular polar family, and the magnitude by which the polar family is altered is propotional to the precession rate. Although the polar family for a non precessing disk was totally unstable, negative precession allowed the disk to maintain stable orbits of moderate inclinations. Thus we were able to fix the nodes of certain circular families in inclined configurations. This will allow us to consider the planetary embryos suggested in (48), although we won't restrict ourselved to the parameters of their simulations, as objects that are consistent with our model. We now proceed to model our system including a precessing disk around the massive planets, along with a planetray embryo acting as an external inclined quadrupole, whose parameters we choose from the equilibria in figure 5.9.

Extended Equations of Motion

We now provide the extended vectorial equations of motion with contributions of a precessing disk, an inner quadrupole from the giant planets, and another quadrupole from the inclined circular planetary embryo.

$$L\frac{d\mathbf{j}}{dt} = +\Gamma\frac{\mathbf{j}\cdot\hat{\boldsymbol{n}_p}}{(1-e^2)^{\frac{5}{2}}}(\mathbf{j}\times\hat{\boldsymbol{n}_p})$$
$$-\Big[2\Phi_3(e)j_n + 2\Phi_4(e)j_n e_u + \Phi_6(e)e_n j_u\Big](\mathbf{j}\times\hat{\boldsymbol{n}_d})$$
$$-\Big[\Phi_6(e)e_n j_n\Big](\mathbf{j}\times\hat{\boldsymbol{u}_d})$$
$$-\Big[\Phi_1(e) + \Phi_4(e)j_n^2 + \Phi_5(e)e_n^2\Big](\mathbf{e}\times\hat{\boldsymbol{u}_d})$$
$$-\Big[2\Phi_2(e)e_n + 2\Phi_5(e)e_u e_n + \Phi_6(e)j_u j_n\Big](\mathbf{e}\times\hat{\boldsymbol{n}_d}) \tag{5.22}$$
$$+\frac{3}{4}\varepsilon_\odot(\mathbf{j}\cdot\hat{\boldsymbol{n}_\odot})(\mathbf{j}\times\hat{\boldsymbol{n}_\odot}) - \frac{15}{4}\varepsilon_\odot(\mathbf{e}\cdot\hat{\boldsymbol{n}_\odot})(\mathbf{e}\times\hat{\boldsymbol{n}_\odot})$$
$$+L\dot{\varpi}_d(\mathbf{j}\times\hat{\boldsymbol{n}_d}) \tag{5.23}$$

$$L\frac{d\mathbf{e}}{dt} = +\Gamma\frac{\mathbf{j}\cdot\hat{\boldsymbol{n}_p}}{(1-e^2)^{\frac{5}{2}}}(\mathbf{e}\times\hat{\boldsymbol{n}_p}) - \frac{\Gamma}{2}\frac{1-e^2-5(\mathbf{j}\cdot\hat{\boldsymbol{n}_p})^2}{(1-e^2)^{\frac{7}{2}}}(\mathbf{j}\times\mathbf{e})$$
$$-\Big[2\Phi_3(e)j_n + 2\Phi_4(e)j_n e_u + \Phi_6(e)e_n j_u\Big](\mathbf{e}\times\hat{\boldsymbol{n}_d})$$
$$-\Big[\Phi_6(e)e_n j_n\Big](\mathbf{e}\times\hat{\boldsymbol{u}_d})$$
$$-\Big[\Phi_1(e) + \Phi_4(e)j_n^2 + \Phi_5(e)e_n^2\Big](\mathbf{j}\times\hat{\boldsymbol{u}_d})$$
$$-\Big[2\Phi_2(e)e_n + 2\Phi_5(e)e_u e_n + \Phi_6(e)j_u j_n\Big](\mathbf{j}\times\hat{\boldsymbol{n}_d})$$
$$-\Big[D_0 + D_1 e_u + D_2 e_n^2 + D_3 j_n^2 + D_4 e_u j_n^2 + D_5 e_u e_n^2 + D_6 j_u e_n j_n\Big](\mathbf{j}\times\mathbf{e})$$
$$+\frac{3}{4}\varepsilon_\odot(\mathbf{j}\cdot\hat{\boldsymbol{n}_\odot})(\mathbf{e}\times\hat{\boldsymbol{n}_\odot}) - \frac{15}{4}\varepsilon_\odot(\mathbf{e}\cdot\hat{\boldsymbol{n}_\odot})(\mathbf{j}\times\hat{\boldsymbol{n}_\odot}) + \frac{3}{2}\varepsilon_\odot(\mathbf{j}\times\mathbf{e})$$
$$+L\dot{\varpi}_d(\mathbf{e}\times\hat{\boldsymbol{n}_d}) \tag{5.24}$$

where as before, components with subscripts are defined with respect to the basis vectors corresponding to the disk, while $\hat{\boldsymbol{n}_\odot}$ corresponds to the orbital angular momentum unit vector of the introduced massive body. And the inner quadrupole strength is defined by:

$$\varepsilon_\odot = GM_\odot\frac{a^2}{a_\odot^3}\frac{1}{(1-e_\odot^2)^{\frac{3}{2}}} \tag{5.25}$$

We then transform to the coplanar-coplanar configuration and look for equilibria.

In this system, we have an interplay of multiple factors at once. Physically speaking, we have a wide range of parameters that we can control. That includes, and is not restricted to:

- The model of the disk (the mass and eccentricity distribution, and the distances over which the disk extends. As we said, for these we adopted DM1 of the referenced work (35)).

- Second, the disk's precession rate orientation and magnitude, and for those we choose a disk regressing because the nodal precession of inclined objects under the disk effect was negative, and we chose a magnitude of regression that does not drastically distort the eccentricity profile of the planar case, while also allowing a circular planetary embryo to exist at a moderate inclination and semi-major axis that is maintained by the distribution of surviving object of Silsbee and Tremaine simulations (48). Based on that, in the sample of results presented below, we used a regression rate: $\dot{\varpi}_d = -0.3 \times 10^{-8} yr^-$.

- Third concerning the planetary embryo, we restricted it to be on a circular orbit. We realize this is not a probable result of (48), but that would allow us to avoid the limitations of the multipoles expansion as the setting is not by any means hierarchical, but higher order terms vanish exactly for a circular orbit. The inclination and semi major axis of the object are dictated by our choice of the precession rate of the disk. In fig 5.9, each rate allows a family of inclined circular equilibiria function of distance. The rate we chose allows for stable equilibria ranging between 145 and 212 AU, with inclinations starting with $57°$ and dropping to zero. Here we had to compromise in choosing the parameters: The more the object is inclined, the more the equilibria we generate would be inclined too, however the more inclined the object the smaller semi-major axis it would have, and that would strengthen its effect, eventually causing more distortion to our desirable profile of eccentricity. Hence in our sample of results, we used an object at 172 AU, inclined at $41°$.

- Finally, we had to choose a mass for the object. The results of (48) show that the distribution of masses allowing for survival falls between $0.1 - 0.5 M_{\oplus}$. In the sample of results presented below, we choose a Mars mass object. However, in what follows we studied the effect of mass on the equilibria.
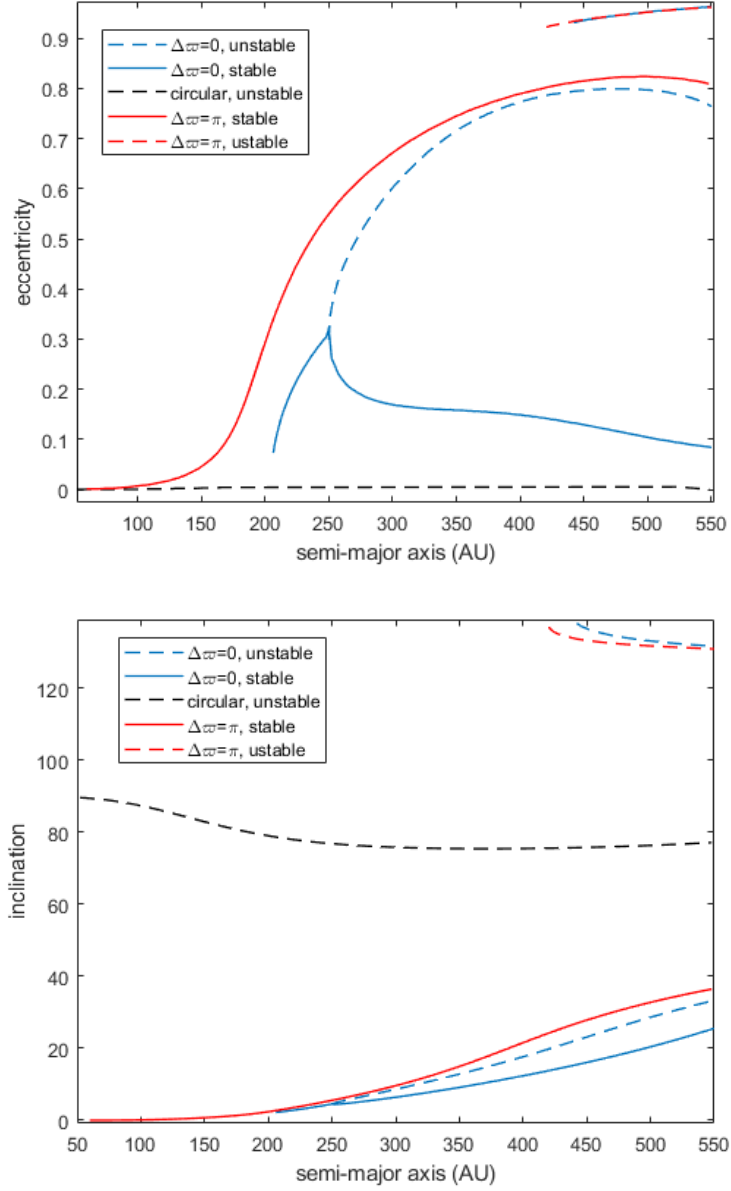
Figure 5.10: Equilibria profiles of the solutions of the extended equations of motion. We chose a disk regressing with a rate= $-0.3 \times 10^{-8} yr^{-}$. This disk allows for a family of stable circular planetary embryos to exist (fig:5.9), we took one of them with inclination $41°$, mass $0.1 M_{\oplus}$, and $a = 172 AU$.
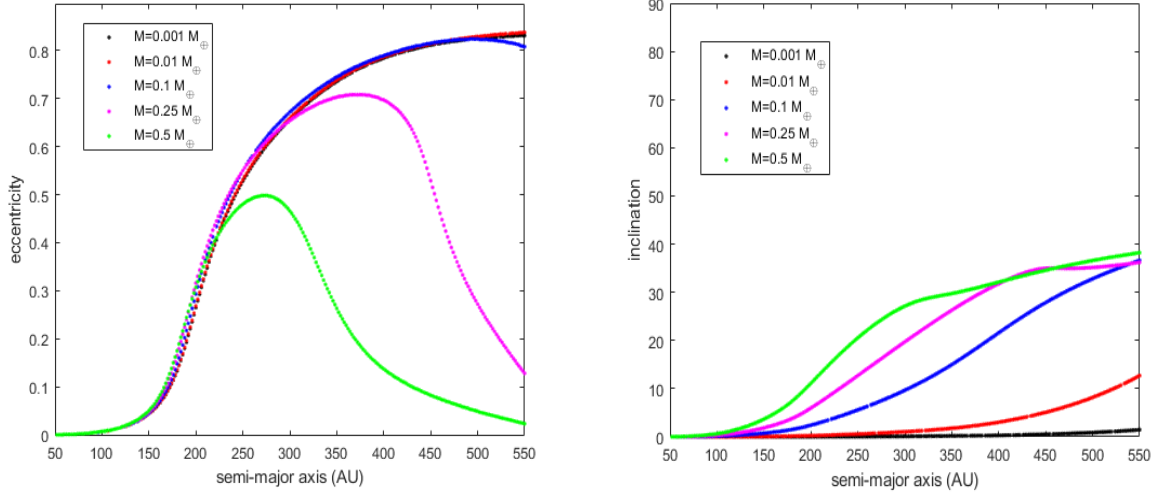
Figure 5.11: Variations in the anti-aligned family for the disk precessing with $-0.3 \times 10^{-8} yr^-$, and the same core used earlier ($a = 172AU, i = 41°$) but for different masses of it.
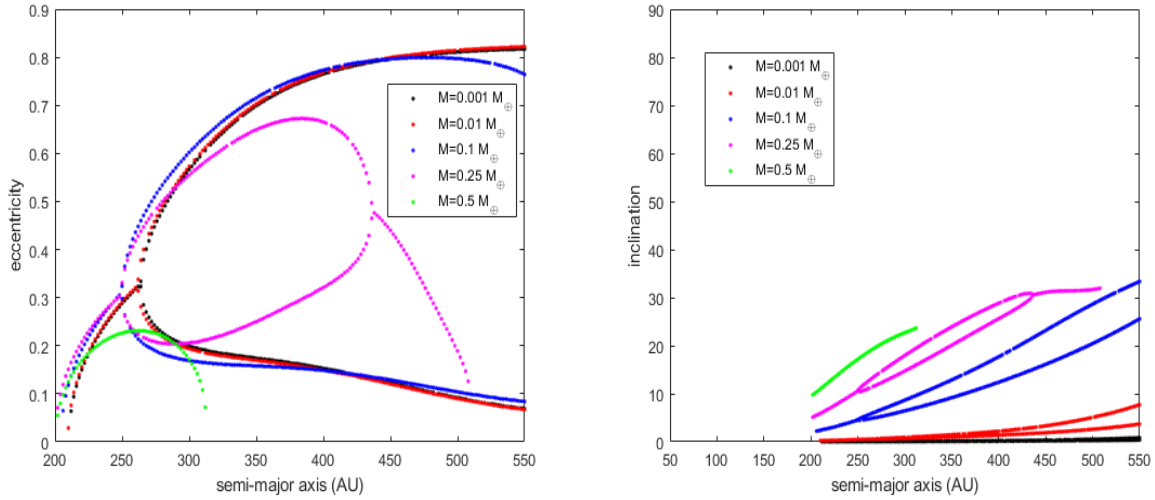
Figure 5.12: Variations in the aligned family for the disk precessing with $-0.3 \times 10^{-8} yr^-$, and the same core used earlier ($a = 172AU, i = 41°$) but for different masses of it.

Our justified choice of parameters allowed us to generate a very promising profile of eccentric inclined equilibria. The interplay between the precessing disk, the giant planets, and the massive object came out in a tuned manner. The disk fixed the apse of our eccentric inclined particles, and while it allowed for circular massive objects to survive, an object of this sort fixed the nodes of our test particles. Eventually that resulted in maintaining the three eccentric families we have: two highly eccentric aligned and anti-aligned families, and another aligned family of low eccentricity, but off the invariant plane! The high eccentricity families decreased in eccentricity because of the disk regression and the effect of the massive object, but retained their stability, specifically our desirable anti-aligned family.

The inclinations of the equilibria followed an increasing trend, The anti-aligned family started at small distances in the plane of the planets, then took of in inclination towards the plane of the inclined massive object. The aligned bifurcation however, emerging at moderate distances started with an inclination and increased in inclination yet remained below the inclination of the object.

In figures. 5.11, 5.12 we studied the effect of the mass of the object on both the aligned and anti-aligned families. We used masses ranging between $0.001-0.5M_\oplus$. The greater the mass of the object the more distortion it produced on the eccentric families, driving them less eccentric. An object with half Earth mass would allow the anti-aligned family to gain eccentricity and peaks at $e = 0.5$ around $270AU$, then loses that eccentricity again. But what we are interested in, is what mass would keep the same eccentric profile inclined. We found out that objects as small as a tenth of Mars would pump the equilibria off plane a couple of degrees at high enough semi-major axis. A mass less than that cannot lift the equilbria off plane. But to produce the desirable inclinations over moderate distances, a mass around $0.1M_\oplus$ is the most appropriate.

Chapter 6

Summary and Conclusions:

We explored dynamics on the Laplace Surface in the classical sense inspired by a history of work extending from Laplace himself, to the recent work of TTN. We questioned how an external perturber that lies on an eccentric orbit would modify the classical topology of equilibria. TTN have also allowed for an eccentric binary, but having restricted multipoles expansion of the perturbation to orbit averaged quadrupolar order, the binary eccentricity only enters as a parameter. Hence for a more accurate account of a non-axisymmetric perturbation we included the Octupole. The Hamiltonian was written in a vectorial form, and was doubly averaged over the orbits to describe the long term deformation of our test orbits. Thus in a secular sense, all of our orbits were analogous to rings of mass distribution described by two vectors: the angular momentum vector and the Laplace-Runge-Lenz vector. This allowed us to describe the dynamics by the Milankovitch equations of motion.

From here on, we were able to explore dynamical equilibria, either by setting the time derivatives of our angular momentum and eccentricity vectors to zero or by phase portraits of our Hamiltonian. Our equilibria of course describe orbits that are non precessing, frozen in space.

The aforementioned history on the subject, along with our theoretical build up including the Octupole theory are expanded in Chapters 1 & 2.

In Chapter 3, we first studied the dynamics of satellites around an oblate planet; with the planet on an eccentric orbit around its host star (the same system studied in TTN except for the eccentric feature of the planet). The Octupole here allows the eccentricity of the planet to enter as a variable rather than a parameter. In a system of scales similar to our Satellite-Earth-Sun system, the multipoles expansion (being a parametric expansion with the ratio of semi-major axes of the inner to outer binary playing the role of the expansion parameter), and in a physical region which is constrained by Hill's radius, the Octupole imposed an additional condition on circular equilibria. This condition, which does not care about the strength of the Octupole through the value of the eccentricity of the outer binary (as long as it's not zero), is not satisfied by the circular equilibria of

the quadrupolar picture. Thus the Laplace surface is destroyed at the octupolar level. However, the Octupole in such a setting turned out to be very weak and did not significantly alter the topology of eccentric equilibria generated at the quadrupolar level, neither did it change their stability. Thus we concluded that in such a system, the Laplace Surface does not survive, and eccentric equilibria would not care if the Earth resided on an eccentric orbit around the Sun.

Nevertheless, in order to investigate the Octupole in a real physical system, we studied the exoplanetary system Kepler-108, that serves as a rare example of mutiplanetary systems with mutual inclinations between the planets, let alone the host star having a wide stellar companion. In this interesting system constituted of two planets, the inner planet plays the role of the inner quadrupole, and the stellar binary contributes as the external perturber, and the outer planet is our test particle. We applied our machinery to this system, assuming the stellar binary is highly eccentric, and explored how the classical Laplace equilibria are modified upon the introduction of the Octupole (The octupole being stronger (relative to the quadrupole) in this case than the previous one. It turns out that losing the Laplace surface of circular equilibria was compromised by the creation of new equilibria. The loci of these equilibria as a function of semi major axis would still follow the alignment trend i.e. aligned with the inner plane at short distances, and with the outer plane at larges distances, and the transition occurs around the Laplace radius. However, the interesting result was that these equilibria which were circular under quadrupoles, are now pumped in eccentricity, and eccentricity function increasing as the orbit enters the outer binary dominated regime. Thus we were able to observe an *Eccentric Laplace Surface* in this case. Although the system needs further analysis, this new surface can explain the current orbital cofiguration of the system.

To exploit the theory more, we investigate a system where the Octupole is of a stronger effect. In the trans-Neptunian region, some of the most distant objects appear to have roughly aligned orbits (both in apse and in node), and they are highly eccentric and moderately inclined. Numerical simulations show that a distant Neptune-mass planet could produce such an accumulation. Thus we try to explain the orbital anomalies of these eTNOs by suggesting they reside in Laplace equilibria planes, where the suggested Planet IX plays the role of the distant perturber, and the giant planets serve as the inner quadrupole. Interestingly enough, we created a structure of equilibria that is unique to the literature. The Octupole in this case is stronger than that in Kepler-108, and the created Eccentric Laplace surface was compromised at a certain semi-major axis in favor of highly eccentric non-linear bifurcations. Unfortunately, we have shown, via a convergence analysis study, that the multipolar series diverges in this setting, and this desirable structure of equilibria in a region where their apoapses are outside the periapse of Planet IX.

However, we intended to study the robustness of this structure of equilibria when subject to multiple variations in the perturbations, such as the mass of the

perturber, the orientation of the perturbation -especially in the case of Planet IX because the significance of the Octupole is in its breaking of symmetry feature- and the addition of higher order terms.

In Chapter 4, we attempted to avoid the limitation of the parametric expansion by modelling the perturbation numerically. This will allow us to correctly model the ring of Planet IX by accounting for the whole of its mass distribution, both in regions inside and outside the particle's orbit. We calculated the gravitational potential of that ring in a spatial grid then expanded the potential in spherical harmonics given their associated modes numerically. This allowed us to create a structure of equilibria that matches the literature in a planar setting, and matches the TNOs in a 3D setting. Specifically, we were able to create a highly eccentric, moderately inclined, family of equilibria that is antialigned with the planet.

With that we concluded our investigation of the modification of Laplace Surface dynamics after studying the effect of weak, moderate, and strong Octupole regimes via expanding the external perturbation both in analytically in multipoles, and semi-analytically in spherical harmonics.

In the last chapter, we followed up on a recent work suggesting that the self-gravity of a massive TNOs reservoir, along with the effect of the giant planets, renders the ninth planet dispensable. This work was able to produce a stable highly eccentric family of equilibria that is anti-aligned with the self-gravitating disk of TNOs. However, this work was restricted to planar dynamics, so we intended to add the inclined feature to the equilibria. To do so, we built a self consistent model that constituted of a precessing disk of TNOs, the giant planets, and an inclined planetary embryo that we were inspired to include from successful simulations in the literature. The combined effect of these components resulted in a topology of equilibria that included a stable, highly eccentric, and moderately inclined family of equilibria that is anti-alinged with the disk.

With that we concluded the work of this thesis, having more questions posed than we had at the beginning. We have studied equilibria configurations without addressing the mechanisms that can drive the particles into such configurations. In other words, we have not studied the evolution of our systems when not in equilibria. Although we have some ideas from the literature, we think this is worth a future study. We also think that in our secular description we were able to capture the dominant dynamical behavior. But accounting for resonances as a correction to that can complete the picture. That also is left for future work.

A problem that we have thought about and that is definitely worth further investigation is a setting in which the Octupole is in the inner perturbation rather than the outer one. We can see this configuration in circumbinary planets in a triple stellar system. The inner stellar binary can be on an eccentric orbit if it undergoes Kozai cycles driven by the tertiary companion. And thus the octupole is needed on the inside to correctly account for the potential.

Our use of the numerical toolbox in the expansion of the interaction in spher-

ical harmonics is a story on its own. We believe this method is very promising in modelling gravitational potentials exactly when other models fail. A detailed study of this toolbox is to prove its robustness is definitely needed.

A further study of Kepler-108 system is also required. We have fixed the inner planet for the sake of our study, but a more precise analysis of the system could require solving for the dynamical evolution of both planets; and that's also left for future work.

Appendix A

Linear Stability Analysis:

For completeness, we present the full linear stability analysis used for determining the stability of generated equilibria. As we studied, for $\mathbf{x}$ containing our vectorial elements, a point $\mathbf{x}_0$ is an equilibrium if $\nabla H(\mathbf{x}_0) = 0$. Our study of equilibira stability would be by linearizing the equations of motion assuming $\mathbf{x}_1 = \mathbf{x} - \mathbf{x}_0$ obtaining

$$\dot{\mathbf{x}}_1 = L\mathbf{x}_1 \tag{A.1}$$

Hence we first look for the linearization matrix L by writing $\mathbf{j} = \mathbf{j}_0 + \mathbf{j}_1$ and $\mathbf{e} = \mathbf{e}_0 + \mathbf{e}_1$ then linearizing the equations of motion (B.20) and (2.95) for arbitrary equilibria $\mathbf{j}_0$ and $\mathbf{e}_0$ up to first order in $\mathbf{j}_1$ and $\mathbf{e}_1$. Having found the linearization matrix L, the solution of the first equation, for distinct eigenvalues λ_i, is of the form:

$$\mathbf{x}_1(t) = \sum_{i=1}^{i=2n} c_i \mathbf{v}_i \exp(\lambda_i t) \tag{A.2}$$

where $\mathbf{v}_i$ are the eigenvectors of L. The solution has exponentially growing terms unless all eigenvalues lie on the imaginary axis. Thus our stability analysis reduces

to finding eigenvalues of L (21).

$$
\begin{aligned}
\frac{d\mathbf{j}_1}{d\tau} =& \frac{3}{4}\varepsilon_\odot(\mathbf{j}_0\cdot\hat{\boldsymbol{n}}_\odot)(\mathbf{j}_1\times\hat{\boldsymbol{n}}_\odot) + \frac{3}{4}\varepsilon_\odot(\mathbf{j}_1\cdot\hat{\boldsymbol{n}}_\odot)(\mathbf{j}_0\times\hat{\boldsymbol{n}}_\odot) - \frac{15}{4}\varepsilon_\odot(\mathbf{e}_0\cdot\hat{\boldsymbol{n}}_\odot)(\mathbf{e}_1\times\hat{\boldsymbol{n}}_\odot) \\
& - \frac{15}{4}\varepsilon_\odot(\mathbf{e}_1\cdot\hat{\boldsymbol{n}}_\odot)(\mathbf{e}_0\times\hat{\boldsymbol{n}}_\odot) + \frac{15}{2}\varepsilon_p(\mathbf{j}_0\cdot\hat{\boldsymbol{n}}_{\boldsymbol{p}})(\mathbf{j}_0\times\hat{\boldsymbol{n}}_{\boldsymbol{p}})(\mathbf{e}_0\cdot\mathbf{e}_1)(1-e_0^2)^{-\frac{7}{2}} \\
& + \frac{3}{2}\varepsilon_p(\mathbf{j}_1\cdot\hat{\boldsymbol{n}}_{\boldsymbol{p}})(\mathbf{j}_0\times\hat{\boldsymbol{n}}_{\boldsymbol{p}})(1-e_0^2)^{-\frac{5}{2}} + \frac{3}{2}\varepsilon_p(\mathbf{j}_0\cdot\hat{\boldsymbol{n}}_{\boldsymbol{p}})(\mathbf{j}_1\times\hat{\boldsymbol{n}}_{\boldsymbol{p}})(1-e_0^2)^{-\frac{5}{2}} \\
& - \frac{75}{64}\varepsilon_\odot\varepsilon_\otimes\Big[2(\mathbf{e}_0\cdot\hat{\boldsymbol{u}}_\odot)(\mathbf{j}_0\cdot\hat{\boldsymbol{n}}_\odot)(\mathbf{j}_1\times\hat{\boldsymbol{n}}_\odot) + 2(\mathbf{e}_0\cdot\hat{\boldsymbol{u}}_\odot)(\mathbf{j}_1\cdot\hat{\boldsymbol{n}}_\odot)(\mathbf{j}_0\times\hat{\boldsymbol{n}}_\odot) \\
& + 2(\mathbf{e}_1\cdot\hat{\boldsymbol{u}}_\odot)(\mathbf{j}_0\cdot\hat{\boldsymbol{n}}_\odot)(\mathbf{j}_0\times\hat{\boldsymbol{n}}_\odot) + 2(\mathbf{e}_0\cdot\hat{\boldsymbol{n}}_\odot)(\mathbf{j}_0\cdot\hat{\boldsymbol{u}}_\odot)(\mathbf{j}_1\times\hat{\boldsymbol{n}}_\odot) \\
& + 2(\mathbf{e}_0\cdot\hat{\boldsymbol{n}}_\odot)(\mathbf{j}_1\cdot\hat{\boldsymbol{u}}_\odot)(\mathbf{j}_0\times\hat{\boldsymbol{n}}_\odot) + 2(\mathbf{e}_1\cdot\hat{\boldsymbol{n}}_\odot)(\mathbf{j}_0\cdot\hat{\boldsymbol{u}}_\odot)(\mathbf{j}_0\times\hat{\boldsymbol{n}}_\odot) \\
& - 14(\mathbf{e}_0\cdot\hat{\boldsymbol{n}}_\odot)(\mathbf{e}_0\cdot\hat{\boldsymbol{u}}_\odot)(\mathbf{e}_1\times\hat{\boldsymbol{n}}_\odot) - 14(\mathbf{e}_0\cdot\hat{\boldsymbol{n}}_\odot)(\mathbf{e}_1\cdot\hat{\boldsymbol{u}}_\odot)(\mathbf{e}_0\times\hat{\boldsymbol{n}}_\odot) \\
& - 14(\mathbf{e}_1\cdot\hat{\boldsymbol{n}}_\odot)(\mathbf{e}_0\cdot\hat{\boldsymbol{u}}_\odot)(\mathbf{e}_0\times\hat{\boldsymbol{n}}_\odot) + 2(\mathbf{j}_0\cdot\hat{\boldsymbol{u}}_\odot)(\mathbf{j}_0\cdot\hat{\boldsymbol{n}}_\odot)(\mathbf{e}_1\times\hat{\boldsymbol{n}}_\odot) \\
& + 2(\mathbf{j}_0\cdot\hat{\boldsymbol{u}}_\odot)(\mathbf{j}_1\cdot\hat{\boldsymbol{n}}_\odot)(\mathbf{e}_0\times\hat{\boldsymbol{n}}_\odot) + 2(\mathbf{j}_1\cdot\hat{\boldsymbol{u}}_\odot)(\mathbf{j}_0\cdot\hat{\boldsymbol{n}}_\odot)(\mathbf{e}_0\times\hat{\boldsymbol{n}}_\odot) \\
& + 2(\mathbf{e}_0\cdot\hat{\boldsymbol{n}}_\odot)(\mathbf{j}_0\cdot\hat{\boldsymbol{n}}_\odot)(\mathbf{j}_1\times\hat{\boldsymbol{u}}_\odot) + 2(\mathbf{e}_0\cdot\hat{\boldsymbol{n}}_\odot)(\mathbf{j}_1\cdot\hat{\boldsymbol{n}}_\odot)(\mathbf{j}_0\times\hat{\boldsymbol{u}}_\odot) \\
& + 2(\mathbf{e}_1\cdot\hat{\boldsymbol{n}}_\odot)(\mathbf{j}_0\cdot\hat{\boldsymbol{n}}_\odot)(\mathbf{j}_0\times\hat{\boldsymbol{u}}_\odot) - 7(\mathbf{e}_0\cdot\hat{\boldsymbol{n}}_\odot)^2(\mathbf{e}_1\times\hat{\boldsymbol{u}}_\odot) \\
& - 14(\mathbf{e}_0\cdot\hat{\boldsymbol{n}}_\odot)(\mathbf{e}_1\cdot\hat{\boldsymbol{n}}_\odot)(\mathbf{e}_0\times\hat{\boldsymbol{u}}_\odot) + (\mathbf{j}_0\cdot\hat{\boldsymbol{n}}_\odot)^2(\mathbf{e}_1\times\hat{\boldsymbol{u}}_\odot) + \frac{8}{5}e_0^2(\mathbf{e}_1\times\hat{\boldsymbol{u}}_\odot) \\
& + 2(\mathbf{j}_0\cdot\hat{\boldsymbol{n}}_\odot)(\mathbf{j}_1\cdot\hat{\boldsymbol{n}}_\odot)(\mathbf{e}_0\times\hat{\boldsymbol{u}}_\odot) + \frac{16}{5}(\mathbf{e}_0\cdot\mathbf{e}_1)(\mathbf{e}_0\times\hat{\boldsymbol{u}}_\odot) - \frac{1}{5}(\mathbf{e}_1\times\hat{\boldsymbol{u}}_\odot)\Big]
\end{aligned}
$$
(A.3)

$$\frac{d\mathbf{e}_1}{d\tau} = \frac{3}{4}\varepsilon_\odot(\mathbf{j}_0 \cdot \hat{\boldsymbol{n}}_\odot)(\mathbf{e}_1 \times \hat{\boldsymbol{n}}_\odot) + \frac{3}{4}\varepsilon_\odot(\mathbf{j}_1 \cdot \hat{\boldsymbol{n}}_\odot)(\mathbf{e}_0 \times \hat{\boldsymbol{n}}_\odot) - \frac{15}{4}\varepsilon_\odot(\mathbf{e}_0 \cdot \hat{\boldsymbol{n}}_\odot)(\mathbf{j}_1 \times \hat{\boldsymbol{n}}_\odot)$$

$$- \frac{15}{4}\varepsilon_\odot(\mathbf{e}_1 \cdot \hat{\boldsymbol{n}}_\odot)(\mathbf{j}_0 \times \hat{\boldsymbol{n}}_\odot) + \frac{15}{2}\varepsilon_p(\mathbf{j}_0 \cdot \hat{\boldsymbol{n}}_{\boldsymbol{p}})(\mathbf{e}_0 \times \hat{\boldsymbol{n}}_{\boldsymbol{p}})(\mathbf{e}_0 \cdot \mathbf{e}_1)(1 - e_0^2)^{-\frac{7}{2}}$$

$$+ \frac{3}{2}\varepsilon_p(\mathbf{j}_1 \cdot \hat{\boldsymbol{n}}_{\boldsymbol{p}})(\mathbf{e}_0 \times \hat{\boldsymbol{n}}_{\boldsymbol{p}})(1 - e_0^2)^{-\frac{5}{2}} + \frac{3}{2}\varepsilon_p(\mathbf{j}_0 \cdot \hat{\boldsymbol{n}}_{\boldsymbol{p}})(\mathbf{e}_1 \times \hat{\boldsymbol{n}}_{\boldsymbol{p}})(1 - e_0^2)^{-\frac{5}{2}}$$

$$- \frac{3}{4}\varepsilon_p(\mathbf{j}_0 \times \mathbf{e}_0)\left[5\frac{(\mathbf{e}_0 \cdot \mathbf{e}_1)}{(1 - e_0^2)^{\frac{7}{2}}} - 35\frac{(\mathbf{j}_0 \cdot \hat{\boldsymbol{n}}_{\boldsymbol{p}})^2}{(1 - e_0^2)^{\frac{9}{2}}} - 10\frac{(\mathbf{j}_0 \cdot \hat{\boldsymbol{n}}_{\boldsymbol{p}})(\mathbf{j}_1 \cdot \hat{\boldsymbol{n}}_{\boldsymbol{p}})}{(1 - e_0^2)^{\frac{7}{2}}}\right]$$

$$+ (\mathbf{j}_1 \times \mathbf{e}_0)\left[\frac{3}{2}\varepsilon_\odot - \frac{3}{4}\varepsilon_p\big[(1 - e_0^2)^{-\frac{5}{2}} - 5(\mathbf{j}_0 \cdot \hat{\boldsymbol{n}}_{\boldsymbol{p}})^2(1 - e_0^2)^{-\frac{7}{2}}\big]\right]$$

$$+ (\mathbf{j}_0 \times \mathbf{e}_1)\left[\frac{3}{2}\varepsilon_\odot - \frac{3}{4}\varepsilon_p\big[(1 - e_0^2)^{-\frac{5}{2}} - 5(\mathbf{j}_0 \cdot \hat{\boldsymbol{n}}_{\boldsymbol{p}})^2(1 - e_0^2)^{-\frac{7}{2}}\big]\right]$$

$$- \frac{75}{64}\varepsilon_\odot\varepsilon_\otimes\Big[2(\mathbf{e}_0 \cdot \hat{\boldsymbol{u}}_\odot)(\mathbf{j}_0 \cdot \hat{\boldsymbol{n}}_\odot)(\mathbf{e}_1 \times \hat{\boldsymbol{n}}_\odot) + 2(\mathbf{e}_0 \cdot \hat{\boldsymbol{u}}_\odot)(\mathbf{j}_1 \cdot \hat{\boldsymbol{n}}_\odot)(\mathbf{e}_0 \times \hat{\boldsymbol{n}}_\odot)$$

$$+ 2(\mathbf{e}_1 \cdot \hat{\boldsymbol{u}}_\odot)(\mathbf{j}_0 \cdot \hat{\boldsymbol{n}}_\odot)(\mathbf{e}_0 \times \hat{\boldsymbol{n}}_\odot) + 2(\mathbf{e}_0 \cdot \hat{\boldsymbol{n}}_\odot)(\mathbf{j}_0 \cdot \hat{\boldsymbol{u}}_\odot)(\mathbf{e}_1 \times \hat{\boldsymbol{n}}_\odot)$$

$$+ 2(\mathbf{e}_0 \cdot \hat{\boldsymbol{n}}_\odot)(\mathbf{j}_1 \cdot \hat{\boldsymbol{u}}_\odot)(\mathbf{e}_0 \times \hat{\boldsymbol{n}}_\odot) + 2(\mathbf{e}_1 \cdot \hat{\boldsymbol{n}}_\odot)(\mathbf{j}_0 \cdot \hat{\boldsymbol{u}}_\odot)(\mathbf{e}_0 \times \hat{\boldsymbol{n}}_\odot)$$

$$- 14(\mathbf{e}_0 \cdot \hat{\boldsymbol{n}}_\odot)(\mathbf{e}_0 \cdot \hat{\boldsymbol{u}}_\odot)(\mathbf{j}_1 \times \hat{\boldsymbol{n}}_\odot) - 14(\mathbf{e}_0 \cdot \hat{\boldsymbol{n}}_\odot)(\mathbf{e}_1 \cdot \hat{\boldsymbol{u}}_\odot)(\mathbf{j}_0 \times \hat{\boldsymbol{n}}_\odot)$$

$$- 14(\mathbf{e}_1 \cdot \hat{\boldsymbol{n}}_\odot)(\mathbf{e}_0 \cdot \hat{\boldsymbol{u}}_\odot)(\mathbf{j}_0 \times \hat{\boldsymbol{n}}_\odot) + 2(\mathbf{j}_0 \cdot \hat{\boldsymbol{u}}_\odot)(\mathbf{j}_0 \cdot \hat{\boldsymbol{n}}_\odot)(\mathbf{j}_1 \times \hat{\boldsymbol{n}}_\odot)$$

$$+ 2(\mathbf{j}_0 \cdot \hat{\boldsymbol{u}}_\odot)(\mathbf{j}_1 \cdot \hat{\boldsymbol{n}}_\odot)(\mathbf{j}_0 \times \hat{\boldsymbol{n}}_\odot) + 2(\mathbf{j}_1 \cdot \hat{\boldsymbol{u}}_\odot)(\mathbf{j}_0 \cdot \hat{\boldsymbol{n}}_\odot)(\mathbf{j}_0 \times \hat{\boldsymbol{n}}_\odot)$$

$$+ 2(\mathbf{e}_0 \cdot \hat{\boldsymbol{n}}_\odot)(\mathbf{j}_0 \cdot \hat{\boldsymbol{n}}_\odot)(\mathbf{e}_1 \times \hat{\boldsymbol{u}}_\odot) + 2(\mathbf{e}_0 \cdot \hat{\boldsymbol{n}}_\odot)(\mathbf{j}_1 \cdot \hat{\boldsymbol{n}}_\odot)(\mathbf{e}_0 \times \hat{\boldsymbol{u}}_\odot)$$

$$+ 2(\mathbf{e}_1 \cdot \hat{\boldsymbol{n}}_\odot)(\mathbf{j}_0 \cdot \hat{\boldsymbol{n}}_\odot)(\mathbf{e}_0 \times \hat{\boldsymbol{u}}_\odot) - 7(\mathbf{e}_0 \cdot \hat{\boldsymbol{n}}_\odot)^2(\mathbf{j}_1 \times \hat{\boldsymbol{u}}_\odot)$$

$$- 14(\mathbf{e}_0 \cdot \hat{\boldsymbol{n}}_\odot)(\mathbf{e}_1 \cdot \hat{\boldsymbol{n}}_\odot)(\mathbf{j}_0 \times \hat{\boldsymbol{u}}_\odot) + (\mathbf{j}_0 \cdot \hat{\boldsymbol{n}}_\odot)^2(\mathbf{j}_1 \times \hat{\boldsymbol{u}}_\odot) + \frac{8}{5}e_0^2(\mathbf{j}_1 \times \hat{\boldsymbol{u}}_\odot)$$

$$+ 2(\mathbf{j}_0 \cdot \hat{\boldsymbol{n}}_\odot)(\mathbf{j}_1 \cdot \hat{\boldsymbol{n}}_\odot)(\mathbf{j}_0 \times \hat{\boldsymbol{u}}_\odot) + \frac{16}{5}(\mathbf{e}_0 \cdot \mathbf{e}_1)(\mathbf{j}_0 \times \hat{\boldsymbol{u}}_\odot) - \frac{1}{5}(\mathbf{j}_1 \times \hat{\boldsymbol{u}}_\odot)$$

$$+ \frac{16}{5}(\mathbf{e}_0 \cdot \hat{\boldsymbol{u}}_\odot)(\mathbf{j}_0 \times \mathbf{e}_1) + \frac{16}{5}(\mathbf{e}_0 \cdot \hat{\boldsymbol{u}}_\odot)(\mathbf{j}_1 \times \mathbf{e}_0) + \frac{16}{5}(\mathbf{e}_1 \cdot \hat{\boldsymbol{u}}_\odot)(\mathbf{j}_0 \times \mathbf{e}_0)\Big]$$

$$\text{(A.4)}$$

Now after linearizing the equations we resolve them into their components considering the outer binary triad as our basis; we use the following notation: $(\mathbf{e}_0 \cdot \hat{\boldsymbol{u}}_\odot)$ as e_u and $(\mathbf{e}_1 \cdot \hat{\boldsymbol{n}}_\odot)$ as e_{1n} and so on for the rest.

$$\frac{dj_{1u}}{d\tau} = j_{1v}\left(-\frac{3}{4}\varepsilon_\odot j_n - \frac{3}{2}\varepsilon_p \frac{(\mathbf{j}_0 \cdot \hat{\boldsymbol{n}}_{\boldsymbol{p}})}{(1 - e_0^2)^{\frac{5}{2}}} \cos\phi_\odot - \frac{75}{64}\varepsilon_\odot\varepsilon_\otimes[-2e_u j_n - 2e_n j_u] \right)$$

$$+ e_{1v}\left(\frac{15}{4}\varepsilon_\odot e_n - \frac{75}{64}\varepsilon_\odot\varepsilon_\otimes[14e_u e_n - 2j_n j_u] \right)$$

$$\frac{dj_{1n}}{d\tau} = j_{1v}\left(-\frac{3}{2}\varepsilon_p \frac{(\mathbf{j}_0 \cdot \hat{\boldsymbol{n}}_{\boldsymbol{p}})}{(1 - e_0^2)^{\frac{5}{2}}} \sin\phi_\odot - \frac{75}{64}\varepsilon_\odot\varepsilon_\otimes[2e_n j_n] \right)$$

$$+ e_{1v}\left(-\frac{75}{64}\varepsilon_\odot\varepsilon_\otimes[-7e_n^2 + j_n^2 + \frac{8}{5}e_0^2 - \frac{1}{5}] \right)$$

$$\frac{dj_{1v}}{d\tau} = j_{1u}\left(\frac{3}{4}\varepsilon_\odot j_n - \frac{3}{2}\varepsilon_p \frac{||\mathbf{j}_0 \times \hat{\boldsymbol{n}}_{\boldsymbol{p}}||}{(1 - e_0^2)^{\frac{5}{2}}} \sin\phi_\odot + \frac{3}{2}\varepsilon_p \frac{(\mathbf{j}_0 \cdot \hat{\boldsymbol{n}}_{\boldsymbol{p}})}{(1 - e_0^2)^{\frac{5}{2}}} \cos\phi_\odot \right.$$

$$\left. - \frac{75}{64}\varepsilon_\odot\varepsilon_\otimes[4e_u j_n + 4e_n j_u] \right)$$

$$+ j_{1n}\left(\frac{3}{4}\varepsilon_\odot j_u + \frac{3}{2}\varepsilon_p \frac{||\mathbf{j}_0 \times \hat{\boldsymbol{n}}_{\boldsymbol{p}}||}{(1 - e_0^2)^{\frac{5}{2}}} \cos\phi_\odot + \frac{3}{2}\varepsilon_p \frac{(\mathbf{j}_0 \cdot \hat{\boldsymbol{n}}_{\boldsymbol{p}})}{(1 - e_0^2)^{\frac{5}{2}}} \sin\phi_\odot \right.$$

$$\left. - \frac{75}{64}\varepsilon_\odot\varepsilon_\otimes[4e_u j_u - 6e_n j_n] \right)$$

$$+ e_{1u}\left(-\frac{15}{4}\varepsilon_\odot e_n + \frac{15}{2}\varepsilon_p \frac{(\mathbf{j}_0 \cdot \hat{\boldsymbol{n}}_{\boldsymbol{p}})||\mathbf{j}_0 \times \hat{\boldsymbol{n}}_{\boldsymbol{p}}||}{(1 - e_0^2)^{\frac{7}{2}}} e_u \right.$$

$$\left. - \frac{75}{64}\varepsilon_\odot\varepsilon_\otimes[4j_n j_u - \frac{156}{5}e_n e_u] \right)$$

$$+ e_{1n}\left(-\frac{15}{4}\varepsilon_\odot e_u + \frac{15}{2}\varepsilon_p \frac{(\mathbf{j}_0 \cdot \hat{\boldsymbol{n}}_{\boldsymbol{p}})||\mathbf{j}_0 \times \hat{\boldsymbol{n}}_{\boldsymbol{p}}||}{(1 - e_0^2)^{\frac{7}{2}}} e_n \right.$$

$$\left. - \frac{75}{64}\varepsilon_\odot\varepsilon_\otimes[2j_u^2 - 14e_u^2 - 3j_n^2 + \frac{89}{5}e_n^2 - \frac{8}{5}e_0^2 + \frac{1}{5}] \right)$$

$$\frac{de_{1u}}{d\tau} = j_{1v}\left(\frac{15}{4}\varepsilon_\odot e_n - \left[\frac{3}{2}\varepsilon_\odot - \frac{3}{4}\varepsilon_p\frac{1-e_0^2-5(\mathbf{j}_0\cdot\hat{\boldsymbol{n}}_{\boldsymbol{p}})^2}{(1-e_0^2)^{\frac{7}{2}}}\right]e_n\right.$$
$$\left. - \frac{75}{64}\varepsilon_\odot\varepsilon_\otimes\left[\frac{54}{5}e_u e_n - 2j_u j_n\right]\right)$$
$$+ e_{1v}\left(-\frac{3}{4}\varepsilon_\odot j_n - \frac{3}{2}\varepsilon_p\frac{(\mathbf{j}_0\cdot\hat{\boldsymbol{n}}_{\boldsymbol{p}})}{(1-e_0^2)^{\frac{5}{2}}}\cos\phi_\odot + \left[\frac{3}{2}\varepsilon_\odot - \frac{3}{4}\varepsilon_p\frac{1-e_0^2-5(\mathbf{j}_0\cdot\hat{\boldsymbol{n}}_{\boldsymbol{p}})^2}{(1-e_0^2)^{\frac{7}{2}}}\right]j_n\right.$$
$$\left. - \frac{75}{64}\varepsilon_\odot\varepsilon_\otimes\left[\frac{6}{5}e_u j_n - 2j_u e_n\right]\right)$$

$$\frac{de_{1n}}{d\tau} = j_{1v}\left(\left[\frac{3}{2}\varepsilon_\odot - \frac{3}{4}\varepsilon_p\frac{1-e_0^2-5(\mathbf{j}_0\cdot\hat{\boldsymbol{n}}_{\boldsymbol{p}})^2}{(1-e_0^2)^{\frac{7}{2}}}\right]e_u - \frac{75}{64}\varepsilon_\odot\varepsilon_\otimes\left[-7e_n^2 + j_n^2 + \frac{16}{5}e_u^2 + \frac{8}{5}e_0^2 - \frac{1}{5}\right]\right)$$
$$+ e_{1v}\left(-\frac{3}{2}\varepsilon_p\frac{(\mathbf{j}_0\cdot\hat{\boldsymbol{n}}_{\boldsymbol{p}})}{(1-e_0^2)^{\frac{5}{2}}}\sin\phi_\odot - \left[\frac{3}{2}\varepsilon_\odot - \frac{3}{4}\varepsilon_p\frac{1-e_0^2-5(\mathbf{j}_0\cdot\hat{\boldsymbol{n}}_{\boldsymbol{p}})^2}{(1-e_0^2)^{\frac{7}{2}}}\right]j_u\right.$$
$$\left. - \frac{75}{64}\varepsilon_\odot\varepsilon_\otimes\left[-\frac{16}{5}e_u j_u + 2j_n e_n\right]\right)$$

$$\frac{de_{1v}}{d\tau} = j_{1u}\left(-\frac{15}{4}\varepsilon_\odot e_n - \frac{3}{2}\varepsilon_p\frac{\|\mathbf{e}_0\times\hat{\boldsymbol{n}}_{\boldsymbol{p}}\|}{(1-e_0^2)^{\frac{5}{2}}}\sin\phi_\odot + \frac{30}{4}\varepsilon_p\frac{(\mathbf{j}_0\cdot\hat{\boldsymbol{n}}_{\boldsymbol{p}})}{(1-e_0^2)^{\frac{7}{2}}}\sin\phi_\odot e_0 j_0\right.$$
$$\left. + \left[\frac{3}{2}\varepsilon_\odot - \frac{3}{4}\varepsilon_p\frac{1-e_0^2-5(\mathbf{j}_0\cdot\hat{\boldsymbol{n}}_{\boldsymbol{p}})^2}{(1-e_0^2)^{\frac{7}{2}}}\right]e_n - \frac{75}{64}\varepsilon_\odot\varepsilon_\otimes\left[-\frac{44}{5}e_n e_u + 4j_n j_u\right]\right)$$
$$+ j_{1n}\left(\frac{3}{4}\varepsilon_\odot e_u + \frac{3}{2}\varepsilon_p\frac{\|\mathbf{e}_0\times\hat{\boldsymbol{n}}_{\boldsymbol{p}}\|}{(1-e_0^2)^{\frac{5}{2}}}\cos\phi_\odot - \frac{30}{4}\varepsilon_p\frac{(\mathbf{j}_0\cdot\hat{\boldsymbol{n}}_{\boldsymbol{p}})}{(1-e_0^2)^{\frac{7}{2}}}\cos\phi_\odot e_0 j_0\right.$$
$$\left. - \left[\frac{3}{2}\varepsilon_\odot - \frac{3}{4}\varepsilon_p\frac{1-e_0^2-5(\mathbf{j}_0\cdot\hat{\boldsymbol{n}}_{\boldsymbol{p}})^2}{(1-e_0^2)^{\frac{7}{2}}}\right]e_u - \frac{75}{64}\varepsilon_\odot\varepsilon_\otimes\left[-\frac{6}{5}e_u^2 + 2j_u^2 + 5e_n^2 - 3j_n^2 - \frac{8}{5}e_0^2 + \frac{1}{5}\right]\right)$$
$$+ e_{1u}\left(\frac{3}{4}\varepsilon_\odot j_n + \frac{15}{2}\varepsilon_p\frac{(\mathbf{j}_0\cdot\hat{\boldsymbol{n}}_{\boldsymbol{p}})\|\mathbf{e}\times\hat{\boldsymbol{n}}_{\boldsymbol{p}}\|}{(1-e_0^2)^{\frac{7}{2}}}e_u + \frac{3}{2}\varepsilon_p\frac{(\mathbf{j}_0\cdot\hat{\boldsymbol{n}}_{\boldsymbol{p}})}{(1-e_0^2)^{\frac{5}{2}}}\cos\phi_\odot - \left[\frac{3}{2}\varepsilon_\odot - \frac{3}{4}\varepsilon_p\frac{1-e_0^2-5(\mathbf{j}_0\cdot\hat{\boldsymbol{n}}_{\boldsymbol{p}})^2}{(1-e_0^2)^{\frac{7}{2}}}\right]j_n\right.$$
$$\left. + \frac{15}{4}\varepsilon_p\frac{e_u e_0 j_0}{(1-e_0^2)^{\frac{7}{2}}} - \frac{105}{4}\varepsilon_p\frac{(\mathbf{j}_0\cdot\hat{\boldsymbol{n}}_{\boldsymbol{p}})^2}{(1-e_0^2)^{\frac{9}{2}}}e_u e_0 j_0 - \frac{75}{64}\varepsilon_\odot\varepsilon_\otimes\left[-\frac{12}{5}e_u j_n - 12j_u e_n - \frac{16}{5}e_0 j_0\right]\right)$$
$$+ e_{1n}\left(-\frac{15}{4}\varepsilon_\odot j_u + \frac{15}{2}\varepsilon_p\frac{(\mathbf{j}_0\cdot\hat{\boldsymbol{n}}_{\boldsymbol{p}})\|\mathbf{e}\times\hat{\boldsymbol{n}}_{\boldsymbol{p}}\|}{(1-e_0^2)^{\frac{7}{2}}}e_n + \frac{3}{2}\varepsilon_p\frac{(\mathbf{j}_0\cdot\hat{\boldsymbol{n}}_{\boldsymbol{p}})}{(1-e_0^2)^{\frac{5}{2}}}\sin\phi_\odot - \frac{105}{4}\varepsilon_p\frac{(\mathbf{j}_0\cdot\hat{\boldsymbol{n}}_{\boldsymbol{p}})^2}{(1-e_0^2)^{\frac{9}{2}}}e_n e_0 j_0\right.$$
$$\left. + \left[\frac{3}{2}\varepsilon_\odot - \frac{3}{4}\varepsilon_p\frac{1-e_0^2-5(\mathbf{j}_0\cdot\hat{\boldsymbol{n}}_{\boldsymbol{p}})^2}{(1-e_0^2)^{\frac{7}{2}}}\right]j_u + \frac{15}{4}\varepsilon_p\frac{e_n e_0 j_0}{(1-e_0^2)^{\frac{7}{2}}} - \frac{75}{64}\varepsilon_\odot\varepsilon_\otimes\left[-\frac{44}{5}e_u j_u + \frac{34}{5}e_n j_n\right]\right)$$

Appendix B

The Hexadecapole:

We present the construction of the hexadecapole order used earlier to test the convergence of the multipoles expansion. From the expansion of the gravittional interactin potential, the hexadecapole is of order four in the radius, thus it reads:

$$\frac{-GM_{ep}}{r'}\frac{1}{8}\left(35\frac{(\mathbf{r}\cdot\mathbf{r}')^4}{r'^8} - 30\frac{(\mathbf{r}\cdot\mathbf{r}')^2}{r'^6}r^2 + 3\frac{\mathbf{r}^4}{\mathbf{r}'^4}\right) \tag{B.1}$$

hence

$$\left\langle \phi_{hex}(\mathbf{r},\phi)\right\rangle = \frac{-GM_{ep}}{8r'}\Bigg[\frac{35}{r'^8}\bigg(\left\langle r^4\cos^4\phi\right\rangle(\hat{\boldsymbol{u}}\cdot\mathbf{r}')^4 + 4\left\langle r^4\cos^3\phi\sin\phi\right\rangle(\hat{\boldsymbol{u}}\cdot\mathbf{r}')^3(\hat{\boldsymbol{v}}\cdot\mathbf{r}')$$

$$+ \left\langle r^4\sin^4\phi\right\rangle(\hat{\boldsymbol{v}}\cdot\mathbf{r}')^4 + 4\left\langle r^4\sin^3\phi\cos\phi\right\rangle(\hat{\boldsymbol{u}}\cdot\mathbf{r}')(\hat{\boldsymbol{v}}\cdot\mathbf{r}')^3$$

$$+ 6\left\langle r^4\cos^2\phi\sin^2\phi\right\rangle(\hat{\boldsymbol{u}}\cdot\mathbf{r}')^2(\hat{\boldsymbol{v}}\cdot\mathbf{r}')^2\bigg)$$

$$- \frac{30}{r'^6}\bigg(\left\langle r^4\cos^2\phi\right\rangle(\hat{\boldsymbol{u}}\cdot\mathbf{r}')^2 + \left\langle r^4\sin^2\phi\right\rangle(\hat{\boldsymbol{v}}\cdot\mathbf{r}')^2$$

$$+ 2\left\langle r^4\sin\phi\cos\phi\right\rangle(\hat{\boldsymbol{u}}\cdot\mathbf{r}')(\hat{\boldsymbol{v}}\cdot\mathbf{r}')\bigg) + \frac{3}{r'^4}\left\langle r^4\right\rangle\Bigg] \tag{B.2}$$

Thus we get the following:

$$\left\langle r^4 \cos^4 \phi \right\rangle = \frac{a^4}{2}(6e^4 + 9e^2 + \frac{3}{4}) \tag{B.3}$$

$$\left\langle r^4 \sin^4 \phi \right\rangle = \frac{3}{8}a^4(1 - e^2)^2 \tag{B.4}$$

$$\left\langle r^4 \cos^2 \phi \right\rangle = a^4(\frac{9e^4}{4} + \frac{41}{8}e^2 + \frac{1}{2}) \tag{B.5}$$

$$\left\langle r^4 \sin^2 \phi \right\rangle = \frac{a^4}{2}(\frac{-3e^4}{4} - \frac{1}{4}e^2 + 1) \tag{B.6}$$

$$\left\langle r^4 \cos \phi \sin^3 \phi \right\rangle = 0 \tag{B.7}$$

$$\left\langle r^4 \cos^3 \phi \sin \phi \right\rangle = 0 \tag{B.8}$$

$$\left\langle r^4 \cos^2 \phi \sin^2 \phi \right\rangle = \frac{a^4}{4}(-3e^4 + \frac{5}{2}e^2 + \frac{1}{2}) \tag{B.9}$$

$$\left\langle r^4 \sin \phi \cos \phi \right\rangle = 0 \tag{B.10}$$

$$\left\langle r^4 \right\rangle = a^4(\frac{15}{8}e^4 + 5e^2 + 1) \tag{B.11}$$

Now double averaging over the outer orbit:

$$\left\langle\left\langle \phi_{hex}(\mathbf{r}') \right\rangle\right\rangle = \frac{-GM_{ep}a^4}{8}\left[\frac{2205}{8}\left\langle \frac{(\mathbf{e} \cdot \mathbf{r}')^4}{r'^9} \right\rangle + \frac{105}{2}(-5e^2 + \frac{1}{2})\left\langle \frac{(\mathbf{e} \cdot \mathbf{r}')^2}{r'^7} \right\rangle \right.$$

$$- \frac{735}{4}\left\langle \frac{(\mathbf{e} \cdot \mathbf{r}')^2(\mathbf{j} \cdot \mathbf{r}')^2}{r'^9} \right\rangle + \left\langle \frac{1}{\mathbf{r}'^5} \right\rangle(30e^4 - \frac{15}{2}e^2 + \frac{9}{8})$$

$$\left. - \frac{15}{4}\frac{\left\langle (\mathbf{j} \cdot \mathbf{r}')^2 \right\rangle}{r'^7}(-10e^2 + 3) + \frac{105}{8}\left\langle \frac{(\mathbf{j} \cdot \mathbf{r}')^4}{r'^9} \right\rangle \right] \tag{B.12}$$

Computing these we get:

$$\left\langle \frac{(\mathbf{e} \cdot \mathbf{r}')^4}{r'^9} \right\rangle = \frac{3}{8a_\odot^5(1 - e_\odot)^{\frac{7}{2}}}\left[(\frac{5}{2}e_\odot^2 + 1)e_u^2 + 2(\frac{3}{2}e_\odot^2 + 1)e_u^2 e_v^2 + (\frac{e_\odot^2}{2} + 1)e_v^4 \right] \tag{B.13}$$

$$\left\langle \frac{(\mathbf{j} \cdot \mathbf{r}')^4}{r'^9} \right\rangle = \frac{3}{8a_\odot^5(1 - e_\odot)^{\frac{7}{2}}}\left[(\frac{5}{2}e_\odot^2 + 1)j_u^2 + 2(\frac{3}{2}e_\odot^2 + 1)j_u^2 j_v^2 + (\frac{e_\odot^2}{2} + 1)j_v^4 \right] \tag{B.14}$$

$$\left\langle \frac{(\mathbf{e} \cdot \mathbf{r}')^2(\mathbf{j} \cdot \mathbf{r}')^2}{r'^9} \right\rangle = \frac{1}{8a_\odot^5(1 - e_\odot)^{\frac{7}{2}}}\left[3(\frac{5}{2}e_\odot^2 + 1)e_u^2 j_u^2 + 3(\frac{e_\odot^2}{2} + 1)e_v^2 j_v^2 \right.$$

$$\left. + (\frac{3}{2}e_\odot^2 + 1)(e_u^2 j_v^2 + e_v^2 j_u^2 + 4e_u e_v j_u j_v) \right] \tag{B.15}$$

$$\left\langle \frac{(\mathbf{e} \cdot \mathbf{r}'^2)}{r'^7} \right\rangle = \frac{1}{8a_\odot^5(1 - e_\odot)^{\frac{7}{2}}}\left[(9e_\odot^2 + 4)e_u^2 + (3e_\odot^2 + 4)e_v^2) \right] \tag{B.16}$$

105

$$\left\langle \frac{(\mathbf{j} \cdot \mathbf{r'^2})}{r'^7} \right\rangle = \frac{1}{8a_\odot^5(1 - e_\odot)^{\frac{7}{2}}}\left[(9e_\odot^2 + 4)j_u^2 + (3e_\odot^2 + 4)j_v^2)\right] \tag{B.17}$$

Plugging these in we get:

$$\langle\langle \Phi_{hex} \rangle\rangle = -\frac{315}{512}\varepsilon_\odot\left[\varepsilon_\otimes^2\left(\frac{21}{2}e_n^4 + (16e^2 - 10)e_u^2 - 42e_n^2e_u^2 + (6e^2 - 9)e_n^2\right.\right.$$
$$+ 14e_u^2j_n^2 + (\frac{-72}{7}e^2 + \frac{2}{7})j_u^2 + 14e_n^2j_u^2 + \frac{1}{2}j_n^4$$
$$\left.+ (\frac{-62}{7}e^2 - \frac{1}{7})j_n^2 - 2j_n^2j_u^2 - \frac{68}{7}e^4 + \frac{66}{7}e^2 - \frac{1}{70}\right)$$
$$\frac{\varepsilon_\otimes^2}{e_\odot^2}\left(21e_n^4 + (-20e^2 + 2)e_n^2 + (\frac{20}{7}e^2 - \frac{6}{7})j_n^2 + j_n^4\right.$$
$$\left.\left.+ \frac{16}{7}e^4 - \frac{4}{7}e^2 + \frac{3}{35}\right)\right] \tag{B.18}$$

$$\frac{d\mathbf{j}}{d\tau} = \frac{3}{4}\varepsilon_\odot j_n(\mathbf{j} \times \hat{\boldsymbol{n}}_\odot) - \frac{15}{4}\varepsilon_\odot e_n(\mathbf{e} \times \hat{\boldsymbol{n}}_\odot) + \frac{3}{2}\varepsilon_p\frac{\mathbf{j} \cdot \hat{\boldsymbol{n}}_p}{(1 - e^2)^{\frac{5}{2}}}(\mathbf{j} \times \hat{\boldsymbol{n}}_p)$$
$$- \frac{75}{64}\varepsilon_\odot\varepsilon_\otimes\left[\left[2(e_uj_n + e_nj_u)\mathbf{j} + 2(-7e_ne_u + j_uj_n)\mathbf{e}\right] \times \hat{\boldsymbol{n}}_\odot\right.$$
$$\left.+ \left[2e_nj_n\mathbf{j} + (-7e_n^2 + j_n^2 + \frac{8}{5}e^2 - \frac{1}{5})\mathbf{e}\right] \times \hat{\boldsymbol{u}}_\odot\right]$$
$$+ \frac{315}{256}\varepsilon_\odot\left[\varepsilon_\otimes^2\left((14e_u^2j_n - 2j_nj_u^2 + j_n^3 + (-\frac{62}{7}e^2 - \frac{1}{7})j_n)\mathbf{j} \times \hat{\boldsymbol{n}}_\odot\right.\right.$$
$$+ (14e_n^2j_u - 2j_n^2j_u + (-\frac{72}{7}e^2 + \frac{2}{7})j_u)\mathbf{j} \times \hat{\boldsymbol{u}}_\odot$$
$$+ (-42e_u^2e_n + 14j_u^2e_n + 21e_n^3 + (6e^2 - 9)e_n)\mathbf{e} \times \hat{\boldsymbol{n}}_\odot$$
$$\left.+ (-42e_n^2e_u + 14j_n^2e_u + (16e^2 - 10)e_u)\mathbf{e} \times \hat{\boldsymbol{u}}_\odot\right)$$
$$\left.+ \frac{\varepsilon_\otimes^2}{e_\odot^2}\left((2j_n^3 + (\frac{20}{7}e^2 - \frac{6}{7})j_n)\mathbf{j} + (42e_n^3 + (-20e^2 + 2)e_n)\mathbf{e}\right) \times \hat{\boldsymbol{n}}_\odot\right]$$
$$\tag{B.19}$$

$$\frac{d\mathbf{e}}{d\tau} = \frac{3}{4}\varepsilon_{\odot}j_n(\mathbf{e} \times \hat{\boldsymbol{n}}_{\odot}) - \frac{15}{4}\varepsilon_{\odot}e_n(\mathbf{j} \times \hat{\boldsymbol{n}}_{\odot}) + \frac{3}{2}\varepsilon_p\frac{\mathbf{j} \cdot \hat{\boldsymbol{n}}_{\boldsymbol{p}}}{(1-e^2)^{\frac{5}{2}}}(\mathbf{e} \times \hat{\boldsymbol{n}}_{\boldsymbol{p}})$$

$$+ \left[\frac{3}{2}\varepsilon_{\odot} - \frac{3}{4}\varepsilon_p\frac{1 - e^2 - 5(\mathbf{j} \cdot \hat{\boldsymbol{n}}_{\boldsymbol{p}})^2}{(1-e^2)^{\frac{7}{2}}}\right]\mathbf{j} \times \mathbf{e}$$

$$- \frac{75}{64}\varepsilon_{\odot}\varepsilon_{\otimes}\left[\left[2\big(e_uj_n + e_nj_u\big)\mathbf{e} + 2\big(-7e_ne_u + j_uj_n\big)\mathbf{j}\right] \times \hat{\boldsymbol{n}}_{\odot}\right.$$

$$+ \left[2e_nj_n\mathbf{e} + \big(-7e_n^2 + j_n^2 + \frac{8}{5}e^2 - \frac{1}{5}\big)\mathbf{j}\right] \times \hat{\boldsymbol{u}}_{\odot}$$

$$\left.+ \frac{16}{5}e_u\mathbf{j} \times \mathbf{e}\right]$$

$$+ \frac{315}{256}\varepsilon_{\odot}\left[\varepsilon_{\otimes}^2\left(\big(14e_u^2j_n - 2j_nj_u^2 + j_n^3 + (-\frac{62}{7}e^2 - \frac{1}{7})j_n\big)\mathbf{e} \times \hat{\boldsymbol{n}}_{\odot}\right.\right.$$

$$+ \big(14e_n^2j_u - 2j_n^2j_u + (-\frac{72}{7}e^2 + \frac{2}{7})j_u\big)\mathbf{e} \times \hat{\boldsymbol{u}}_{\odot}$$

$$+ \big(-42e_u^2e_n + 14j_u^2e_n + 21e_n^3 + (6e^2 - 9)e_n\big)\mathbf{j} \times \hat{\boldsymbol{n}}_{\odot}$$

$$+ \big(-42e_n^2e_u + 14j_n^2e_u + (16e^2 - 10)e_u\big)\mathbf{j} \times \hat{\boldsymbol{u}}_{\odot}$$

$$\left.+ \big(16e_u^2 + 6e_n^2 - \frac{72}{7}j_u^2 - \frac{62}{7}j_n^2 - \frac{136}{7}e^2 + \frac{66}{7}\big)\mathbf{j} \times \mathbf{e}\right)$$

$$+ \frac{\varepsilon_{\otimes}^2}{e_{\odot}^2}\left(\big(2j_n^3 + (\frac{20}{7}e^2 - \frac{6}{7})j_n\big)\mathbf{e} \times \hat{\boldsymbol{n}}_{\odot} + \big(42e_n^3 + (-20e^2 + 2)e_n\big)\mathbf{j} \times \hat{\boldsymbol{n}}_{\odot}\right.$$

$$\left.\left.+ \big(\frac{20}{7}j_n^2 - 20e_n^2 + \frac{32}{7}e^2 - \frac{4}{7}\big)\mathbf{j} \times \mathbf{e}\right)\right] \tag{B.20}$$

Coplanar Coplanar solutions, for $\alpha = \phi_\odot - \phi$, are determined by the following equations:

$$0 = \frac{3}{4}\varepsilon_p(1-e^2)^{-\frac{3}{2}}\sin(2\phi) - \frac{3}{8}\varepsilon_\odot(1+4e^2)\sin 2\alpha$$

$$-\frac{75}{64}\varepsilon_\odot\varepsilon_\otimes e\left[-\frac{7}{2}(1+e^2)\cos\alpha\sin 2\alpha\right.$$

$$\left. + (2+5e^2)\sin^3\alpha + \frac{1}{5}(1-8e^2)\sin\alpha\right]$$

$$+\frac{315}{128}\varepsilon_\odot\varepsilon_\otimes^2\left[-\sin 4\alpha\left(\frac{27}{8}e^4 + \frac{23}{8}e^2 + \frac{5}{16}\right)\right.$$

$$+ \sin 2\alpha\left(\frac{5}{14}e^4 + \frac{1}{28}e^2 - \frac{1}{56}\right)$$

$$+ \frac{1}{e_\odot^2}\left(\sin 4\alpha\left(-\frac{11}{4}e^4 + \frac{1}{4}e^2 - \frac{1}{8}\right)\right.$$

$$\left.\left. + \sin 2\alpha\left(\frac{5}{7}e^4 + \frac{1}{14}e^2 - \frac{1}{28}\right)\right)\right] \qquad \text{(B.21)}$$

$$0 = \frac{3}{4}\varepsilon_p e(1-e^2)^{-2}(1-3\cos^2\phi) - \frac{3}{4}\varepsilon_\odot e(1-e^2)^{\frac{1}{2}}(1-4\sin^2\alpha)$$

$$-\frac{75}{64}\varepsilon_\odot\varepsilon_\otimes(1-e^2)^{\frac{1}{2}}\left[(3e^2-1)\cos^3\alpha(\frac{1}{5}-\frac{24}{5}e^2)\cos\alpha\right.$$

$$\left. + (1+\frac{15}{2}e^2)\sin\alpha\sin 2\alpha\right]$$

$$+\frac{315}{128}\varepsilon_\odot\varepsilon_\otimes^2(1-e^2)^{\frac{1}{2}}\left[-\cos 4\alpha\left(\frac{27}{8}e^3 + \frac{23}{16}e\right) + \cos 2\alpha\left(\frac{5}{7}e^3 + \frac{1}{28}e\right)\right.$$

$$+ \frac{57}{56}e^3 - \frac{51}{112}e$$

$$+ \frac{1}{e_\odot^2}\left(-\cos 4\alpha\left(\frac{11}{4}e^3 - \frac{1}{8}e\right)\right.$$

$$\left.\left. + \cos 2\alpha\left(\frac{10}{7}e^3 + \frac{1}{14}e\right) + \frac{25}{28}e^3 - \frac{43}{56}e\right)\right]$$

# Appendix C

Convergence Study:

We study the convergence of the interaction potential series expansion. For simplicity at first, we reduce the Hamiltonian to the planar case where the inner quadrupole, outer effect, and the test particle orbit all lie in the same plane and we expand up to the 7th order. Then we study the 3D series.

The analysis shows that multipoles expansion converges in the Moon-Earth-Sun system where the ratio of semi-major axes is very small; it also converges in our TNOs study, but only in regions below 280AU, and it diverges otherwise, both for planar and non-planar dynamics. A family of highly eccentric equilibira in the TNO study case survives the orders addition indicating a sort of asymptotic convergence and structural stability in that region. This family is the family of interset in matching the parameters of the studies eTNOs, both in inclinations and eccentricities. However, we say that another method is needed to study such systems. We start by the planar Hamiltonian expanded up to the 7th order.

$$
\begin{aligned}
H = {} & -\frac{1}{2}\varepsilon_p(1-e^2)^{-\frac{3}{2}} \\
& -\frac{3}{8}\varepsilon_\odot\Big(\frac{2}{3}+e^2\Big) \\
& +\varepsilon_\odot\varepsilon_\otimes\Big(\frac{15}{64}e\cos\Delta\varpi(3e^2+4)\Big) \\
& -\varepsilon_\odot\frac{\varepsilon_\otimes^2}{e_\odot^2}\bigg[\frac{315}{512}\Big(\frac{23}{14}e^4+\frac{26}{7}e^2+\frac{12}{35}\Big)e_\odot^2 \\
& \qquad\qquad +\frac{315}{512}\Big(\frac{3}{7}e^4+\frac{8}{7}e^2+\frac{8}{35}\Big)\bigg] \\
& +\varepsilon_\odot\frac{\varepsilon_\otimes^3}{e_\odot^3}\bigg[\frac{15}{64}\Big(\frac{35}{16}e^5+\frac{35}{4}e^3+\frac{7}{2}e\Big)\Big(\frac{3}{2}e_\odot^3+2e_\odot^2\Big)\cos\Delta\varpi \\
& \qquad\qquad +\frac{35}{128}\Big(\frac{63}{16}e^5+\frac{21}{2}e^3\Big)\Big(\frac{e_\odot^2}{2}\Big)\cos 3\Delta\varpi\bigg] \\
& -\varepsilon_\odot\frac{\varepsilon_\otimes^4}{e_\odot^4}\bigg[\frac{25}{256}\Big(\frac{35}{16}e^6+\frac{105}{8}e^4+\frac{21}{2}e^2+1\Big)\Big(\frac{15}{8}e_\odot^4+5e_\odot^2+1\Big) \\
& \qquad\qquad +\frac{105}{512}\Big(\frac{45}{16}e^6+15e^4+9e^2\Big)\Big(\frac{5}{4}e_\odot^4+\frac{5}{2}e_\odot^2\Big)\cos 2\Delta\varpi\bigg] \\
& \qquad\qquad +\frac{63}{256}\Big(\frac{99}{16}e^6+\frac{165}{8}e^4\Big)\Big(\frac{5}{16}e_\odot^4\Big)\cos 4\Delta\varpi\bigg] \\
& +\varepsilon_\odot\frac{\varepsilon_\otimes^5}{e_\odot^5}\bigg[\frac{175}{1024}\Big(\frac{315}{128}e^7+\frac{315}{16}e^5+\frac{189}{8}e^3+\frac{9}{2}e\Big)\Big(\frac{18}{5}e_\odot^5\frac{15}{2}e_\odot^3+3e_\odot\Big)\cos\Delta\varpi \\
& \qquad\qquad +\frac{189}{1024}\Big(\frac{495}{128}e^7+\frac{825}{32}e^5+\frac{165}{8}e^3\Big)\Big(\frac{15}{16}e_\odot^5+\frac{5}{2}e_\odot^3\Big)\cos 3\Delta\varpi\bigg] \\
& \qquad\qquad +\frac{231}{1024}\Big(\frac{1287}{128}e^7+\frac{1287}{32}e^5\Big)\Big(\frac{3}{16}e_\odot^5\Big)\cos 5\Delta\varpi\bigg]
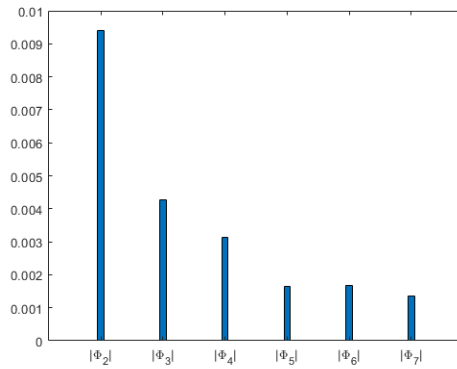\end{aligned}
\tag{C.1}
$$
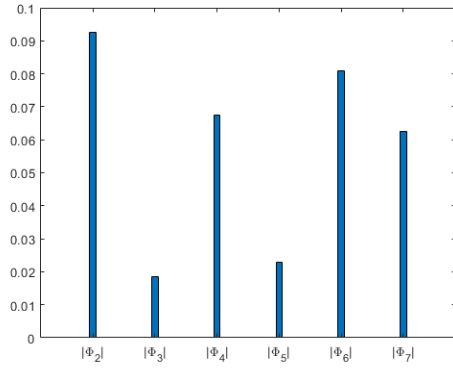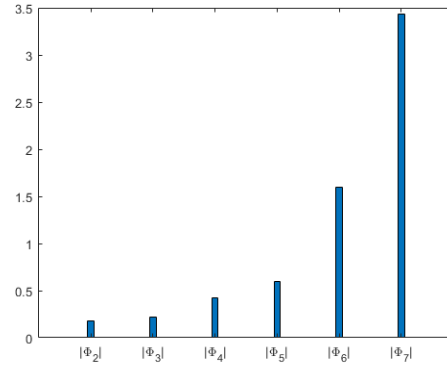
(a) e=0.1, a=400au (b) e=0.8, a=400au
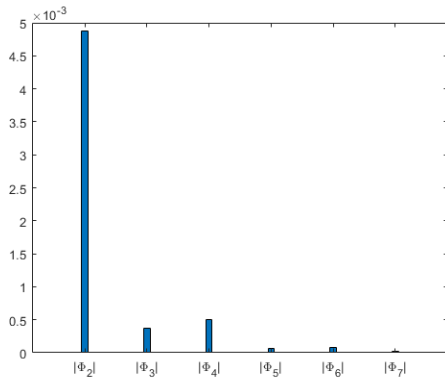
(c) e=0.1, a=150au (d) e=0.8, a=150au

Figure C.1: Numerical values of the orders in the potential expanded in equation (132) for different parameters of the solar binary case at $a_\odot = 700$a.u. and $e_\odot = 0.6$
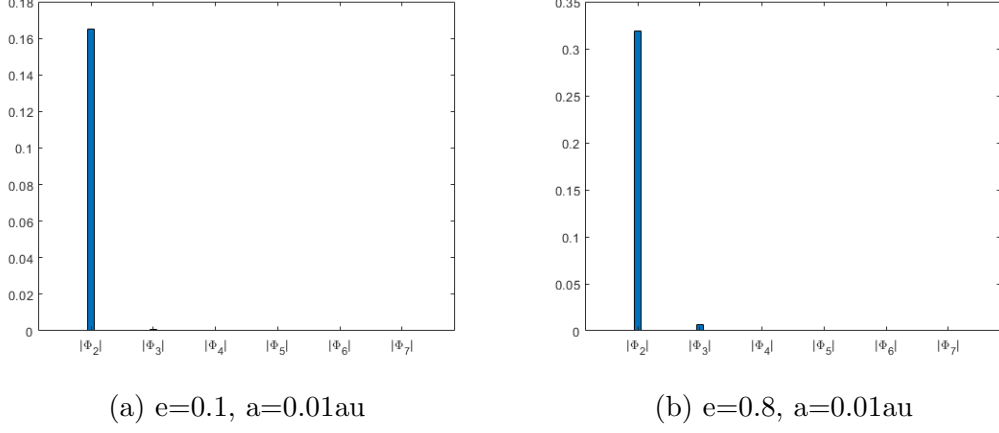
111

(a) e=0.1, a=0.01au

(b) e=0.8, a=0.01au

Figure C.2: Same numerical study for the Earth-Moon-Sun system with $e_\odot = 0.6$. $r = 0.01$a.u. defines the Hill's radius.

We also study these effects for off-plane dynamics. The potential up to the hexadecapole in 3D, for coplanar-coplanar description, with $\alpha = \phi_\odot - \phi$ is:
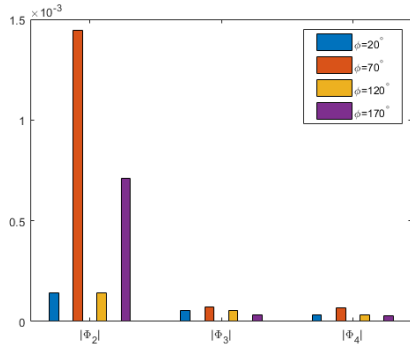
$$
\begin{aligned}
H = & -\frac{3}{8}\varepsilon_\odot \left(4e^2 \cos^2 \alpha + \cos^2 \alpha - 3e^2 - \frac{1}{3} \right) \\
& + \frac{15}{64}\varepsilon_\odot\varepsilon_\otimes \left(20e^3 \cos^2 \alpha + 15e \cos^3 \alpha - 17e^3 \cos \alpha - 11e \cos \alpha \right) \\
& - \frac{315}{512}\varepsilon_\odot\varepsilon_\otimes^2 \Bigg[\frac{1}{70}(1890e^4 + 1610e^2 + 175)\cos^4 \alpha + \frac{1}{70}(-1990e^4 + -1620e^2 + -170)\cos^2 \alpha \\
& \qquad + \frac{43}{14}e^4 + \frac{27}{7}e^2 + \frac{19}{70} \\
& \qquad + \frac{1}{e_\odot^2}\left(\frac{1}{35}(770e^4 - 7e^2 + 35)\cos^4 \alpha + \frac{1}{35}(-870e^4 + 60e^2 - 30)\cos^2 \alpha \right. \\
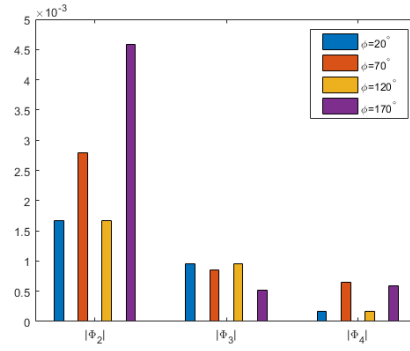& \qquad\qquad \left. + \frac{23}{7}e^4 + \frac{10}{7}e^2 + \frac{3}{35} \right) \Bigg]
\end{aligned}
\tag{C.2}
$$
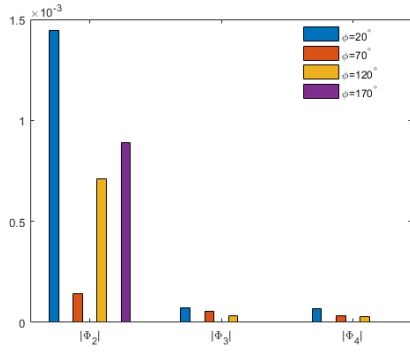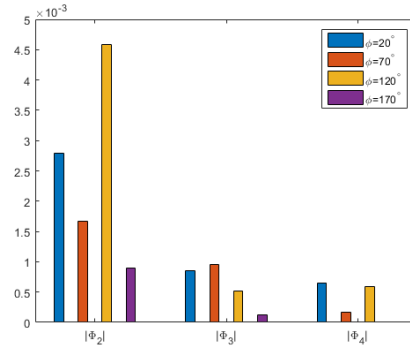
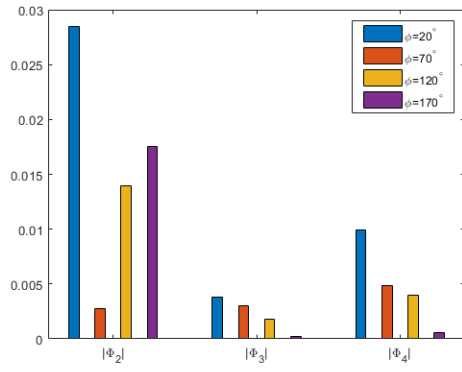(a) $\phi_\odot = 20°$, $e = 0.1$, $a = 100$a.u.   (b) $\phi_\odot = 20°$, $e = 0.8$, $a = 100$a.u.
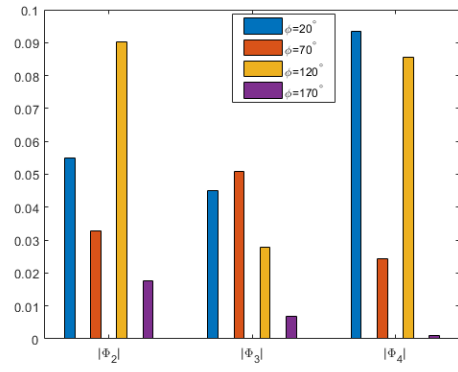
(c) $\phi_\odot = 70°$, $e = 0.1$, $a = 100$a.u.   (d) $\phi_\odot = 70°$, $e = 0.8$, $a = 100$a.u.

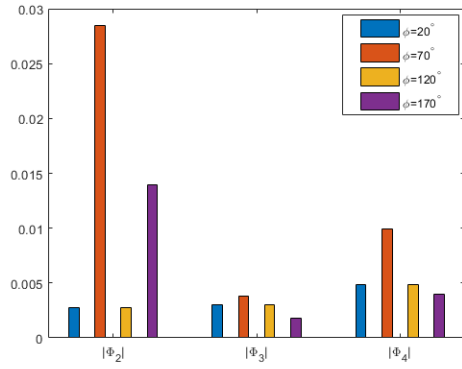Figure C.3: Numerical values of (133) for different parameters of the solar binary case at $a_\odot = 700$a.u. and $e_\odot = 0.6$. Particle at $a = 100$ a.u.

(a) $\phi_{\odot} = 20°$, $e = 0.1$, $a = 270$a.u.

(b) $\phi_{\odot} = 20°$, $e = 0.8$, $a = 270$a.u.

(c) $\phi_{\odot} = 70°$, $e = 0.1$, $a = 270$a.u.
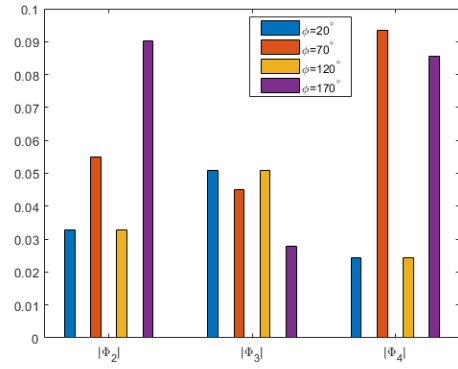
(d) $\phi_{\odot} = 70°$, $e = 0.8$, $a = 270$a.u.

Figure C.4: Same setting but particle at $a = 270$ a.u. The series still diverges except for low eccentricity solutions, and not for all inclinations.

Bibliography

[1] P. S. Laplace, *Traité de mécanique céleste*, vol. 1. de l'Imprimerie de Crapelet, 1799.

[2] R. Allan and G. Cook, "The long-period motion of the plane of a distant circular orbit," *Proceedings of the Royal Society of London. Series A. Mathematical and Physical Sciences*, vol. 280, no. 1380, pp. 97–109, 1964.

[3] P. Goldreich, "Inclination of satellite orbits about an oblate precessing planet," *The Astronomical Journal*, vol. 70, p. 5, 1965.

[4] M. Lidov, "The evolution of orbits of artificial satellites of planets under the action of gravitational perturbations of external bodies," *Planetary and Space Science*, vol. 9, no. 10, pp. 719–759, 1962.

[5] Y. Kozai, "Secular perturbations of asteroids with high inclination and eccentricity," *The Astronomical Journal*, vol. 67, p. 591, 1962.

[6] E. B. Ford, B. Kozinsky, and F. A. Rasio, "Secular evolution of hierarchical triple star systems," *The Astrophysical Journal*, vol. 535, no. 1, p. 385, 2000.

[7] G. Li, S. Naoz, B. Kocsis, and A. Loeb, "Eccentricity growth and orbit flip in near-coplanar hierarchical three-body systems," *The Astrophysical Journal*, vol. 785, no. 2, p. 116, 2014.

[8] W. R. Ward, "Orbital inclination of iapetus and the rotation of the laplacian plane," *Icarus*, vol. 46, no. 1, pp. 97–107, 1981.

[9] S. Tremaine, J. Touma, and F. Namouni, "Satellite dynamics on the laplace surface," *The Astronomical Journal*, vol. 137, pp. 3706–3717, 2009.

[10] A. J. Rosengren and D. J. Scheeres, "Laplace plane modifications arising from solar radiation pressure," *The Astrophysical Journal*, vol. 786, no. 1, p. 45, 2014.

[11] S. Charnoz, R. Canup, A. Crida, and L. Dones, "The origin of planetary ring systems," *arXiv preprint arXiv:1703.09741*, 2017.

[12] B. J. Buratti and J. A. Mosher, "Comparative global albedo and color maps of the uranian satellites," *Icarus*, vol. 90, no. 1, pp. 1–13, 1991.

[13] D. Tamayo, J. Burns, D. Hamilton, and P. Nicholson, "Chaotic dust orbits at uranus may explain hemispherical color asymmetries on its regular satellites," in *EPSC-DPS Joint Meeting 2011*, p. 47, 2011.

[14] D. Tamayo, J. A. Burns, D. P. Hamilton, and P. D. Nicholson, "Dynamical instabilities in high-obliquity systems," *The Astronomical Journal*, vol. 145, no. 3, p. 54, 2013.

[15] D. Hestenes, *New Foundations for Classical Mechanics*. Kluwer Academic Publishers, 1999.

[16] J. P. Rozelot and C. Damiani, "History of solar oblateness measurements and interpretation," *The European Physical Journal H*, vol. 36, pp. 407–436, Nov 2011.

[17] C. Murray and S. Dermott, *Solar System Dynamics*. Press Syndicate of the University of Cambridge, 1999.

[18] D. Brouwer, "Solution of the problem of artificial satellite theory without drag," *The Astronomical Journal*, vol. 64, p. 378, 1959.

[19] H. Goldstein, *Classical Mechanics*. Addison-Wesley, 1980.

[20] R. R. Allan and G. N. Ward, "Planetary equations in terms of vectorial elements," *Proceedings of the Cambridge Philosophical Society*, vol. 59, p. 669, 1963.

[21] V. I. Arnold, *Mathematical Methods of Classical Mechanics*. Springer, 1980.

[22] J. Laskar and G. Boué, "Explicit expansion of the three-body disturbing function for arbitrary eccentricities and inclinations," *Astronomy & Astrophysics*, vol. 522, p. A60, 2010.

[23] J. J. Lissauer, R. I. Dawson, and S. Tremaine, "Advances in exoplanet science from kepler," *Nature*, vol. 513, no. 7518, p. 336, 2014.

[24] C. J. Burke, S. T. Bryson, F. Mullally, J. F. Rowe, J. L. Christiansen, S. E. Thompson, J. L. Coughlin, M. R. Haas, N. M. Batalha, D. A. Caldwell, *et al.*, "Planetary candidates observed by kepler iv: Planet sample from q1-q8 (22 months)," *The Astrophysical Journal Supplement Series*, vol. 210, no. 2, p. 19, 2014.

[25] D. C. Fabrycky, J. J. Lissauer, D. Ragozzine, J. F. Rowe, J. H. Steffen, E. Agol, T. Barclay, N. Batalha, W. Borucki, D. R. Ciardi, *et al.*, "Architecture of kepler's multi-transiting systems. ii. new investigations with twice as many candidates," *The Astrophysical Journal*, vol. 790, no. 2, p. 146, 2014.

[26] S. Tremaine and S. Dong, "The statistics of multi-planet systems," *The Astronomical Journal*, vol. 143, no. 4, p. 94, 2012.

[27] J. F. Rowe, S. T. Bryson, G. W. Marcy, J. J. Lissauer, D. Jontof-Hutter, F. Mullally, R. L. Gilliland, H. Issacson, E. Ford, S. B. Howell, *et al.*, "Validation of kepler's multiple planet candidates. iii. light curve analysis and announcement of hundreds of new multi-planet systems," *The Astrophysical Journal*, vol. 784, no. 1, p. 45, 2014.

[28] S. M. Mills and D. C. Fabrycky, "Kepler-108: A mutually inclined giant planet system," *The Astronomical Journal*, vol. 153, no. 1, p. 45, 2017.

[29] W. Xu and D. Fabrycky, "Exciting mutual inclination in planetary systems with a distant stellar companion: the case of kepler-108," *arXiv preprint arXiv:1904.02290*, 2019.

[30] J. R. Touma and S. Sridhar, "The disruption of multiplanet systems through resonance with a binary orbit," *Nature*, vol. 524, no. 7566, p. 439, 2015.

[31] J. Wang, D. A. Fischer, J.-W. Xie, and D. R. Ciardi, "Influence of stellar multiplicity on planet formation. iv. adaptive optics imaging of kepler stars with multiple transiting planet candidates," *The Astrophysical Journal*, vol. 813, no. 2, p. 130, 2015.

[32] A. Morbidelli and H. F. Levison, "Scenarios for the origin of the orbits of the trans-neptunian objects 2000 cr105 and 2003 vb12 (sedna)," *The Astronomical Journal*, vol. 128, no. 5, p. 2564, 2004.

[33] R. S. Gomes, T. Gallardo, J. A. Fernández, and A. Brunini, "On the origin of the high-perihelion scattered disk: The role of the kozai mechanism and mean motion resonances," *Celestial Mechanics and Dynamical Astronomy*, vol. 91, no. 1-2, pp. 109–129, 2005.

[34] K. Batygin and M. E. Brown, "Evidence for a distant giant planet in the solar system," *The Astronomical Journal*, vol. 151, no. 2, p. 22, 2016.

[35] A. Sefilian and J. Touma, "Shepherding in a self-gravitating disk of trans-neptunian objects," *The Astronomical Journal*, vol. 157, p. 59, 2019.

[36] C. Migaszewski and K. Goździewski, "A secular theory of coplanar, non-resonant planetary system," *Monthly Notices of the Royal Astronomical Society*, vol. 388, no. 2, pp. 789–802, 2008.

[37] C. Migaszewski and K. Goździewski, "Equilibria in the secular, non-co-planar two-planet problem," *Monthly Notices of the Royal Astronomical Society*, vol. 395, no. 4, pp. 1777–1794, 2009.

[38] H. Beust, "Orbital clustering of distant kuiper belt objects by hypothetical planet 9. secular or resonant?," *Astronomy & Astrophysics*, vol. 590, p. L2, 2016.

[39] B. A. Smith and R. J. Terrile, "A circumstellar disk around β pictoris," *Science*, vol. 226, no. 4681, pp. 1421–1424, 1984.

[40] A.-M. Lagrange, D. Gratadour, G. Chauvin, T. Fusco, D. Ehrenreich, D. Mouillet, G. Rousset, D. Rouan, F. Allard, É. Gendron, *et al.*, "A probable giant planet imaged in the β pictoris disk-vlt/naco deep l'-band imaging," *Astronomy & Astrophysics*, vol. 493, no. 2, pp. L21–L25, 2009.

[41] P. Kalas and D. Jewitt, "Asymmetries in the beta pictoris dust disk," *The Astronomical Journal*, vol. 110, p. 794, 1995.

[42] Y. K. Okamoto, H. Kataza, M. Honda, T. Yamashita, T. Onaka, J.-i. Watanabe, T. Miyata, S. Sako, T. Fujiyoshi, and I. Sakon, "An early extrasolar planetary system revealed by planetesimal belts in β pictoris," *Nature*, vol. 431, no. 7009, p. 660, 2004.

[43] W. R. Dent, M. Wyatt, A. Roberge, J.-C. Augereau, S. Casassus, S. Corder, J. Greaves, I. de Gregorio-Monsalvo, A. Hales, A. Jackson, *et al.*, "Molecular gas clumps from the destruction of icy bodies in the β pictoris debris disk," *Science*, vol. 343, no. 6178, pp. 1490–1492, 2014.

[44] A.-M. Lagrange, A. Boccaletti, J. Milli, G. Chauvin, M. Bonnefoy, D. Mouillet, J. Augereau, J. Girard, S. Lacour, and D. Apai, "The position of β pictoris b position relative to the debris disk," *Astronomy & Astrophysics*, vol. 542, p. A40, 2012.

[45] I. Snellen and A. Brown, "The mass of the young planet beta pictoris b through the astrometric motion of its host star," *Nature Astronomy*, vol. 2, no. 11, p. 883, 2018.

[46] P. Kervella, F. Arenou, F. Mignard, and F. Thévenin, "Stellar and substellar companions of nearby stars from gaia dr2-binarity from proper motion anomaly," *Astronomy & Astrophysics*, vol. 623, p. A72, 2019.

[47] T. J. Dupuy, T. D. Brandt, K. M. Kratter, and B. P. Bowler, "A model-independent mass and moderate eccentricity for β pic b," *The Astrophysical Journal Letters*, vol. 871, no. 1, p. L4, 2019.

[48] K. Silsbee and S. Tremaine, "Producing distant planets by mutual scattering of planetary embryos," *The Astronomical Journal*, vol. 155, no. 2, p. 75, 2018.